Nanoencapsulation of bioactive compounds for food applications

Mariarenata Sessa

Unione Europea

UNIVERSITÀ DEGLI
STUDI DI SALERNO

Department of Industrial Engineering

Ph.D. Course in Chemical Engineering
(X Cycle-New Series)

NANOENCAPSULATION OF BIOACTIVE COMPOUNDS FOR FOOD APPLICATIONS

Supervisor
Prof. Giovanna Ferrari

Ph.D. student
Mariarenata Sessa

Scientific Referees
Dr. Ing. Francesco Donsì
Dr. Rong Cao

Ph.D. Course Coordinator
Prof. Paolo Ciambelli

“An unexamined life is not worth living”

Socrates

Acknowledgements

I gratefully acknowledge the support given by my scientific supervisors, Prof. Giovanna Ferrari and Dr. Francesco Donsì. I wish to thank Prof. Giovanna Ferrari for her professional and scientific advices. A special thanks to Dr. Francesco Donsì for his incomparable guidance and unequaled support, but also for his extreme patience with me in these three years. I'm sincerely grateful to him for having fueled in me the passion for the research and for believing deeply in me.

I also want to express my gratitude to Dr. Rong Cao for kindly inviting me to join his research group at the Guelph Food Research Centre, Agriculture and AgriFood Canada, and for giving me precious suggestions and encouragements. My special thanks to all Dr. Cao's research group, especially to Dr. Amy Proulx and Dr. Ronghua Liu for being so helpful in the *in vitro* and *ex vivo* experiments.

I would like to acknowledge all the people who work and have worked at ProdAl Scarl for sharing with me pleasant days during the whole period of my PhD. Especially thanks to my friend Marianna, to Mariangela Falcone and Mariarosaria Vincensi for their assistance with the HPLC analysis and to Raffaele Taddeo and Luigi Esposito for their help in plant maintenance.

I would like to thank my colleagues who accompanied me through all happy and tough times of our PhD course, and in particular way to my friend Titti with whom I "virtually" shared the long canadian evenings.

Finally, I'm very grateful to my parents, who always supported my choices and helped me to overcome every difficulty.

I would like to dedicate this work to my beloved Saverio, who makes special every moment of my life. Thanks for always being by my side.

Publications

Donsì, F.; Annunziata, M.; **Sessa, M.**; Ferrari, G. (2011) Nanoencapsulation of essential oils to enhance their antimicrobial activity in foods. *Lwt-Food Science and Technology,* 44, 1908-1914.

Sessa, M.; Tsao, R.; Liu, R.; Ferrari, G.; Donsì, F. (2011) Evaluation of the stability and antioxidant activity of nanoencapsulated resveratrol during *in vitro* digestion. *Journal of Agricultural and Food Chemistry,* 59, 12352-12360.

Donsì, F.; **Sessa, M.**; Ferrari, G. (2011) Effect of emulsifier type and disruption chamber geometry on the fabrication of food nanoemulsions by high pressure homogenization. *Industrial & Engineering Chemistry Research,* in press.

Donsì, F., **Sessa, M.**, Ferrari, G., Mediouni, H., Mgaidi, A. (2011) Encapsulation of bioactive compounds in nanoemulsion-based delivery systems. In: Editors: Taoukis, P.S., Stoforos, N.G., Karathanos, V.T., Saravacos, G.D. Proceedings of the 11th International Congress on Engineering and Food (ICEF11), Athens (Greece), May 22-26, 2011, vol. 1, p. 681-682.

Amendola, D., Donsì, F., **Sessa, M.**, Ferrari, G., De Faveri, D.M., Spigno, G. (2011). Nanoemulsions of grape marc extract as natural additives to improve hazelnut paste shelf-life. In: Editors: Taoukis, P.S., Stoforos, N.G., Karathanos, V.T., Saravacos, G.D. Proceedings of the 11th International Congress on Engineering and Food (ICEF11). Athens (Greece), May 22-26, 2011, vol. 1, p. 165-166.

Donsì, F., Annunziata, M., **Sessa, M.**, Ferrari, G. (2011) Nanoemulsion-based delivery systems for the encapsulation of essential oils to be used as antimicrobials in foods. In: Editors: Tavman, S., Ötleş, S., Baysal, T., Göksungur, Y., Kişla, D., Dirim, N., Koca, N. Proceedings of the

International Food Congress Novel Approaches in Food Industry (NAFI 2011). Cesme (Turchia), May 26-29, 2011, vol. 1, p. 16-21.

Donsì, F.; **Sessa, M.**; Ferrari, G. (2011) Nanometric-size delivery systems of bioactive compounds for nutraceutical and food industries. In: *Bionanotechnology: A Revolution in Biomedical Sciences & Human Health*, John Wiley & Sons, submitted.

Sessa, M., Casazza, A.A:, Perego, P., Tsao, R., Ferrari, G., Donsì, F. (2012) Exploitation of polyphenolic extracts from grape marc as natural antioxidants by encapsulation in lipid-based nanodelivery systems. *Food and Bioprocess Technology*, submitted.

Sessa, M., Donsì, F, Ferrari, G., Proulx, A., Tsao, R. (2012) Bioavailability of encapsulated resveratrol into nanoemulsion-based delivery systems. *Nanomedicine: Nanotechnology, Biology, and Medicine*, submitted.

Oral communications

Encapsulation of bioactive compounds in nanoemulsion-based delivery systems. 11th International Congress on Engineering and Food (ICEF11). Athens (Greece), May 22-26, 2011.

Recent advances in the use of HPH technique @ ProdAl. Advanced in UHPH process (FUNENTECH workshop). Barcelona (Spain), December 15, 2011.

Index

List of figures

List of tables

Abstract

The increase in dietary-intake-related illnesses, such as obesity, cardiovascular diseases, hypertension, diabetes and cancer, have made in recent years the development of health-and-wellness promoting foods a priority of the food industry. Clinical studies have demonstrated tangible health benefits that may be derived from the intake of bioactive compounds. However many difficulties are associated with their inclusion in food matrices, due to a very low solubility in water and easy degradation by hostile environmental conditions once extracted from plant tissues. Furthermore, poor solubility also means lower absorption in the gastrointestinal tract and, therefore, limited bioavailability. In the food industry, it has become apparent that there is a pressing need for edible delivery system to efficiently encapsulate, protect and release bioactive compounds when developing functional foods.

This thesis was addressed to the study and engineering of nanoencapsulation systems, above all nanoemulsions and solid lipid nanoparticles, with superior capabilities of a) protecting the encapsulated bioactive compounds from interaction with food ingredients, keeping their functional properties and preventing the deterioration of the food itself (i.e. oxidation of fat), b) reducing the impact on the organoleptic properties of food and c) improving the absorption and bioavailability of the bioactives, due to the subcellular size of the nanocapsules, which may potentially enhance passive transport mechanisms (i.e. related to the concentration gradient) across the intestinal wall.

The research activity has contributed to the advance of the knowledge in the field of the science of colloids, through the specific investigation of the effects of formulation and process parameters, which influence nanoemulsion production, as well as to a deeper comprehension of the technological and biological aspects of the incorporation of the nanoencapsulated compounds in food matrices and explication of their activity.

Three different classes of bioactive compounds were chosen as model systems of the experimental work, namely curcumin, resveratrol and essential oils. Both curcumin and resveratrol are antioxidant compounds

with markedly low solubility both in aqueous and lipid phase, hence requiring the development of specific formulations. In contrast, essential oils can be easily blended with oils, but require their diffusion through the aqueous phase to attack the cell membrane of microorganisms and act as antimicrobials.

Therefore, novel formulations were developed using a combination of hydrophilic (sugar ester, defatted soy lecithin, polysorbate 20) and lipophilic emulsifiers (soy lecithin, glycerol monooleate) to encapsulate resveratrol in peanut oil droplets and disperse it in aqueous systems at a concentration of 100 mg/L, ten times higher than the therapeutic blood concentration. In the same way, curcumin has been encapsulated in solid lipid particles, using stearic acid as lipid phase, at a maximum concentration 1600 times higher than the solubility of curcumin in water (0.6 mg/L).

Once the formulation was defined, the issue of the actual fabrication of the nanometric delivery systems was faced from a fundamental point of view. In particular, the production of food nanoemulsions by high pressure homogenization (HPH) has been investigated, focusing on the effect on droplet nanonization of emulsifier type and concentration, as well as of the geometry of the homogenization chamber. The reported results showed that the kinetic parameters of the emulsification process can be primarily correlated with the interfacial and dynamic properties of the emulsifiers, while the fluid-dynamics regime established in the homogenization chamber contributes only to a lesser extent. Nevertheless, the correct design of the homogenization chamber may help in obtaining uniform fluid-dynamic conditions, which ensure a narrow droplet size distribution.

The issues related to the physicochemical stability of nanoencapsulated bioactive compounds was faced for resveratrol and curcumin, trying to improve the formulation based on the inputs derived from accelerated ageing studies, that could simulate the food processing and the shelf life of the final product. The results obtained demonstrated that the nanoemulsions based on soy lecithin/sugar esters and Tween 20/glycerol monooleate can better encapsulate resveratrol in the lipid matrix, protecting it both during accelerated ageing and gastro-intestinal digestion and promoting a sustained release. Moreover, these formulations, having smaller mean droplet diameters (below 200 nm), remained physically stable also after the digestion process, allowing the resveratrol to reach the intestinal wall entrapped in the lipid droplets.

The subcellular dimension and the compatibility with cell membranes of the developed formulations also resulted in a higher permeability through the intestinal wall, which was simulated studying the transport through Caco-2 cell monolayers grown on permeable supports. Generally, the apparent permeability of most compounds falls in a range of 1×10^{-7} cm/sec (poorly transported compound) to 1×10^{-5} cm/sec (well-transported compound). The apparent permeability of resveratrol encapsulated in different nanoemulsion-

based delivery systems resulted always in the range indicated, demonstrating that nanoencapsulation can improve passive transport mechanisms. In particular, soy lecithin/sugar esters-based formulation showed an higher permeability due to the presence of soy lecithin, which, having a structure similar to the phospholipid bilayers of the cellular membrane, favours the absorption and the entrapment of the oil droplets in the microvilli and their consequent transport through the cell membrane.

Another remarkable result of the present thesis is that for the first time the effect of the delivery systems on the antioxidant activity of nanoencapsulated compounds was investigated, using a biological-based approach that integrated the classical chemical approaches. More specifically, an improved cellular assay was developed, that enabled to measure exclusively the residual activity of nanoencapsulated bioactive that penetrated inside Caco-2 cells, giving precious information on the combination of the mass transfer promotion and protection by the delivery systems.

Finally, the technological issue related to the incorporation into fruit juices of essential oils encapsulated into nanometric delivery systems was investigated, having as goal the design of systems that are able to enhance antimicrobial activity of the bioactive compounds, while minimizing the impact on the quality attributes of the final product. The results showed that, due to the higher antimicrobial activity of the nanoencapsulated essential oils, lower antimicrobial concentrations are required for a bactericidal action with a minimal alteration of the organoleptic properties of the juice.

Chapter I
Introduction and background

I.1 Interest of the study

Several factors sustain the exponential growth of functional foods and nutraceuticals registered during the last years in the world food market, such as the increasing demand of the Western societies for natural products, together with the increasing consumers' awareness that eating habits should not be merely based on the nutritive aspects of the food, but also on the health-beneficial effects that may derive from its consumption.

Therefore, incorporation in foods and in nutraceutical formulations of bioactive compounds, in order to improve food quality, such as shelf-life, taste or aspect, without the need of synthetic additives, as well as to develop novel functionalities, especially related to health promotion, such as antioxidant, antiradical and antitumor abilities, is highly desired from manufacturing companies and is object of intensive investigations from food scientists, food engineers and food technologists.

In particular, the issues related to efficiently delivering bioactive compounds through the food matrices, improving their uptake and bioavailability, while minimizing the impact on the organoleptic and qualitative properties of the products, call for a heavy involvement of nanotechnology in the development of suitable encapsulation systems.

Currently, the market of nanotechnology products in the food industry is worth about US$ 1 billion, including mainly nanometric delivery systems of bioactive compounds, applied to packaging coatings, to health promoting products, as well as to beverages, and it is foreseen to grow to more than US$20 billion in the next decade (Chau et al., 2007).

In this chapter, the nanometric size delivery systems most suitable for food applications will be discussed, such as nanoemulsions and solid lipid nanoparticles, focusing on high pressure homogenization as production method. Finally, it will be highlighted the ability of the nanoencapsulation to increase the dispersion in aqueous systems of bioactive compounds, which are poorly soluble in water, to protect them from chemical degradation, to

improve their antioxidant and antimicrobial activities and to increase their bioavailability.

I.2 Food-grade nanometric delivery systems

The development of functional foods through the addition of bioactive compounds holds many technological challenges. There is a pressing need for edible delivery system to encapsulate, protect and release bioactive compounds within the food industry. From a technological point of view, an efficient nanometric size delivery system should benefit from the following characteristics (McClements et al., 2007):

- *Food grade ingredients*: the delivery system should be formulated with food-grade, possibly all-natural, ingredients using solvent-free fabrication methods. In particular, one major challenge is to replace some of the polymers and surfactants used in the pharmaceutical industry with food-grade alternatives (Acosta, 2009).
- *Food incorporation:* the delivery system should be able to incorporate the bioactive compounds into the food matrices with high physicochemical stability and minimal impact on the organoleptic properties of the product (Donsi et al., 2011a).
- *Protection against degradation:* the delivery system should be able to protect the encapsulated bioactive compounds from the interaction with other food ingredients, as well as from degradation due to temperature, light, pH, during food manufacturing, storage, and preparation (McClements et al., 2007).
- *Uptake and bioavailability:* the delivery system should maximize the uptake of the encapsulated compounds upon consumption and their transport to the sites of action (Acosta, 2009). In addition, controlled release in response to specific environmental stimulus may be desirable (McClements et al., 2007).
- *Industrial scalability:* the fabrication of the delivery systems should be easily scalable to industrial production (Donsi et al., 2010a, Donsi et al., 2010d).

In the following, the nanometric size delivery systems most suitable for food applications, such as nanoemulsions and solid lipid nanoparticles, will be discussed.

I.2.1 Nanoemulsions

Nanoemulsions are heterogeneous systems consisting of two immiscible liquids, with one liquid phase being dispersed as nanometric droplets into another continuous liquid phase and stabilized through an appropriate emulsifier. In particular, O/W nanoemulsions, which are of prevalent interest

for food delivery systems, are composed of oil droplets dispersed in an aqueous medium and stabilized by a food-grade surfactant or biopolymeric layer, with mean droplet size typically ranging from 20 to 200 nm (Sagalowicz and Leser, 2010, Chen et al., 2011). The selection of emulsifier type is important to control the interfacial properties (charge, thickness, droplet size and rheology), as well as the response of nanometric oil droplets to environmental stresses (pH, ionic strength, temperature and enzyme activity).

Differently from microemulsions, which are thermodynamically stable systems and form spontaneously, nanoemulsions are kinetically stable and require energy to be formed. Due to their being metastable systems, nanoemulsions can be diluted with water without any change occurring in the droplet size distribution. Nanoemulsions are in fact highly stable to gravitational separation thanks to the small droplet sizes, which means that Brownian motion effects dominate over gravitational forces (McClements, 2005). In addition, nanoemulsions show a lower tendency to droplet aggregation than conventional emulsions, because the strength of the net attractive forces acting between droplets usually decreases with decreasing droplet diameters (McClements, 2005). However, coalescence phenomena due to Ostwald ripening can affect nanoemulsions stability, leading to a significant growth in droplet size over time. Ostwald ripening is a mechanism whereby the larger droplets grow at the expense of the smaller ones because of molecular diffusion of oil between droplets through the continuous phase. This process is driven by the Kelvin effect where the small lipid droplets have higher local oil solubility than the larger droplets, because of the difference in Laplace pressure (Wooster et al., 2008).

Therefore, being its rate dictated by the solubility of the oil in the continuous phase, Ostwald ripening can be kept at minimum by selecting oil with low aqueous phase solubility. More specifically, the aqueous phase solubility of oils decreases linearly with increasing oil molar volume: therefore, nanoemulsions based on low molar volume oils are more likely subjected to Ostwald ripening destabilization than nanoemulsions based on large molar volume oils consisting of long chain triglycerides. When formulation with an oil relatively soluble in the continuous phase cannot be avoided, such as in the case of essential oils nanoemulsions, Ostwald ripening can be reduced by adding a second oil with lower water solubility, in order to change the partitioning of the most soluble oil between lipid and aqueous phase (Sagalowicz and Leser, 2010).

The nanoencapsulation of bioactive compounds in O/W nanoemulsions is an effective approach for incorporating poorly water-soluble compounds in foods. The bioactive molecules, depending on the formulation used, in terms of ingredients and composition, as well as preparation procedures, might have different localizations within an O/W nanoemulsion. For example, the bioactive compound can be entrapped in the inner oil phase (bioactive-

enriched core) or can diffuse into the outer stabilizer film (bioactive-enriched shell), as shown in Figure I.1. Its localization influences the stability, release and the bioavailability of the nanoencapsulated compound.

The migration of the bioactive molecules from the inner oil phase to the stable surfactant layer of O/W nanoemulsions, as a consequence of more intense production conditions by high pressure homogenization (increasing number of passes and higher processing temperatures) is reported to increase the protection of bioactive molecules against chemical degradation (Baspinar et al., 2010). On the other side, the entrapment of the bioactive molecules in the emulsifier layer is likely to reduce the possibility of a controlled release mechanisms.

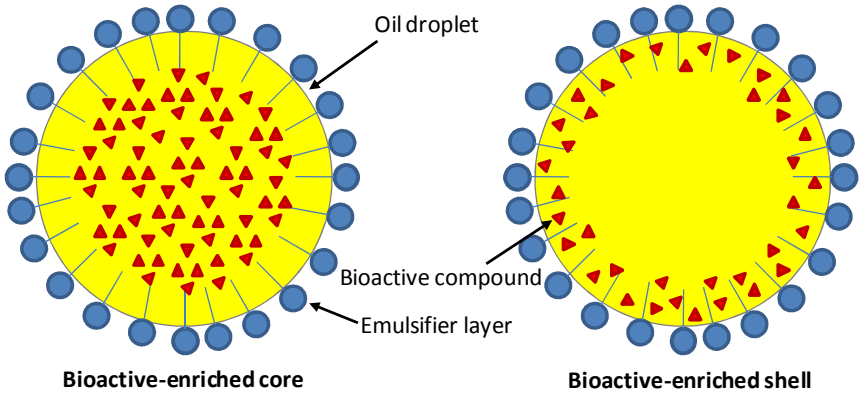

Figure I.1 *Possible localizations of bioactive molecules into O/W nanoemulsions.*

In general, the immobilization of bioactive compounds in the lipid matrix of the nanoemulsions, thanks to the nanometric size of the encapsulation system, can potentially contribute: (a) to improve the dispersibility of poorly water soluble compounds in aqueous solutions, minimizing the tendency to separate the different phases (aqueous and lipid); (b) to protect the bioactive compounds by interaction with food ingredients, keeping their functional properties and preventing the deterioration of the food itself (i.e., oxidation of fat); (c) to reduce the impact on the organoleptic properties of food; (d) to improve the absorption and bioavailability of the encapsulated bioactive compound, thanks to the subcellular size of the nanocapsules, which enhances passive transport mechanisms (related to the concentration gradient) across the cell membrane.

In Table I.1, some example of applications of nanoemulsions to the delivery of bioactive compounds are reported, with special emphasis on some of the above aspects.

For example, O/W nanoemulsions produced by high pressure homogenization technique were reported to improve the solubility in water of carotenoids, such as β-carotene (Yuan et al., 2008).

Alcohol-free O/W nanoemulsions, using hyaluronic acid as stabilizer, were developed for transdermal delivery of lipophilic active ingredients, such as α-tocopherol (Kong et al., 2011), demonstrating that, without any chemical enhancers, a good skin permeability can be achieved, with improved mass transfer through the stratum corneum and deep diffusion into the dermis.

Table I.1 *Examples of nanoemulsion-based delivery systems.*

Bioactives	**Formulation/ preparation**	**Application**	**Advantages**	**Ref.**
β-carotene	*Oil phase*: medium chain triglyceride oil *emulsifier*: Tween 20-80 *continuous phase*: water Emulsification via high pressure homogenization	Functional food preparation	Improved solubility of carotenoids into aqueous systems	(Yuan et al., 2008)
α-tocopherol	*Oil phase*: methylene chloride *emulsifier*: Tween 80 - Span 20 *continuous phase*: hyaluronic acid and glycerol monostearate solution Emulsification via solvent evaporation	Transdermal delivery vehicles for drugs and cosmetic applications	Enhanced permeability and diffusion into deeper dermis	(Kong et al., 2011)
Curcumin	*Oil phase*: medium chain triglycerols *emulsifier*: Tween 20 *continuous phase*: water Emulsification via high pressure homogenization	Oral administration	Enhancement and targeting of anti-inflammation activity	(Wang et al., 2008)

Nanoemulsions were also shown to enhance the beneficial effects of encapsulated bioactive compound when orally administered. For example, using a mouse ear inflammation model, anti-inflammation activity of curcumin was shown to be better targeted, when encapsulated in O/W nanoemulsions. In particular, the synergistic combination of two key features of the nanoemulsion-based delivery system, such as the nanometric droplet size and the presence of a lipid (medium chain triglycerides) in the emulsion formulation, enhanced both the transport through the intestinal walls and cell uptake, allowing the orally-administred curcumin to reach the target sites (the mouse ears) to explicate their full anti-inflammation activity (Wang et al., 2008).

Additional nanoemulsion applications involve sublingual and intranasal delivery of drugs, exploiting the mucoadhesive properties and the ability to enhance the permeability of the mucous layer through an adequate interfacial formulation (Kumar et al., 2008).

The deposition of a multiple layer of emulsifiers and/or polyelectrolytes around nanoemulsion oil droplets via layer-by-layer electrostatic deposition technique may positively affect the absorption properties in the gastrointestinal tract (McClements and Li, 2010).

Different types of primary stabilizers as well as biopolymers for subsequent layer-by-layer deposition were used in order to provide the right properties to emulsion droplets for successful applications, such as low molecular weight surfactants, proteins, polysaccharides.

I.2.2 Solid lipid nanoparticles

Solid lipid nanoparticles (SLNs) are similar to the nanoemulsions, consisting of emulsifier coated lipid droplets dispersed within an aqueous phase, with the main difference that the lipid phase is at the solid or semi-solid state.

In general, to produce loaded SLNs, a lipid phase, where the bioactive compounds have been dispersed, is emulsified in aqueous phase at about 10 °C above the melting point of the lipid, via common dispersing techniques, such as colloid milling, ultrasound, solvent evaporation and high pressure homogenization (HPH).

In particular, the HPH technique has emerged as the most reliable and powerful technique for the preparation of SLNs (Mehnert and Mader, 2001), with two approaches being mainly used: hot and cold homogenization. Hot homogenization is carried out at temperatures above the melting point of the lipids obtaining an hot O/W nanoemulsion, which is then rapidly cooled at room temperature to induce fat crystallization. In contrast, in cold homogenization a coarse dispersion of lipids at solid state is mechanically comminuted to the nanosize and subsequent dispersed in a aqueous solution in presence of a suitable emulsifier. With the cold homogenization method,

the thermal exposure of the encapsulated compounds is minimized, but larger particles and broader size distribution are obtained, in comparison to hot homogenization (Mehnert and Mader, 2001).

The main difficulty associated with the repeatability of the SLNs production is associated to the control of the lipid crystallization, which is significantly dependent on the temperature history of the system, on the presence of impurities in the lipid phase, as well as on droplet size (Sagalowicz and Leser, 2010).

In comparison to nanoemulsions, SLNs exhibit an increased chemical protection against degradation, a higher encapsulation efficiency (> 90%) and a better controlled release, due to the immobilization of the encapsulated bioactive compound in the solid lipid matrix. As schematically shown in Figure I.2, the bioactive compounds within solid lipid nanoparticles can be either dispersed in the interstices of the fat crystals (bioactive-enriched core), or on the surface of the lipid nanoparticle protected by the emulsifier layer (bioactive-enriched shell) (Fathi et al., 2011).

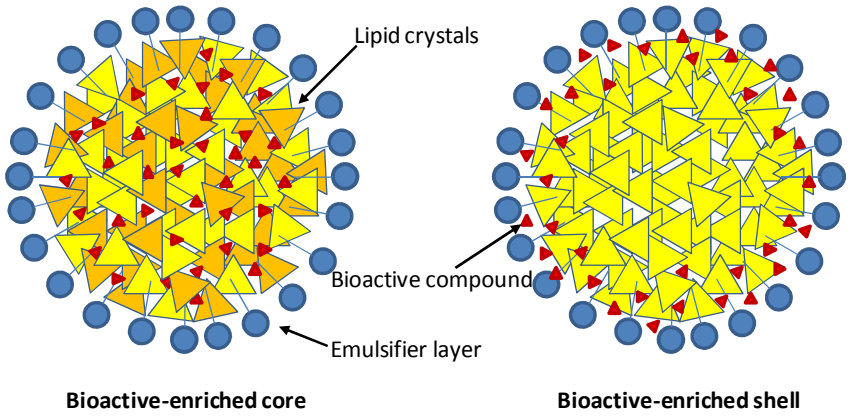

Figure I.2 *Possible localizations of a bioactive molecules into SLNs.*

Whether a bioactive enriched core or a bioactive enriched shell is formed depends on the solid lipid phase. A lipid phase consisting of fats of different types and with different properties as well as crystallization kinetics, will exhibit an inner core characterized by voids and defects of the crystalline structure, where the bioactive molecules can be preferentially hosted. In contrast, a lipid phase with a more ordered crystalline structure, for example consisting of a single type of fats, will offer less space for the bioactive molecules. In this case, during crystallization upon lipid cooling, the bioactive compounds are phase separated, either enriching the emulsifier shell or being expelled into the aqueous phase.

SLNs with a bioactive-enriched core are able to keep the encapsulated bioactive compounds away from any hydrophilic reactive species dispersed

in the aqueous phase, as well as to promote a sustained release of the encapsulated active material upon oral administration (Muller et al., 2002).

On the other side, SLNs with a bioactive-enriched shell are more indicated to provide a delayed release of the bioactive compounds.

Typically, two or more lipids with different melting points, e.g., mixtures of purified triglycerides, waxes or fatty acids, are used rather than an individual lipid to increase the loading capacity and retention of encapsulated lipophilic components, which can fit better into the more imperfect crystalline structure formed (Schubert and Muller-Goymann, 2005).

Further development of the SLNs brought to the so-called nanostructure lipid carriers, consisting of a disperse phase made of a mix of solid and liquid lipids (Muller et al., 2002). The nanostructure lipid carriers, due to the decreased melting point of the lipid phase, can be produced at lower temperatures, reducing the extent of degradation of the thermolabile compounds. Moreover, they are also claimed to have smaller particle sizes than SLNs, as well as to exhibit a sustained release mechanism in the gastrointestinal tract (Zhuang et al., 2010).

Table I.2 shows some examples of SLN-based delivery systems for applications in different fields, such as food, pharmaceutics and cosmetics.

Table I.2 *Examples of solid lipid nanoparticles-based delivery systems.*

Bioactives	**Formulation/ preparation**	**Application**	**Advantages**	**Ref.**
D-limonene	Palm oil soy lecithin hot HPH	Solubilization and dispersion in foods	Increased antimicrobial activity	(Donsi et al., 2010c)
Curcumin	Hydrogenated soya phosphatidylcholine, distearoyl phosphatidyl ethanolamine, cholesterol and triolein hot HPH	Pharmaceutical application against breast cancer	Increased cellular uptake and cytotoxicity.	(Mulik et al., 2010)
Vitamin A	Glyceryl behenate	Transdermal delivery	Increased skin permeation and release rate in comparison to nanoemulsions	(Jenning et al., 2000)

SLNs formulated with palm oil and soy lecithin were successfully used to increase the dispersibility and antimicrobial activity of essential oils, as well as to incorporate them into fruit juices, with minimal impact on the organoleptic properties of the product (Donsi et al., 2010c).

However, SLNs are underused for food applications, because they require the formulation with solid lipids, such as saturated ones, which are not preferred in terms of nutrition and health (Sagalowicz and Leser, 2010).

For pharmaceutical applications, SLNs are intensively studied in the field of controlled drug release.

The therapeutic efficacy of curcumin encapsulated in transferring conjugated solid lipid nanoparticles was tested against breast cancer, with the results that the cellular uptake was increased and the sustained release of the encapsulated curcumin was favored (Mulik et al., 2010).

In addition, SLNs were also used to control the penetration of several bioactive compounds into the skin, making them attractive for cosmetic applications and topical delivery. For example, skin permeation and release rate of vitamin A was increased when encapsulated into SLNs instead of nanoemulsions (Jenning et al., 2000).

I.3 Production of nanometric delivery systems

Nanometric size delivery systems can be produced by a top-down approach, by mechanical comminution of larger entities into homogeneously sized particles with desired functional properties (i.e. nanoemulsions and solid lipid nanoparticles), by bottom-up approach, assembling the molecular building blocks into structured systems (i.e. micelles, microemulsions, some biopolymeric nanoparticles), as well as by a mixed approach, where molecular assembly and nanonization are combined together (i.e. liposomes, cubosomes, hexosomes, some biopolymeric nanoparticles, multilayer emulsions).

The bottom-up approach is based on self-assembling of molecules into nanometric structured systems exhibiting functional properties, in a process driven by the balance of attraction and repulsion forces tending to thermodynamic equilibrium.

The forces between the building blocks can be controlled by environmental factors, such as temperature, concentration, pH and ionic strength of the system, as well as applying external stimuli, such as pressure, shear or electric and magnetic fields (Sanguansri and Augustin, 2006), with the input of mechanical energy being limited to keep the system perfectly mixed (Acosta, 2009).

Since the nanostructures formed through bottom-up approach exist at the thermodynamic equilibrium, any environmental modification would bring to nanostructures disassembly, therefore limiting their use and incorporation in real food systems, which involves mixing with other ingredients and

thermal, pressure or shear stresses during product manufacturing. As a consequence, a stabilization step is required, to freeze the self-assembled nanostructures in the desired size and functional state. Such stabilization step can be conducted through physical or chemical changes, such as rapid quench cooling, sudden solvent dilution or evaporation, as well as chemical reactions, which are required to be more rapid than the system kinetics of attaining a novel equilibrium state.

In the fabrication of nanostructured delivery systems via bottom-up approaches, the poorly water-soluble bioactive compound is first dissolved or dispersed in an organic solvent, and then precipitated through a non-solvent addition, which is typically water for food applications, in the presence of stabilizers, such as surfactants or hydrocolloids (Acosta, 2009, Gao et al., 2011). Eventually, a polymer, which is soluble in the internal solvent but insoluble in the external one, may be added to the system (Acosta, 2009).

The precipitation of the bioactive compound in nanoparticles may be induced by rapid solvent diffusion into the aqueous phase, such as in supercritical fluid technology, by evaporative precipitation into aqueous solution, spray-freezing into liquid process, and emulsion-solvent evaporation.

On the other side, the top-down approaches for the production of nanometric particulate systems are mainly based on comminution by mechanical size reduction techniques without using chemical solvents.

Figure I.3 reports a schematization of the different types of particle stressing exerted in comminution processes.

At macroscopic level, comminution can be carried out by stressing the particles to be disrupted between two surfaces through the combination of compression and shear, in systems such as roller mills and media mills. Obviously in this case the minimum achievable particle size depends on the coupling of the mill surfaces that exert the stress, and, in general, it is > 1 mm.

In order to obtain finer particles, comminution should be based on more focused particle stressing. For example, in impact mills the particles are accelerated towards a surface where they impact, with the stress intensity depending on the kinetic energy of the particles.

An even more focused particle or droplet stressing is based on the transmission of the stress to the particles through a surrounding fluid, where intense fluid mechanical stresses occur. The energy is transferred from the sheared, elongated, or turbulent fluid to the particles, with a stress intensity significantly smaller than in the case of contact with solid surface, but of significantly higher efficiency.

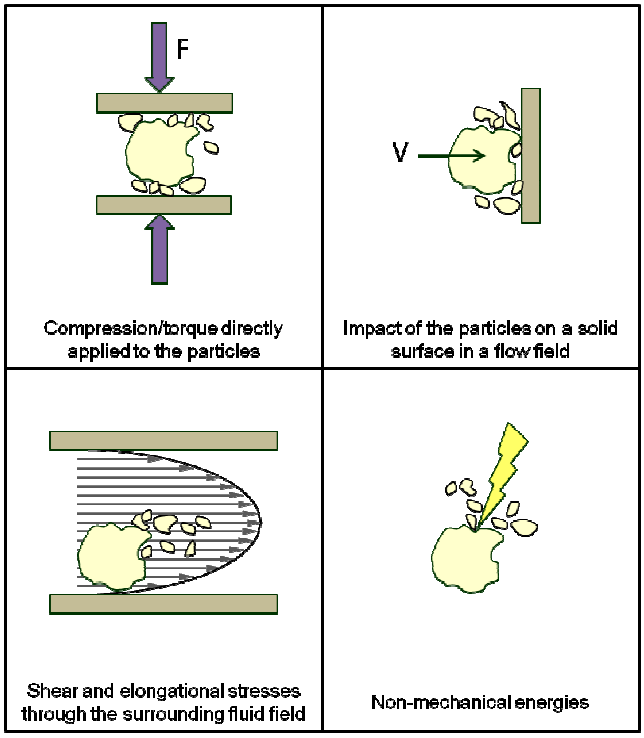

Figure I.3 *Particle stressing in comminution processes.*

In particular, the most used systems for nanonization processes in the food and nutraceutical industry, colloid or media milling and high pressure homogenization, are based mainly on stress transmission through a surrounding fluid, eventually in combination with the impact on solid surfaces.

Particle stressing through non-mechanical energies, such as electrical or thermal, at the moment do not represent viable systems for the production of nanometric particles and droplets.

Comminution processes are very energy-intensive, with the required energy exponentially increasing at decreasing the particle size. In fact, as the particle size decreases, the number of defects that allow crack propagation and particle disruption is reduced and the intermolecular forces significantly increase.

On the other side, mechanical nanonization processes require minimal use of chemical additives in the formulation of nanometric systems, which represents the main advantage over chemical comminution processes (Acosta, 2009).

Current challenges to the nanonization processes are the efficient use of shear or particle collision to break down larger entities in fine nanoscale

aggregates with minimal energy consumption, while preventing re-aggregation and segregation of small and large particles (Acosta, 2009). At the same time, the issues of industrial scalability and cost-effectiveness attract increasing interest, in view of the transfer of the technology to the market.

I.3.1 High pressure homogenization

High pressure homogenization (HPH) is the most suitable currently available technique for the production of uniformly nanosized emulsions, suspensions and dispersions, when evaluated in terms of ease of operation, industrial scalability, reproducibility and high throughput (Schultz et al., 2004).

The high pressure homogenization process can be described as the production of a homogeneous size distribution of particles or droplets suspended in a liquid, by forcing the liquid under the effect of high pressure through a specifically designed disruption chamber.

A typical HPH system consists therefore of a high-pressure generator, a disruption or homogenization chamber, as well as a temperature control system, as shown in the simplified schematics of Figure I.4. From the feed tank, the process liquid is pressurized in a set of pressure intensifiers, such as positive-displacement pumps coupled with piston-cylinder pressure intensifiers, whose phase-delayed movement guarantees an almost uniform flow at the desired pressure level.

HPH working pressures are in the range of 100-300 MPa, with higher operating pressures requiring an increase in equipment costs, which is not balanced by a significant gain in size reduction of the processed emulsions and suspensions.

The homogenization chamber, where the emulsion droplets are disrupted into finer droplets due to the fluid-mechanical stresses generated by the sudden pressure drop, can be realized in different geometries, ranging from a simple orifice plate to colliding jets and radial diffuser assemblies (Schultz et al., 2004). In Figure I.4, some examples of valve geometries are also given.

The simplest valve geometry is represented by an orifice plate of appropriate size to generate the desired pressure level at the process flow rate. Because of their simplicity, orifice valves are widely used in hands-on experimental systems (Brosel and Schubert, 2000) as well as in commercial units (Bee International, Inc., USA).

In the flat-bead valve assembly (Figure I.4-V1), typical of Manton–Gaulin APV (USA), Emulsiflex Avestin (Canada) and GEA Niro Soavi (Italy) commercial models, the process fluid is radially and outwardly dispersed through a narrow gap between the valve piston and seat, with the resulting jet impinging on an impact ring. The flat-bead valve assembly is widely used in the preparation of nanosuspensions (Donsi et al., 2010d,

Moschwitzer et al., 2004), nanoemulsions (Donsi et al., 2010c) and solid-lipid nanoparticles (Souto et al., 2005).

Another valve assembly, which is a hybrid between a radial diffuser and a colliding jet assembly, is sketched in Figure I.4-V2. In such homogenization valve, equipping commercial models of Stansted Fluid Power Ltd (UK), the radial jet originating around the pressurized valve piston, converges to the inner core of the valve, where reciprocally colliding jet fringes contribute to increase the fluid dynamic stresses on the fluid. This geometry resulted more efficient in cell disruption (Donsi et al., 2009) than in nanoemulsion formation (Donsi et al., 2011c).

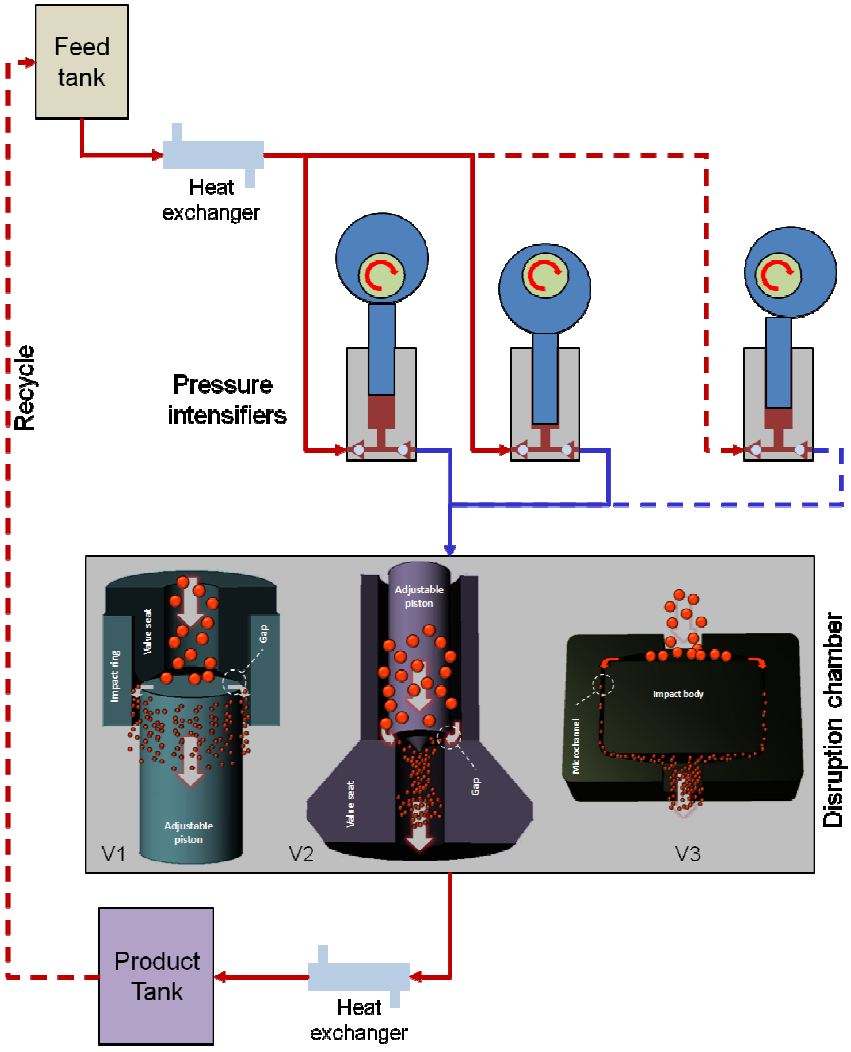

Figure I.4 *Schematics of a high pressure homogenization system.*

The colliding jet assembly shown in Figure I.4-V3 shows the simplified schematics of the interaction chambers of Microfluidizer (Microfluidics Corp., USA) systems. The pressurized process fluid is divided into two microchannels and then recombined in a reacting chamber where the liquid jets collide, dissipating the energy input almost instantaneously at the point of impact. As the reaction chamber of the microfluidizer is static and contains no moving parts, a high level of reproducibility is ensured in nanoemulsion preparation (Paquin, 1999). On the other side, processing of dispersions and suspensions is limited by the impossibilities of unclogging by varying the gap opening (i.e. by moving the valve piston).

An efficient heat exchanging system is required immediately downstream of the homogenization chamber to cool down the process fluid, whose temperature is increased proportionally to the pressure drop due to frictional heating (0.15-0.20 °C/MPa), in order to prevent the degradation of thermolabile compounds. In addition, temperature control of the process fluid upstream of the pressurization stage may be needed when multiple HPH passes are performed to reach the desired particle or droplet size distribution, as well as in the production of solid lipid nanoparticles, when the temperature should be consistently maintained above the melting temperature of the lipids to avoid their uncontrolled crystallization in the system and consequent clogging.

Droplet or particle break-up occurs in the homogenization chamber thanks to droplet deformation, induced by the fluid-dynamic stresses arising from the combination of turbulence, elongational and shear stress, as well as cavitation within the homogenization chamber.

In standard homogenization chambers, such as radial diffusers or Microfluidizer chambers, the inertial forces in the turbulent flow determined by the valve geometry are mainly responsible for droplet disruption, together with cavitation induced by pressure and velocity fluctuations (Shirgaonkar et al., 1998). In contrast, in orifice valves, where a laminar flow region is established due to the small size of the orifice gap (in some cases as low as 100 μm), break-up can be ascribed to shear forces in elongational flow, as well as to the perturbation occurring in the region following the elongational flow.

The severity of the HPH process and hence the intensity of the fluid-mechanical stresses can be regulated by controlling the operating pressure, the number of passes through the disruption valve, the inlet temperature, as well as the homogenizer valve design, while the scale of operation does not appear to influence the extent of particle break-up, as shown in the case of microorganism cells (Donsi et al., 2009).

In general, the flow regime established in the HPH valve and downstream controls the extent of mechanical disruption of suspended particles and microbial cells with break-up occurring when the fluid-dynamic stresses exceed the particle or cell wall resistance.

In contrast, the emulsification process by HPH consists of two phenomena: the deformation and disruption of the droplets and the consequent droplet stabilization due to the adsorption of the emulsifier molecules at the newly formed O/W interfaces (Brosel and Schubert, 2000). Consequently, product properties and, in particular, the rate of adsorption of emulsifier at the newly formed interfaces contribute to control the size distribution of the nanoemulsion droplets.

Especially in the case of food applications, where the product formulation poses severe limits to the amount and type of emulsifiers to be used, recoalescence phenomena can be problematic. As a consequence, the advantage of a high-pressure homogenization chamber in comparison with another is not the more efficient droplet break-up, but rather droplet stabilization against coalescence after disruption (Schultz et al., 2004).

In the comminution of solid particles into nanoparticles, high pressure homogenization results in lower polydispersity than media milling, which instead require a stage of removal of microparticles and of the residues of abrasion of the used beads or balls.

High pressure homogenization can therefore be considered a highly-recommended technique to reduce particle size efficiently with high reproducibility and to process highly concentrated systems. It can be widely applied to create stable nanoemulsions, as well as dispersions of solid nanoparticles. Moreover, HPH technique enjoys various advantages such as simplicity, high efficiency and needlessness of organic solvents.

I.4 Protection of bioactive compounds by nanoencapsulation

The protection of bioactive compounds against degradation and interaction with food ingredients occurs through the encapsulation in nanometric delivery systems. For this reason an efficient nanodelivery system must be stable in the food matrices over long periods of time. However, some of the conditions that a nanoemulsion encounters during processing (e.g. heating, high-shear mixing) are not conducive to stability. Therefore it is necessary to understand, and ideally to eliminate, the sources of instability in such nanometric delivery systems.

A nanoemulsion may become unstable due to different types of physical and chemical processes. Physical instability, such as creaming, flocculation, coalescence, phase inversion, results in an alteration of the spatial distribution or structural organization of the molecules, whereas chemical instability, such as oxidation and hydrolysis, results in the alteration of the type of molecules present.

Instability during nanoemulsion formation occurs if there is insufficient surfactant to cover the entire oil-water interface created by the homogenizer.

The surfactant has an important role to prevent immediate aggregation or coalescence and its properties largely determine the behaviour of the nanoemulsion.

Sufficiently large droplets suspended in aqueous medium of low viscosity or yield stress will cream. The creaming rate depends on the square of the droplet diameter, emphasizing the need for efficient homogenization.

Creaming itself does not destabilize an emulsion, but the high concentration of oil droplets in the creamed layer promotes interactions that lead to flocculation, aggregation or coalescence. For two droplets to coalescence, they must first approach to close proximity, then the film of water separating them must drain, and finally the resultant Newton black film must rupture and allow the two droplets' contents to flow together (McClements, 2005). In many cases the repulsive forces between droplets is sufficient to limit droplet approach and film drainage while in other cases the mechanical strength of the film can resist rupture. Coarse emulsions are prone to coalescence as the lower internal pressure allows significant deformation of large droplets to form a polyhedral structure separated by large planar films vulnerable to rupture. On the other hand, fine emulsions act as hard spheres and to overcome the disjoining pressure and to force droplets into close proximity separated by a Newton black film an external pressure must be applied.

Flocculation and aggregation of the oil droplets in an emulsion arise from the inability of the adsorbed surfactant layer to prevent the close approach of the droplets. Although the two terms are almost synonymous, flocculation is generally regarded as being weaker than aggregation, because even in the combined state the particles are further away from one another; flocculation is therefore more readily reversed, at least temporarily, by shaking or stirring. The particles tend to aggregate because of attractive inter-atomic forces, but aggregation is opposed by repulsive charge interactions, which arise from adsorbed emulsifier.

Figure I.5 summarises the mechanisms of physical instability of emulsions highlighting that creaming and flocculation can often readily be reversed by gentle agitation, while coalescence is a irreversible phenomenon.

The research has historically focused mainly on the physical aspects of emulsion stability in foods. Nevertheless, there are many types of chemical reactions that can have adverse effects on the quality of food emulsions: for example, lipid oxidation, hydrolysis, flavor or color degradation, bioactive degradation due to a chemical interaction of nutraceutical compound with food components.

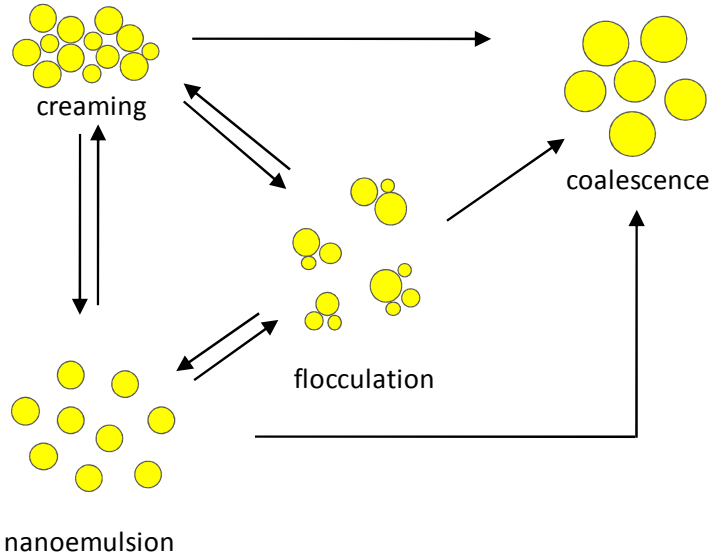

Figure I.5 *Mechanisms of physical instability in nanoemulsions.*

Djordjevic et al. have studied the chemical and physical stability of O/W emulsions containing limonene, an important flavor component of citrus oils (Djordjevic et al., 2008). Since limonene is lipid soluble, it is often added to foods as an oil-in-water emulsion. However, o/w emulsions containing limonene are susceptible to both physical instability and oxidative degradation, leading to loss of aroma and formation of off-flavors. They showed that whey protein isolate could protect limonene in O/W°emulsion droplets more effectively than gum Arabic. The ability of whey protein isolate to decrease the oxidative deterioration of limonene could be due to the formation of a cationic emulsion droplet interface, which can repel prooxidative metals. Yuan et al. have investigated the influence of emulsifier type and concentration, homogenization pressure, temperature and number of cycles on the properties and stability of O/W nanoemulsions of β–carotene (Yuan et al., 2008). They showed that the physical stability of the nanoemulsions decreased with an increase of temperature but increased with pressure and homogenization cycles.

I.5 Increase of bioavailability of nanoencapsulated bioactives

Many bioactive compounds are poorly absorbed and quickly metabolized once they have been ingested and, therefore, they are prevented from reaching the target organs in active form. Nanometric size delivery systems can contribute to increase the bioavailability of bioactive compounds through their protection during the digestive processes, as well as their

improved uptake in the gastrointestinal tract and enhanced transport to the target sites.

First of all, "bioavailability" and "uptake" should be clearly distinguished, because they are often inappropriately used interchangeably. The term bioavailability indentifies the fraction of an ingested component that enters in the bloodstream (Holst and Williamson, 2008). On the other hand, the uptake defines the fraction of ingested component that is absorbed through the intestinal walls. Although these two phenomena can be related, a nutraceutical compound absorbed through the intestine may not be bioavailable, due to the complexity of the biological mechanisms involved in the digestion of nutrients (Acosta, 2009).

The first stage of digestion occurs in the mouth once the ingested food is mixed with saliva and broken down in smaller pieces by mastication.

Subsequently, the food is subjected in the stomach to a complex series of physical and chemical changes: it is exposed to a highly acidic environment (pH 1-3), then to enzyme hydrolysis (e.g., pepsin) and to a complex stress profile due to the various contractions of the stomach. Therefore, the resistance of the nanometric delivery system to the environment gastric digestion may be an important requisite, if the encapsulated bioactive compound is chemically unstable at acidic pH. Moreover, through the creation of physical barriers (i.e., coating a lipid droplet with multilayer emulsifiers or encapsulating droplets within a hydrogel) between the encapsulated compound and the surrounding aqueous phase, where the digestive enzymes are normally located, it is possible to control the enzyme accessibility to their specific substrates within the delivery systems (Mun et al., 2006).

As the digested food leaves the stomach and enters in the small intestine, it is mixed with the digestive juices containing the bile salts, which emulsify the lipids and hydrophobic compounds present and transport them to the enterocyte cells, where they are absorbed, as sketched in Figure I.6.

The absorption of bioactive compounds through the intestinal walls occurs by two main mechanisms, based on active and passive transport, respectively. Active transport is the movement of the active ingredient against its concentration gradient, due to specific channels on the surface of the epithelial cells. The cells use their own energy, such as adenosine triphosphate (ATP), to capture the active compounds. Passive transport is instead regulated by a simple diffusion across the epithelial membrane, which occurs along the concentration gradient.

The ability to control the particle size of the encapsulation system is of primary importance for increasing the adsorption of encapsulated components, improving the passive transport through the intestinal walls thanks to the subcellular size of the nanoparticles. Moreover, particle size and surface moieties can control the retention time in the gastrointestinal tract, either favoring the particles entrapment in the mucous layer, or

promoting their direct uptake, as schematically shown in Figure I.6 (Hussain et al., 2001). In particular, several works on the determination of the correlation between uptake/bioavailability and particle size of the delivery system, clearly showed that when reducing the particle size below 500 nm higher nanoparticles uptake and higher absorption of the encapsulated active compound can be achieved (Acosta, 2009).

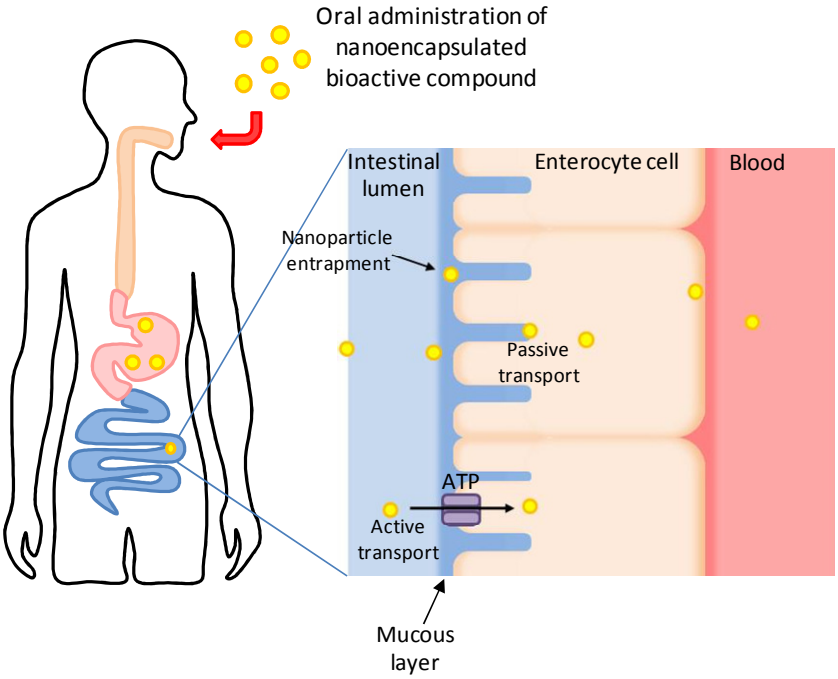

Figure I.6 *Schematic mechanism of uptake and bioavailability of nanoencapsulated bioactive compound.*

The delivery systems of nanometric scale provide a larger surface area for interaction with the biological substrates than the corresponding micrometric size carriers. Moreover, an efficient design of the interfacial properties of the nanocapsules can improve the controlled release of the encapsulated compound to its target site, while avoiding any undesired instantaneous release (Mozafari et al., 2008). Two mechanisms of controlled release are possible, as shown in Figure I.7: delayed release, with the bioactive compound being released after a certain lag time, and sustained release, with concentration of the bioactive compound being maintained constant over a prolonged release time (Fathi et al., 2011). In particular, delayed release is used for achieving the protection of nutrients during gastric digestion and the release in the intestinal tract. On the other hand, sustained release can be

employed for extending the release time of certain drugs, such as insulin, reducing the frequency of administration.

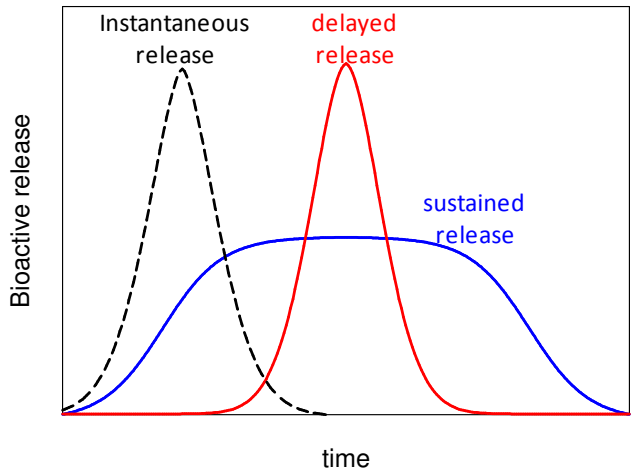

Figure I.7 *Mechanisms of release of bioactive compounds.*

Different factors, such as ingredients, shape and dimensions of carrier, may influence the release of the encapsulated material. For example, McClements and coworkers have critically analyzed different delivery systems, such as nanoemulsions, multilayer emulsions, solid lipid nanoparticles and filled hydrogel particles, in terms of potential control of the digestion and release of bioactive lipophilic components within the gastro intestinal tract (McClements and Li, 2010).

Another important aspect to take into account in the design and formulation of efficient delivery systems, is that lipid-based systems can improve the bioavailability of many poorly soluble bioactive compounds, being the absorption path of the bioactive ingredients affected by the co-administration of fats (Porter et al., 2008). In contrast, although most orally administered compounds gain access to the systemic circulation via the portal vein, some highly lipophilic compounds are transported directly to the systemic circulation via the intestinal lymphatics, therefore requiring a different forlumation to improve their bioavailability.

In summary, the ability to maintain the particle size of the delivery systems into the nanometric range is of primary importance not only for increasing the dispersibility of poorly soluble bioactive compounds in food matrices, as well as for preserving the organoleptic properties of the product, e.g., taste, aroma, texture, and appearance, but also for controlling the release of the encapsulated compounds, improving their absorption into the body, and hence for ensuring the overall efficacy of the delivery systems.

Chapter II
Scope of the work

II.1 Objectives

In recent years there was an intensive research focusing on the encapsulation of bioactive compounds in the pharmaceutical field, but just a few researches were specific to the food field. More specifically, no systematic study was conducted in terms of development, design and production of nanodelivery systems and of the interaction of nanoencapsulated bioactive compounds with food. Based on these considerations, the general objective of this thesis is **the rational design of efficient nanometric delivery systems, above all nanoemulsions and solid lipid nanoparticles, made of natural food ingredients, to incorporate bioactive compounds**.

To achieve this goal the following specific objectives have been set:

- Design of efficient formulations, in terms of lower emulsifier content, to improve the solubility of bioactive compounds, scarcely soluble in water and in aqueous systems, such as food matrices.
- Improve the scalability of food-grade nanodelivery systems production through a deep understanding of high pressure homogenization process and a specific investigation of the interface interactions and the forces that regulate the formation and the thermodynamic and kinetics stabilization of a nanoemulsion.
- Increase the physicochemical stability of nanoencapsulated bioactive compounds that can be easily degraded from environmental conditions.
- Improve the bioavailability of functional ingredients, so that they can arrive in their most active form to the target sites, without being rapidly metabolized.

- Promote the incorporation in real foods, by an improved understanding of the interactions of nanoencapsulated bioactive compounds with food ingredients, as well as of the effect on the nutritional and organoleptic properties of their implementation in food matrices.

The research activity will pursue the above objectives, specifically focusing on the encapsulation in food nanoemulsions of model bioactive compounds: polyphenols, such as resveratrol and curcumin, for the crescent interest on their beneficial effects on human health, especially an high antioxidant activity, and essential oils, in order to retain and possibly enhance the antimicrobial activity.

II.2 Working plan

The research was organized taking into account all the aspects related to the design and engineering of a delivery system for the nanoencapsulation of bioactive compounds, which are able to protect them against degradation and increase their bioavailability. In particular, to achieve the stated objectives, the research activity has been divided into the following steps, as shown schematically in Figure II.1:

- *Formulation procedures for high solubility:* Definition of the criteria for the choice of a suitable formulation to increase the solubility of bioactive compounds in an aqueous system by means of the construction of the pseudo ternary phase diagram, which allows to evaluate, based on the composition of the emulsifiers and the lipid phase, the physically stable formulations. Curcumin, a polyphenolic compound which is insoluble in water and poor soluble in oil, will be chosen as model compound.
- *Investigation of HPH process parameters:* The mechanisms of production of food nanoemulsions by high pressure homogenization (HPH) will be investigated, focusing on the effect on droplet nanonization of emulsifier type and concentration, as well as of the geometry of the homogenization chamber. Moreover, several food-grade emulsifiers will be characterized, in comparison with artificial ones, in terms of their interfacial and dynamic properties, by pendant drop measurements.
- *Physical and chemical stability:* Investigation of the physicochemical stability of encapsulated bioactive compounds into nanoemulsion-based delivery systems under accelerated ageing conditions (high temperature, UV light exposition and low/high pH).
- *Bioavailability of encapsulated compounds:* Studying of the efficiency of nanometric delivery systems to increase the

bioavailability of bioactive compounds, using *in vitro* and *ex vivo* assays. In particular, the stability of the encapsulated compound during the digestion process will be evaluated, simulating *in vitro* gastric and intestinal digestion. The transport through the intestinal wall will be simulated, observing the transport through Caco-2 cell monolayers grown on permeable supports. The release profile of the bioactive compound from the nanocapsules will be performed by a dialysis bag method. For these experiments, resveratrol, having a very low bioavailability and a rapid metabolism, will be used as model. Furthermore, the effect of nanometric delivery systems on the antioxidant activity of the encapsulated compounds will be evaluated using a chemical and a biological-based approach.

- *Antimicrobial activity:* Evaluation of the effect of the delivery systems on the antimicrobial activity of essential oils, such as a terpene mixture and D-limonene, encapsulated into food-grade nanoemulsions. The analysis will be performed by determining the minimum inhibitory concentration (MIC) and minimum bactericidal concentration (MBC) for three different classes of microorganisms (*Lactobacillus delbrueckii, Saccharomyces cerevisiae, Escherichia coli*).
- *Incorporation in real foods:* The alteration of the organoleptic properties of fruit juices after the incorporation of nanoencapsulated antimicrobials will be investigated.

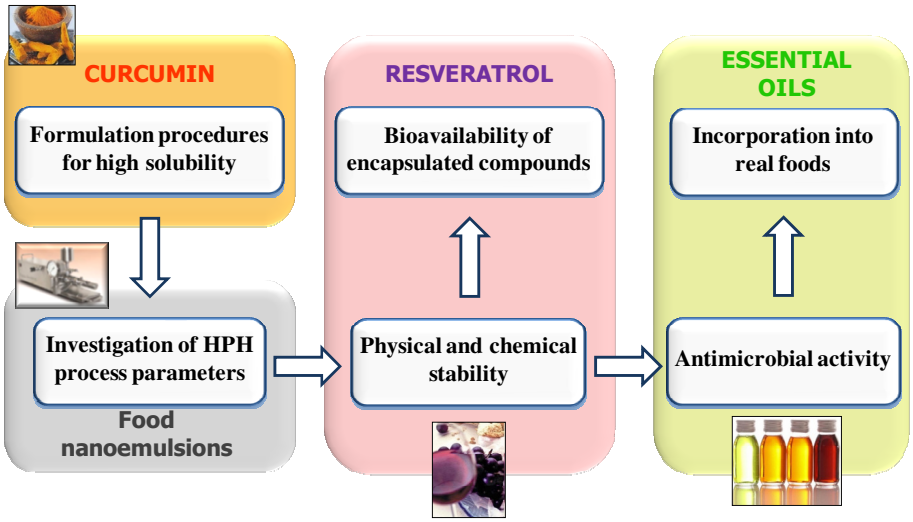

Figure II.1 *Sketch of the research activities related to the nanoencapsulation of bioactive compounds.*

Chapter III
Formulation procedures for high solubility

This chapter explains the procedures used for the formulation of the delivery systems to be used for increasing the dispersability in aqueous systems of bioactive compounds, which are poorly soluble in water (i.e. curcumin). The approach adopted is based on the investigation of stability/instability regions of oil in water emulsion systems encapsulating curcumin at varying composition of the food nanoemulsions, in terms of content of emulsifiers and lipid phase, and the consequent construction of the corresponding pseudo-ternary phase diagrams.

III.1 Introduction

In the field of nutraceuticals and functional foods, there is a growing interest in exploiting the nanoemulsions to solve the problems of solubility and stability of nutraceuticals and food additives in aqueous solution.

For example, curcumin, because of its polyphenolic structure, is not only water insoluble, but also scarcely dissolved by organic phases, thus requiring the encapsulation in suitable delivery systems to increase its solubility in aqueous systems, such as food matrices, and improve its bioavailability, which is solubility-limited.

Knowledge of the equilibrium phase behaviour of emulsion systems, such as oil/water/emulsifier(s), has proven to be an interesting tool to study the emulsification process in terms of drop size and stability. However, the majority of the concepts developed to predict emulsion properties are focused on emulsifier's characteristics. More specifically, the affinity of an emulsifier for oil or water depends on formulation parameters, which are taken into account through a concept called hydrophilic–lipophilic deviation

(HLD) (Salager, 1988). This number can be positive or negative, indicating the emulsifier's affinity for oil or water phase respectively.

When HLD is coupled with the composition (volume fraction of water in oil/water system), a two dimensional map is constructed called formulation–composition map. On this 2D map the boundary which separates the morphology of one type of emulsion from another normally forms a stair-like structure. A typical example of formulation–composition map of an emulsion system is shown in Figure III.1. The vertical line below and above the HLD = 0 is known as catastrophic inversion line, while the horizontal line (HLD = 0) is known as transitional inversion line. The knowledge of catastrophic inversion line appears in dynamic condition, i.e. during emulsion production, but transitional inversion line is the result of phase behavior of oil/water/emulsifier system at equilibrium (Salager, 1988). This map is advantageous for formulation protocol of an emulsion to get the desired properties in a predictive and more controlled way.

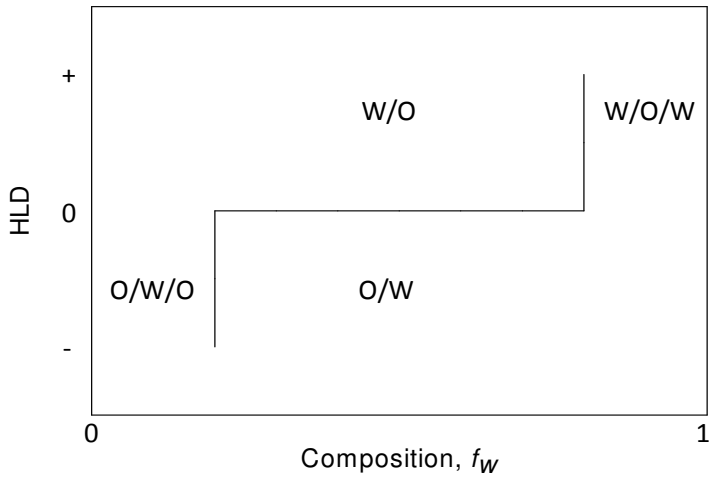

Figure III.1 *A generalized formulation–composition map on two-dimensional plot (Salager, 1988).*

In food emulsion systems, such map is rare due to the complexities associated with (i) emulsifiers (i.e. phospholipids or proteins) and (ii) oil phase (mostly triglycerides). In particular, the phase behavior at equilibrium of even a simple food emulsion system is not easy to observe (Thakur et al., 2007).

For this reason, the region or composition of food nanoemulsions is usually defined or identified by constructing ternary-phase diagrams.

Ternary diagrams are employed to depict mixtures of three components. With the help of these diagrams, every state of the three-phase system for a specific temperature and specific pressure can be described. In case of nanoemulsion development, the diagrams are called pseudo-ternary phase diagrams, since a nanoemulsion is a complex system of oil, water and emulsifiers (surfactant and cosurfactant) and between these phases there is no thermodynamic equilibrium, but kinetic stabilization. Surfactant and cosurfactant is prepared in defined mixtures and is presented on one axis in the ternary phase diagram.

III.2 Material and methods

III.2.1 Materials

Curcumin (85% pure, with 11% demethoxycurcumin and 4% bisdemethoxycurcumin as impurities) was obtained from Sabinsa Corporation (Piscataway, NJ) and used without further purification.

Primary emulsion formulation was based on stearic acid (Sigma-Aldrich s.r.l., Milan, Italy), palm oil (Fluka, Germany) or hydrogenated palm oil (a kind gift from Prodotti Gianni, Milan, Italy) as organic phase, and the combination of lipophilic and hydrophilic emulsifiers. Lipophilic emulsifiers were soy lecithin Solec IP (a kind gift from Solae Italia s.r.l., Milan, Italy) and glycerol monooleate (Sigma-Aldrich s.r.l., Milan, Italy). Hydrophilic compounds were sugar ester P1670 (a kind gift from Prodotti Gianni, Milan, Italy) and defatted soy lecithin Solec FS-B (a kind gift from Solae Italia s.r.l., Milan, Italy). Bidistilled water was used as continuous phase.

III.2.2 Screening of Emulsion Formulations

The pseudo-ternary phase diagram of curcumin encapsulated into O/W emulsion system, using a lipophilic and hydrophilic emulsifier mole ratio of 1:0.5, was constructed in order to identify stable formulations .

The emulsions were prepared by mixing the separately prepared aqueous and oil phases. Curcumin (0.1 wt%) was first dissolved in the oil and mixed with the lipophilic emulsifier at a temperature above the lipid melting point (75 °C for stearic acid and 50 °C for palm oil). The aqueous phase containing the hydrophilic emulsifier was heated up to 75 °C under slight mixing. Nine different samples were initially prepared by mixing the aqueous phase with the lipid phase in different proportions (from 1:9 to 9:1).

After high speed homogenization (HSH) using an *Ultra Turrax T25* blender (IKA Labortechnik, *Jahnke und Kunkel, Germany*) at 24000 rpm for 4 min at a temperature above the lipid melting point to obtain a primary emulsion, part of the sample was collected in a tube for stability investigation, while the other part was serially diluted in water and treated

again by HSH to generate the other points of the phase diagram, which were all sampled and stored at room temperature. After 24 h from preparation the state of the emulsified systems was visually evaluated and classified in physically unstable or stable systems.

Samples which resulted fluid enough to be sucked and pumped by the intensifier of the Nano DeBEE system, were further treated by HPH.

III.3 Construction of a pseudo-ternary phase diagram for the evaluation of stable formulations

The emulsion-based nanometric delivery systems are produced in two step: the formation of the primary emulsions prepared by high speed homogenization (HSH), followed by high pressure homogenization (HPH) for the formation of the secondary nanoscale emulsions. The limiting step to produce stable nanoemulsions for improving the solubility in an aqueous system of a compound poorly soluble in water, is the choice of the optimal composition, in terms of emulsifier and lipid contents, to obtain stable primary emulsions. The stability of the primary emulsions was evaluated thanks to the construction of a pseudo-ternary phase diagram. In particular, a pseudo-ternary phase diagram was used as a compositional map for the identification of the optimal conditions to obtain kinetically stable emulsions, through the reduction of the droplet size and minimization of the amount of emulsifier to be used.

In the triangular phase diagram of Figure III.2, the first vertex corresponds to water, the second to curcumin (0.1 wt%) solubilized in stearic acid, and the third to a combination of a lipophilic and hydrophilic emulsifier in 1:0.5 ratios. In particular, glycerol monooleate and sugar ester (Figure III.2a), lipophilic soy lecithin and sugar ester (Figure III.2b), lipophilic and defatted soy lecithins (Figure III.2c) have been used as emulsifiers.

As shown in Figure III.2, different regions of stability/instability can be identified. The unstable systems include: the “heterogeneous liquid” case, characterized by the physical separation of aqueous and oil phases and settling of curcumin, which precipitated to the bottom of the tube; the “heterogeneous cream” case, where two layers were observed with excess water at the bottom and the emulsion on top with settling of curcumin; the “heterogeneous solid” case, which consists of solid coarse particles in which the curcumin is completely insoluble.

It was observed that the unstable zone of the diagram is confined to its lower part, while the stable conditions all exist above the imaginary water dilution line that starts from the middle of the right side of the phase diagram and reaches the water vertex.

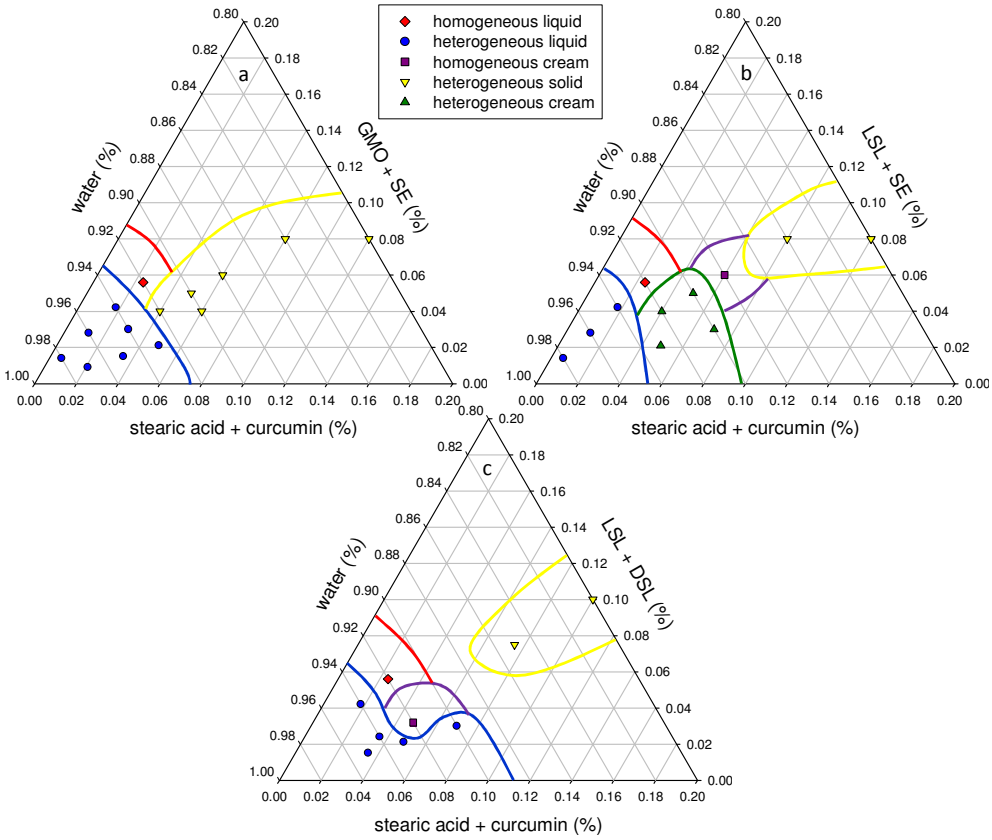

Figure III.2 *The pseudo-ternary phase diagrams of curcumin–encapsulated emulsion using stearic acid as lipid phase and a combination of (a) lipophilic soy lecithin, LSL, and sugar ester, SE, (b) lipophilic soy lecithin, LSL, and defatted soy lecithin, DSL, and (c) glycerol monooleate, GMO, and sugar ester, SE, as emulsifiers.*

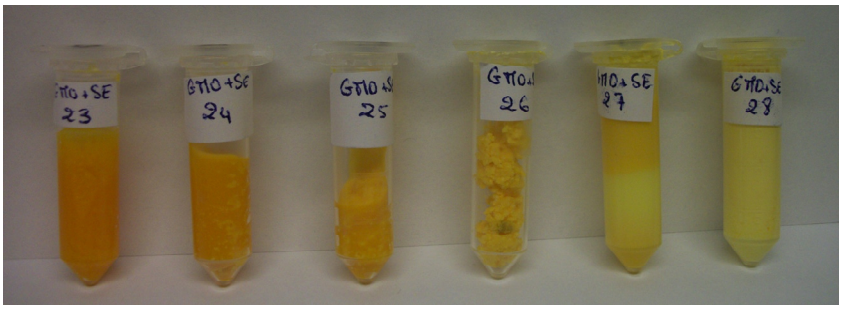

Figure III.3 *Samples collected for the evaluation of the stability/instability regions of the pseudo-ternary phase diagram. From left to right: homogeneous cream, heterogeneous cream, heterogeneous solid, heterogeneous and homogeneous liquid.*

The stable systems that were obtained were divided into two large categories: the "homogeneous liquid" case, which included stable oil in water emulsions that exhibited a Newtonian flow behavior, and "homogeneous cream" case, which included the emulsion systems with a macroscopically non-Newtonian behavior.

In Figure III.3 the pictures of some samples collected for the evaluation of the stability/instability regions of the pseudo-ternary phase diagram were reported to illustrate the different cases.

The "homogeneous liquid" systems were considered to be the primary emulsions for further processing by HPH and comminution to nanometric size for the production of the secondary emulsions.

In Table III.1 were reported the composition of the stable primary emulsions, that were further homogenized with high-pressure homogenizer at 200 MPa for 10 cycles of homogenization to reduce the sizes of the droplets and obtain curcumin-encapsulated O/W emulsions. After HPH processing, just a formulation, C/LSL-SE, remained stable without settling of curcumin and was prepared for further studies.

Table III.1 *Composition of the "homogeneous liquid" systems that has been used as primary emulsions during the production by HPH of O/W emulsion for curcumin delivery.*

Homogeneous liquid	Composition
C/GMO-SE	0.1% curcumin 3.73% glycerol monooleate 1.87% sugar ester 2.4% stearic acid 91.9% water
C/LSL-SE	0.1% curcumin 3.73% lipophilic soy lecithin 1.87% sugar ester 2.4% stearic acid 91.9% water
C/LSL-DSL	0.1% curcumin 3.73% lipophilic soy lecithin 1.87% defatted soy lecithin 2.4% stearic acid 91.9% water

We also tried to increase the curcumin's concentration from 0.05 to 0.2 wt% and observe the stability of the emulsions to find the maximum concentration that can be encapsulated without precipitation.

For curcumin concentration >0.1 wt%, there was a settling of curcumin on the bottom of the test tube. So we can conclude that 1000 mg/L is the maximum concentration of curcumin that can be encapsulated in stearic acid-based emulsions, resulting 1600 times higher than the solubility of curcumin in water, which is 0.6 mg/L (Donsi et al., 2010d).

Moreover, in order to check the effect of the oil phase, palm oil and hydrogenated palm oil have been used as lipid phase instead of stearic acid.

It has been observed that only the stearic acid gives stable submicron emulsions; on the contrary, in the formulations with palm oil and hydrogenated palm oil as lipid phase, the curcumin encapsulated has been suddenly released, precipitating on the bottom of the test tube.

Chapter IV
Investigation of HPH process parameters

In this chapter the production of food nanoemulsions by high pressure homogenization technique (HPH) was investigated, focusing on the effect of emulsifier type and concentration as well as of the geometry of the homogenization chamber on the mean droplet diameter obtained. The kinetics of the emulsification process was determined by dynamic light scattering measurements on the emulsions produced at different pressure levels and number of HPH passes, in four different homogenization chamber geometries.

Moreover, several food-grade emulsifiers, such as soy lecithins, pea proteins, modified starch and sugar ester, were characterized in terms of their interfacial and dynamic properties, by pendant drop measurements and compared with synthetic compounds, such as Tween 80 and SDS.

The results show that the kinetic parameters of the emulsification process can be primarily correlated with the interfacial and dynamic properties of the emulsifiers, while the fluid-dynamics regime establishing in the homogenization chamber contributes only to a lesser extent. Nevertheless, the correct design of the homogenization chamber may help in obtaining uniform fluid-dynamic conditions, which ensure a narrow droplet size distribution.

IV.1 Introduction

Emulsification at nanometric sizes can be conducted by means of energy intensive systems, such as colloid milling, ultrasonication and high pressure homogenization (Stang et al., 2001, Schultz et al., 2004). At the moment, high pressure homogenization (HPH) appears to be the most suitable technique for industrial applications, because of the ease of operation,

scalability, reproducibility and high throughput (Liedtke et al., 2000, Schultz et al., 2004).

The emulsification process by HPH can be schematically represented by two stages, one consisting in the deformation and disruption of the droplets, with the consequent increase of the surface area of the emulsion, and the other in the droplet stabilization by means of the adsorption of the emulsifier molecules at the newly formed interfaces (Brosel and Schubert, 1999, Hakansson et al., 2009b, Hakansson et al., 2009a).

Disruption occurs in the homogenization chamber when droplet deformation, induced by the fluid-dynamic stresses occurring partly in the discharge gap and mainly in the interaction chamber (Brosel and Schubert, 1999), reaches a critical level.

The fluid-dynamic stresses arise from the combination of different factors, such as turbulence, elongational and shear stress, as well as cavitation (Floury et al., 2004b, Floury et al., 2004a). Which of these factors is dominant depends on the equipment used, operating conditions, process fluid properties and droplet composition.

For a given valve geometry, disruption is also influenced by product properties and operating conditions (Stang et al., 2001). While the viscosity of the continuous phase does not play a significant role on the disruption efficiency, the disperse phase viscosity or the viscosity ratio, defined as the ratio of the viscosity of the disperse phase to the viscosity of the emulsion phase (η_d/η_{em}) or of the continuous phase (η_d/η_c) (Stang et al., 2001, Qian and McClements, 2011), represents an important parameter.

For example, the inertial forces generated in the highly turbulent region are identified as responsible of droplet disruption for disperse phases of low viscosity (Middelberg, 1995, Floury et al., 2004b). At higher disperse phase viscosities, the mechanisms of disruption due to the laminar elongational flow become instead predominant (Stang et al., 2001, Kleinig and Middelberg, 1998), because the lifetime of turbulent eddies is too short to critically deform highly viscous droplets (Stang et al., 2001).

Another mechanism that contributes to droplet disruption is cavitation. Turbulent flow conditions favor cavitation due to fluid velocity and pressure fluctuations that can cause the formation and disruption of vapor cavities (Kleinig and Middelberg, 1998).

Donsì and coworkers devoted numerous efforts to clarifying the mechanisms of inactivation by HPH of cells suspended in a liquid, which is a disruption-dominated process, using different valve geometries and scale of operation (Donsi et al., 2009), deriving the indications that the flow regime established in the HPH valve and downstream of it controls the extent of mechanical disruption (Donsi et al., 2009).

Obviously, HPH emulsification is complicated by the recoalescence phenomena following disruption, which depends not only on the flow regime but also on emulsifier properties. For a very fast-adsorbing emulsifier, the

mean droplet diameter can be well correlated to the energy density delivered to the system by the HPH system by a power law (Stang et al., 2001, Schultz et al., 2004):

$$d_{em} = C \cdot E_V^{-b} \qquad \text{(IV.1)}$$

In eq. (IV.1), d_{em} is the mean droplet diameter and E_V is the energy density, which corresponds to the pressure drop in the homogenization valve times the number of HPH passes (Schultz et al., 2004), while C and b are kinetic constants, which depend on the efficiency of droplet disruption (C) and on the flow conditions in the interaction chamber (b). Typical values of b range from 1 for laminar elongational flow to about 0.6 for inertial forces in turbulent flow and 0.75 for shear forces in turbulent flow (Stang et al., 2001). Values of C are instead affected by the emulsion properties and interfacial activity of the emulsifier. The lower interfacial tension induced by the emulsifier may in fact facilitate droplet deformation and disruption (Brosel and Schubert, 1999).

For slow-adsorbing emulsifiers, the mean droplet diameter is instead controlled by interfacial adsorption velocity, which is the main determinant of the stabilization of the newly formed droplets, and hence of the minimum droplet size that can be obtained in the homogenizer.

Despite considerations on droplet surface coverage suggest that the mean droplet diameter should be inversely proportional to emulsifier concentration (McClements, 1999), the theoretical minimum diameter is never achieved, because adsorption at the interface is a dynamic process, which is in competition with coalescence phenomena (Qian and McClements, 2011). In particular, the adsorption and coalescence phenomena, which can be both correlated to the collision of emulsifier molecules with oil droplets (adsorption) and to inter-droplet collisions (coalescence), are characterized by comparable time scales in the case of macromolecular emulsifiers (Nilsson and Bergenstahl, 2006).

Recoalescence phenomena, being prevented by emulsifier adsorption at newly formed interfaces (Brosel and Schubert, 1999), are therefore affected by emulsifier type and concentration (Qian and McClements, 2011). Nevertheless, especially in food formulation, due to ingredient and taste constraints, it is not always possible choosing the optimal emulsifier or adding it at high concentration (Schultz et al., 2004).

In general, small-molecule emulsifiers, such as Tween 20 and SDS, can lead, under similar processing conditions, to smaller droplet size than larger molecules, such as proteins (Qian and McClements, 2011), which can also undergo denaturation upon HPH, losing their interfacial and emulsifying properties (Qian and McClements, 2011, Floury et al., 2002b, Floury et al., 2002a, Donsi et al., 2010b).

The aim of this chapter is to contribute to the fundamental investigation of the HPH-assisted emulsification process at the nanometric size, using

food-grade ingredients. In particular, the effect of different food-grade emulsifiers, such as modified starch, vegetable proteins, sugar ester and soy lecithin, whose interfacial and dynamic properties are thoroughly characterized, are critically assessed in comparison with artificial emulsifiers, such as SDS and Tween 80. In addition, also the effect of different homogenization chamber geometries is investigated, in order to identify the key determinants of the emulsification process.

IV.2 Material and methods

IV.2.1 Materials

All O/W emulsions tested in the present work were formulated using sunflower oil (Sagra, Lucca, Italy) as disperse phase and bidistilled water as continuous phase. Different hydrophilic compounds were tested as emulsifiers, which were dissolved in the aqueous medium prior to lipid mixing. Among small-molecule surfactants, polysorbate 80 (Tween 80) and sodium dodecyl sulphate (SDS), both acquired from Sigma-Aldrich s.r.l. (Milan, Italy), a sugar ester (sucrose palmitate P-1670), a kind gift from Prodotti Gianni (Milan, Italy), as well as a defatted soy lecithin (Solec FS-B), a generous gift from Solae Italia s.r.l. (Milan, Italy), were tested. Among functional polysaccharides, a modified starch (Cleargum® CO01) and pea proteins isolates (Nutralys® F85M), both a generous gift from Roquette Italia S.p.A. (Alessandria, Italy), were used as emulsifying agents.

IV.2.2 Experimental method

IV.2.2.1 Interfacial tension measurements

Interfacial tension at the water-oil interface, with different emulsifier loadings in the aqueous solution (from 0.01 g/L to 50 g/L), was measured by means of the pendant drop method. Measurements were conducted on a droplet of aqueous solution, of volume ranging between 5 and 10 μL, produced by means of a micrometric syringe in water-saturated sunflower oil contained in a transparent cuvette. This configuration was preferred for technical reasons to the reverse configuration (oil droplet in water), after it was experimentally verified that the same results were obtained in the two cases.

A CAM200 apparatus (KSV Instruments, Finland), consisting of an experimental cell, an illuminating and viewing system to visualize the drop as well as a data acquisition system, was used to determine the interfacial tension from the pendant drop profile. Images of the drop were captured and digitalized, the drop contour was extracted for the determination of the radius of curvature at the apex necessary for the calculation of interfacial

tension. Interfacial tension was automatically determined via software by fitting the shape of the captured drop images to the Young-Laplace equation which relates interfacial tension to drop shape.

Eq. (IV.2) reports the Young-Laplace equation, where ϕ is the angle made by the tangent at the point (X, Z), s is the linear distance along the drop profile and $d\phi/ds$ corresponds to the radius of curvature at the point (X, Z) and β is the shape parameter, given by eq. (IV.3), where g is the gravitational constant, ρ is the effective density of the liquid drop, σ is the surface or interfacial tension, and q is the radius of curvature at the origin.

$$\frac{d\phi}{ds} = 2 + \beta Z - \frac{\sin\phi}{X} \qquad \text{(IV.2)}$$

$$\beta = -\frac{g\sigma q^2}{\rho} \qquad \text{(IV.3)}$$

The evolution of the interfacial tension over 10^4 s from the instant of drop formation was monitored by sequential acquisition of drop images at specified time intervals.

The reported results are the average of 3 measurements.

IV.2.2.2 Emulsion production by high pressure homogenization

Primary emulsions were obtained by homogenizing water-emulsifier-oil mixtures (10% sunflower oil in water and emulsifier concentration in the emulsion ranging from 50 to 10 and 2.0 g/L) through high speed homogenization (HSH) using an Ultra Turrax T25 apparatus (IKA® Werke GmbH & Co., DE) equipped with a S25 N18 G rotor operated at 24000 rpm for 5 min at 4°C. Primary emulsions were then reduced into very fine secondary emulsions (nanoemulsions) by HPH either in a Nano DeBEE Electric Bench-top Laboratory Machine (Bee International, Inc., South Easton, MA) or in a bench-scale nm-GEN 7400 homogenizer (Stansted Power Fluids, Stansted, UK).

The operating pressure ranged from 70 to 280 MPa, while the number of homogenization passes was varied from 1 to 10. The inlet temperature was set at 4°C and the outlet temperature, which increased because of frictional heating during pressure drop, was rapidly reduced back to 4 °C in a heat exchanger placed immediately downstream of the homogenization valve.

Sampling was conducted on the primary emulsion (0 HPH passes) and after 1, 2, 3, 5, 7 and 10 HPH passes for mean droplet size measurements.

Experiments were conducted in duplicate.

IV.2.2.3 Homogenization chamber geometry

HPH-assisted emulsification process was conducted using two different HPH systems with four different configurations of the homogenization chamber, which are schematically depicted in Figure IV.1.

The Nano DeBEE machine was characterized by an orifice valve fitted in a modular homogenization chamber, whose geometry could be simply regulated. In contrast, the Stansted homogenizer was characterized by a piston valve geometry of the homogenization valve, previously described (Donsi et al., 2009).

Homogenization chamber configurations Z5, Z5-cf and Z8 (Figure IV.1) were all realized in the Nano DeBEE system, and differed in the orifice size and downstream flow pattern. The zirconia orifice nozzle mounted in the systems was available in two different sizes, 130 µm (Z5 and Z5-cf) and 200 µm (Z8). In all cases the process fluid was forced under high pressure (70-280 MPa) through the orifice, generating an extremely high velocity jet. This was the first step in the droplet disruption process. Subsequently, the high velocity jet entered a series of 5 interaction chambers, where the disruption process was completed. The homogenization chamber geometry with different interaction chambers was designed to create a combination of fluid-mechanical stresses, in order to completely break apart the droplets, while favouring emulsifier adsorption at the interface.

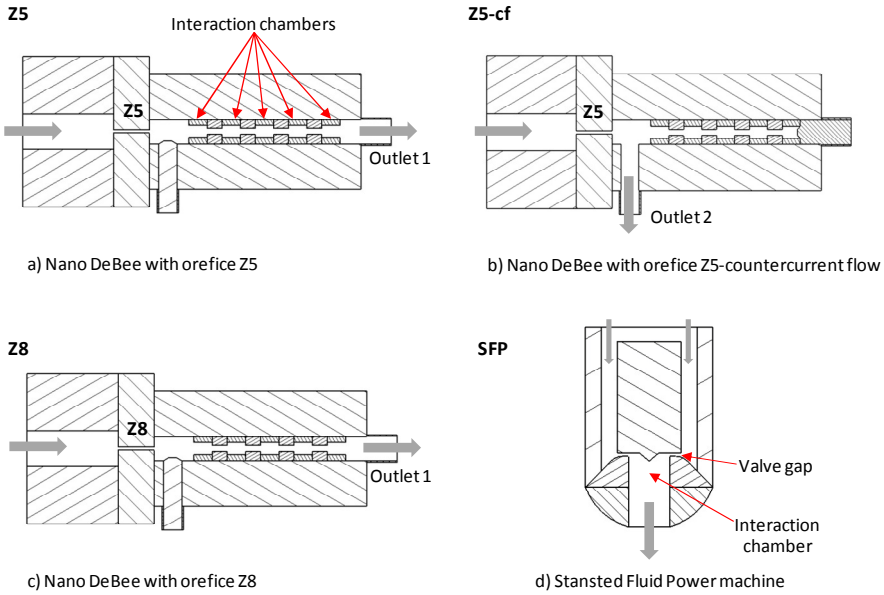

Figure IV.1 *Simplified sketch of the different geometries of the homogenization chambers tested.*

Z5 and Z8 configurations were operated in standard mode, with the outlet in the same direction of the fluid jet. In contrast, Z5-cf configuration was characterized by the outlet perpendicularly located immediately downstream of the orifice. The flow inversion induced either after the interaction chambers (as claimed by the manufacturer), or before them, theoretically improves turbulent fluid-fluid interactions and therefore droplet disruption.

SFP configuration was realized in the Stansted Fluid Power machine and was characterized by a movable piston, whose position with respect to the valve seat determined the gap opening and hence the operating pressure (Figure IV.1). In the investigated pressure range (70-140 MPa), gap opening varied between 2 and 5 μm. More details on the relationship between gap opening, flow rate and operating pressure are given elsewhere (Donsi et al., 2009, Floury et al., 2004a). In the SFP geometry, the pressurized flow is radially dispersed from the volume surrounding the piston to the inner interaction chamber through the annular gap formed by the piston and the valve seat. In the interaction chamber, the combination of shear and elongational stresses, turbulence and cavitation causes the droplet disruption (Donsi et al., 2009).

IV.2.2.4 Photon Correlation Spectroscopy

A photon correlation spectrometer (HPPS, Malvern Instruments, Malvern, UK) was used for the particle size measurement of the emulsion droplets, whose characteristic size was always comprised in the instrument sensitivity range (1–6000 nm). The droplet size distribution was characterized in terms of the mean droplet size (*Z-diameter*) and width of the distribution (polydispersity index, *PDI*) at 25 °C by measuring the backscattered (173°) light through samples diluted 1:100 with bidistilled water to avoid multiple scattering effects within polystyrene cuvettes. The intensity-intensity autocorrelation function, G(q,t), generated by the measurements was automatically analyzed through cumulant analysis coupled with the Stokes-Einstein equation (Stepanek, 1993) by the software provided by the manufacturer, with only refractive index and viscosity of the dispersant medium (water) required (1.332 and 0.895 mPa s respectively, at 25 °C) as input parameters.

IV.2.2.5 Viscosity measurement of the nanoemulsions

Viscosity measurements of the emulsion samples treated at different pressures were conducted using a dynamic shear rheometer (TA Instruments, New Castle, DE) with a shear rate profile from 0.1 to 1000 s^{-1}. All the measurements were performed at 25 °C.

IV.2.2.6 Density measurement of the nanoemulsions

Density measurements of the emulsion samples treated at different pressures were conducted using a density-meter Densito 30PX (Mettler-Toledo, Inc., Columbus, OH) at 25 °C.

IV.2.3 Data fitting

IV.2.3.1 Dynamic interfacial tension

The dynamic interfacial tension $\sigma(t)$ of the tested emulsifiers was measured as a function of time. The pronounced decrease of $\sigma(t)$ with advancing time was attributed to the migration and reorganization of the emulsifier at water-oil interface (Shi et al., 2004). Accordingly, a kinetic model, eq. (IV.4), which enables the detailed description of the rate of transport of the different emulsifiers tested, was implemented by minor modifications of a literature model, validated for macromolecules (Shi et al., 2004).

$$\sigma(t) = \sigma_f + (\sigma_1 - \sigma_f) \cdot \exp\left(-\frac{t}{\tau_1}\right) + (\sigma_2 - \sigma_f) \cdot \exp\left(-\frac{t}{\tau_2}\right) \qquad \text{(IV.4)}$$

In eq. (IV.4), σ_f is the asymptotic interfacial tension for $t \rightarrow \infty$, and σ_1, σ_2, τ_1 and τ_2 are the dynamic parameters that describe the decay kinetics of the interfacial tension over time until a stationary value is reached. More specifically, τ_1 and τ_2 represent the characteristic times of decay of $\sigma(t)$ to the asymptotic value, with τ_1 corresponding to the migration of the emulsifier to the water-oil interface, and τ_2 to the reorganization of the emulsifier at water-oil interface and to the eventual configurational changes of macromolecules at interfaces (Nilsson and Bergenstahl, 2006). In general, τ_1 values are expected to be lower than τ_2.

IV.2.3.2 Emulsification process

The effect on the mean droplet size (d_{em}) of the emulsifier type and concentration, as well as of the geometry of the homogenization chamber was modeled as function of the energy density according to eq. (IV.1) (Stang et al., 2001).

In eq. (IV.1) E_V is the specific energy delivered to the emulsion by the HPH device, that is the mechanical energy input per unit volume of the zone where the droplets are disrupted (Stang et al., 2001), and that can be calculated as the homogenization pressure times the number of HPH passes.

C and b are kinetic parameters, with a precise physical meaning. C is the mean droplet size of the primary emulsion for a unit specific energy, and therefore indicates the emulsifying ability of the used emulsifier upon mild

homogenization (prior to HPH). b represents the kinetic constant of reduction of the mean droplet size and therefore indicates how fast the droplets are disrupted. Better emulsification is attained for $b \rightarrow 1$, while a worse performance is characterized by $b \rightarrow 0$.

In comparison with the model of eq. (IV.1), also the model reported in eq. (IV.5) was tested for fitting the experimental data, with the main difference consisting in a different exponent for operating pressure ΔP_h (b) and for number of passes n (f):

$$d_{em} = C'' \cdot \Delta P_h^{-b} \cdot n^{-f} \qquad \text{(IV.5)}$$

The polydispersity index, PDI, was instead fitted with eq. (IV.6):

$$PDI = C' \cdot E_V^{-b'} \qquad \text{(IV.6)}$$

IV.3 Results

IV.3.1 Interfacial tension and adsorption kinetics

The surface activity of several hydrophilic emulsifiers (modified starch, pea proteins, SDS, Tween 80, sugar ester, as well as soy lecithin) was characterized by measuring the dynamics of the interfacial tension at the O/W interface at different concentration in the aqueous phase, in comparison with the interfacial tension of a pure water-sunflower oil system. Results are reported in Figure IV.2.

The interfacial tension of the pure water-sunflower oil system is about 27.5 mN/m at t = 0, exhibiting a reduction of less than 3 mN/m over a period of 104 s, which must be ascribed to the presence of impurities in the oil phase.

When a hydrophilic emulsifier is present in the aqueous phase, its adsorption at the O/W interface goes through three different stages affecting the interfacial tension: (a) the diffusion from the bulk to the boundary layer insisting at the interface, (b) the molecular adsorption at the interface and the penetration in the oil phase, and (c) the eventual molecular reorganization at the interface (Liu et al., 2011).

In pendant drop experiments, the diffusional transport is the rate-determining step only in the adsorption process of small molecules from dilute solutions. In the case of macromolecules, such as globular proteins, reorganization at the interface upon unfolding may become the rate-limiting factor (Liu et al., 2011). In addition, during high pressure homogenization, the turbulent regime that establishes immediately downstream of the disruption valve makes the diffusional transport of the emulsifier to the

interface less important, with faster turbulence-controlled convective transport instead dominating (Nilsson and Bergenstahl, 2006).

In the experiments reported in Figure IV.2, the diffusion step is too fast to be detected with the experimental method used, with a few seconds elapsing between the droplet formation and the first recorded image. As a consequence, the value of the interfacial tension measured at t = 0 always exhibits a jump down with respect to the pure water-oil system, which is larger at higher emulsifier concentrations (Figure IV.2), and whose extent can be considered a qualitative measurement of the degree of diffusion of the emulsifier to the interface (Nino et al., 2005).

From Figure IV.2 it is possible to identify two different characteristic times of exponential decay of σ as a function of t, with the shortest time being the inverse of a first-order constant of penetration into the oil phase and the longest time corresponding to the inverse of the rate constant of rearrangement at the interface (Liu et al., 2011). This is more evident for macromolecular emulsifiers, such as modified starch and pea proteins, whose conformational changes increase the number of interfacial contacts per protein molecule, thereby increasing the effective concentration of adsorbed segments and lowering the tension (Beverung et al., 1998).

Moreover, the dynamics of the different stages of adsorption, and especially reorganization at the interface, can last even hours or days (Beverung et al., 1998), therefore preventing, in some cases, the attaining of an equilibrium interfacial tension, even after long equilibration times (10000 s).

Figure IV.2 shows that the values of $\sigma(t)$ exhibit a decreasing trend both with increasing time and concentration, because the adsorption of the emulsifier at the O/W interface is a dynamic process, driven by the concentration gradient and by the adsorption properties of the emulsifier. As a result, it is possible to classify the emulsifiers both in terms of the asymptotic interfacial tension, which would be attained for $t \rightarrow \infty$ (σ_f) and by the characteristic times of adsorption at the interface (τ_1, τ_2).

For example, modified starch, pea proteins and lecithin exhibited a very low surface activity at low concentration (from 10^{-2} to 1 g/L), with the interfacial tension being very slightly reduced, in contrast with SDS, Tween 80 and sugar ester, whose surface activity was measurably higher already in the low concentration range. In particular, sugar ester resulted to be the emulsifier with the fastest adsorption kinetics and higher surface activity at the lowest concentrations, causing the detachment of the pendant drop after less than 20 s at 10^{-1} g/L, as well as the inability to stabilize a drop at higher concentrations.

In order to derive some quantitative parameters for the characterization of the different emulsifiers, the experimental curves of Figure IV.2 were fitted with eq. (IV.4) (solid lines in Figure IV.2), with the corresponding parameters reported in Table IV.1.

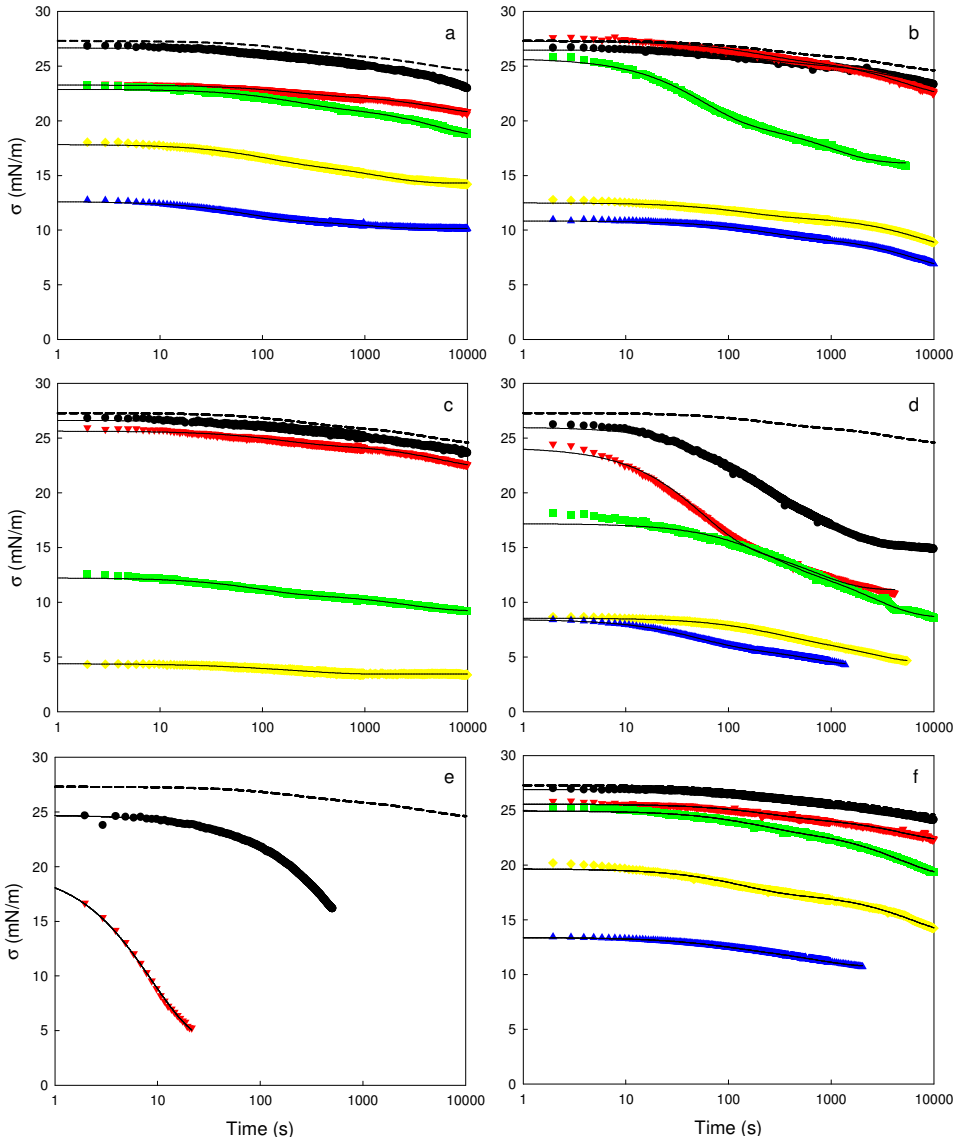

Figure IV.2 *Dynamic interfacial tension, σ, of different emulsifiers, modified starch (a), pea proteins (b), SDS (c), Tween 80 (d), sugar ester (e) and defatted soy lecithin (f), solubilized in water at the following concentrations: 10^{-2} g/L (●), 10^{-1} g/L (▼), 1.0 g/L (■), 10 g/L (◆) and 50 g/L (▲) compared with the dynamic interfacial tension of water in sunflower oil (dashed line). Experimental data are fitted with eq. (IV.4) (solid lines).*

In all cases, data fitting were extremely accurate, as shown by the values of the coefficient of determination R^2, which are always close to 1.

Some emulsifiers, such as sugar esters, Tween 80 and SDS, showed significantly shorter characteristic times for reaching the O/W interface (τ_1) and being displaced on the same interface (τ_2), with possible implications on the attainable mean droplet size during emulsification. In fact, fast adsorption kinetics of the emulsifier can significantly reduce recoalescence phenomena in the homogenization chamber (Brosel and Schubert, 1999, Stang et al., 1994, Stang et al., 2001). In contrast, pea proteins and modified starch exhibited the longer τ_2 values, due to the slower reorganization of large biopolymeric molecules at the interface after adsorption.

Table IV.1 *Kinetic parameters from the fitting of the curves of Figure IV.2 with eq.(IV.4) for different emulsifier types and concentrations.*

Emulsifier	C_{em} (g/L)	σ_f (mN/m)	σ_1 (mN/m)	τ_1 (s)	σ_2 (mN/m)	τ_2 (s)	R^2
Modified starch	10^{-2}	22.3	23.4	170	25.5	10000	0.994
	10^{-1}	20.6	21.4	170	22.4	5000	0.996
	1.0	18.4	20.0	190	21.3	5000	0.995
	10	14.3	16.0	100	16.2	1400	0.996
	50	10.2	11.8	66	11.0	910	0.993
Pea proteins	10^{-2}	22.2	23.7	180	25.7	5000	0.995
	10^{-1}	23.0	24.1	180	25.4	5000	0.995
	1.0	16.1	22.0	55	19.9	1000	0.997
	10	8.00	9.2	140	11.3	10000	0.997
	50	6.10	7.5	210	9.50	10000	0.999
SDS	10^{-2}	23.7	24.6	150	25.7	3300	0.986
	10^{-1}	22.2	23.4	140	24.5	5000	0.989
	1.0	9.20	10.7	88	10.7	2500	0.992
	10	3.40	3.7	44	4.10	290	0.971
Tween 80	10^{-2}	15.0	20.3	120	20.7	1000	0.999
	10^{-1}	11.2	19.9	52	15.5	710	0.996
	1.0	8.6	12.3	220	13.5	2500	0.995
	10	4.50	6.10	240	6.90	2500	0.999
	50	4.20	6.60	48	6.00	620	0.999
Sugar ester	10^{-2}	10.8	11.6	31	23.9	560	1.000
	10^{-1}	3.70	12.0	9.0	11.5	9.0	0.999
Soy lecithin	10^{-2}	23.9	24.9	220	25.9	5000	0.997
	10^{-1}	22.1	23.3	220	24.4	5000	0.991
	1.0	18.9	20.6	180	23.3	5000	0.997
	10	13.4	15.6	130	17.5	5000	0.994
	50	10.7	11.6	79	12.5	670	0.999

Among the kinetic parameters reported in Table IV.1, those expected to affect most the mean droplet size during HPH-emulsification are the asymptotic value of the interfacial tension σ_f, as well as the characteristic times of the interface adsorption and penetration into the oil phase τ_1 and of reorganization at the interface τ_2. On the other side, the values of parameters σ_1 and σ_2, obtained from the data fitting, can be considered to depend mainly on the diffusional transport to the interface, and hence are of less interest in the HPH process. In fact, downstream of gap of the homogenization chamber a turbulent regime is established, where emulsifier is transported to the O/W interface mainly by fast convective mechanisms. In addition, the trend of the values of σ_1 and σ_2 with emulsifier type and concentration, can be well correlated to σ_f, and therefore do not represent truly independent indicators of emulsifiers surface activity.

The σ_f values of modified starch and soy lecithin exhibited the same trend, with significant activity becoming evident only above $C_{em} > 1$ g/L. Pea proteins were characterized by slightly better interfacial properties, with their σ_f values lower than for modified starch and lecithin in the high concentration range (1-50 g/L). SDS exhibited a remarkable decrease in σ_f only for $C_{em} > 0.1$ g/L. Tween 80 resulted to be very active already at very low concentration, while sugar ester was apparently required in extremely small quantities in order to explicate excellent surface activity.

IV.3.2 Effect of emulsifier type and concentration on mean droplet diameter

The effect of emulsifier concentration on the mean droplet size as a function of the specific energy of homogenization was studied in the Z5 configuration, with the results being reported in Figure IV.3. In particular, the *Z-diameter* is plotted as a function of the energy density E_v, with the emulsifier concentration indicated by colors, the operating pressure ΔP_h by different symbols and the number of passes n that can be calculated from E_v and ΔP_h ($E_v = n \cdot \Delta P_h$).

For all the emulsifiers, the experimental data are grouped according to the emulsifier concentration, with a linear trend in the log-log diagram of Figure IV.3, which qualitatively appears to depend only on the energy density, rather than on the pressure level or number of passes separately. In fact, data points at the same E_v but different ΔP_h (and hence different n values) are always superimposed, suggesting that the mean droplet diameter is not strongly dependent on how the energy is delivered to the system. The suitability of the model of eq. (IV.1) to fit the experimental data of Figure IV.3 was quantitatively assessed in comparison with the model reported in eq. (IV.5), where the disrupting effects of operating pressure and number of passes are uncoupled by allowing for different exponent parameters.

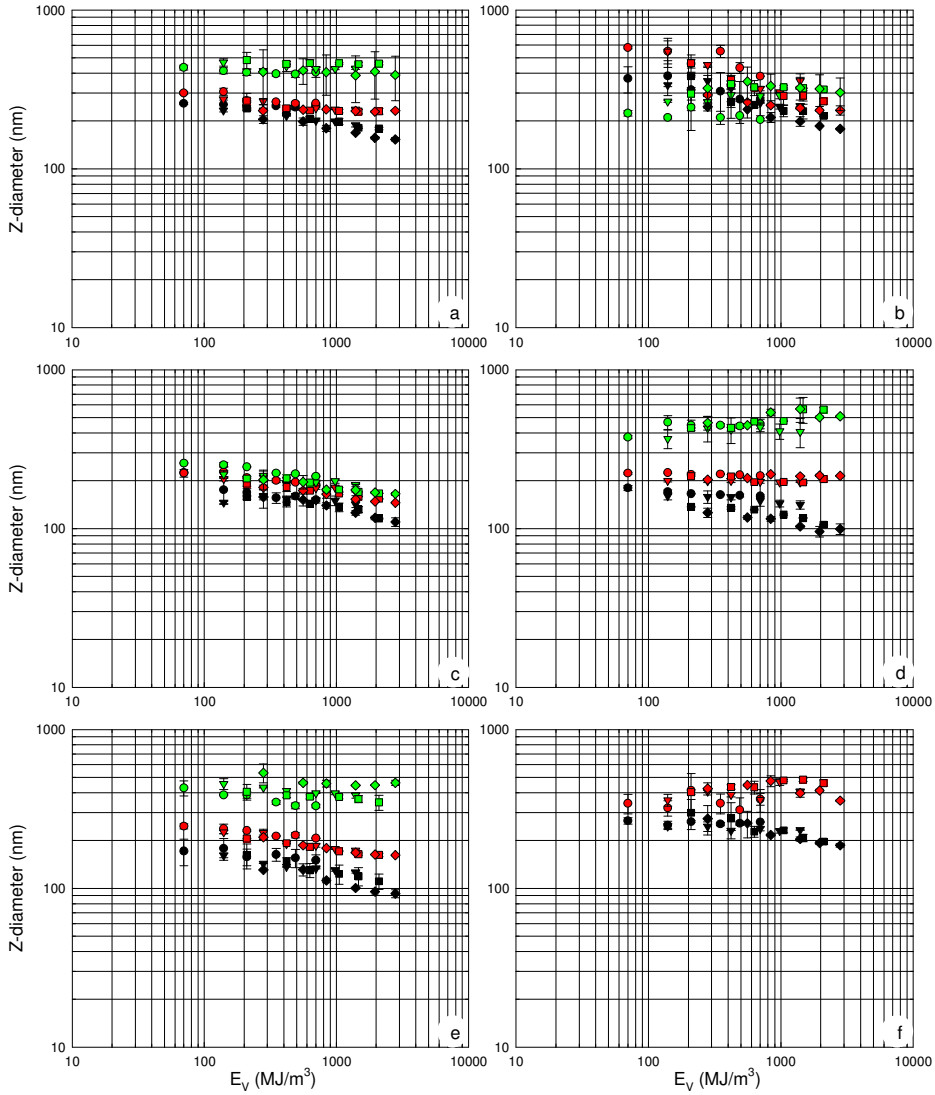

Figure IV.3 *Effect of emulsifier concentration on the mean droplet size, Z-diameter, as a function of the energy density, E_V, for modified starch (a), pea proteins (b), SDS (c), Tween 80 (d), sugar ester (e) and soy lecithin (f). Experimental data: emulsifier concentration of 2.0 g/L (green symbols), 10 g/L (red symbols) and 50 g/L (black symbols); pressure of 70 MPa* (○), *140 MPa* (▽), *210 MPa* (□) *and 280 MPa* (◇)*; the number of passes can be calculated as E_v divided pressure.*

The parity plots of Figure IV.4 show that both models can fit the experimental data quite accurately, with R^2 values ranging from 0.961 for the model of eq. (IV.5) to 0.933 for the model of eq. (IV.1). Being the improvement in fitting accuracy deriving from the introduction of an additional parameter in eq. (IV.5) only marginal, the energy density-based model of eq. (IV.1) was applied to fitting all the experimental data.

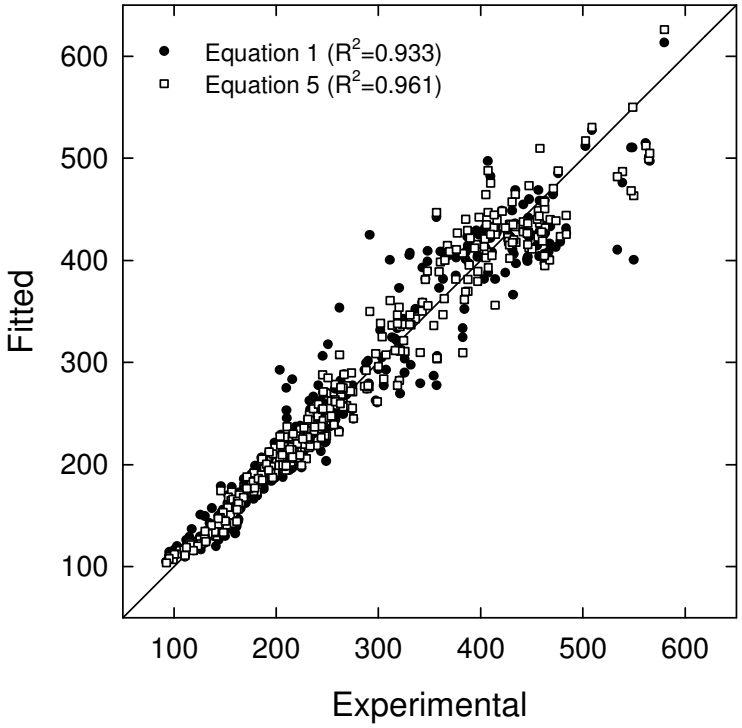

Figure IV.4 *Parity plots reporting fitted values, according to the models of eqs. (IV.1) and (IV.5), vs. experimental values of Figure IV.3.*

Figure IV.3 shows that for all the emulsifiers, at the highest concentration investigated (50 g/L), the efficiency of droplet disruption increased with the energy density. Therefore, at the most severe conditions (10 HPH passes at 280 MPa, corresponding to 2800 MJ/m^3) the smallest mean droplet diameter was achieved, which depended on emulsifier surface and dynamic properties.

Based on the smallest achievable *Z-diameter*, the best emulsifying efficiency was observed for sugar ester (90 nm), followed by Tween 80 (95 nm), SDS (110 nm), modified starch (150 nm), pea protein (180 nm) and soy lecithin (190 nm). Interestingly, the emulsifying efficiency could be well

correlated with the parameters σ_f, τ_1 and τ_2, reported in Table IV.1, as described in the Discussion section.

For some emulsifiers, such as SDS, a very modest difference was observed among the *Z-diameter* vs. E_v curves at 2.0, 10 and 50 g/L, while in the other cases the differences were quite significant. In fact, if the emulsifier concentration is too low, its contribution against recoalescence is negligible, and increasing the energy density does not contribute to decrease the mean droplet size. This was observed for sugar ester, modified starch and pea proteins at 2.0 g/L, and for Tween 80 and soy lecithin also at 10 g/L. In addition, for Tween 80 and soy lecithin, a low emulsifier concentration had a detrimental effect on HPH-assisted droplet disruption, with an observed increase in mean droplet diameter, which can be attributed to increased coalescence at higher pressures and for multiple HPH passes when emulsifier surface coverage is insufficient.

In summary, production of emulsions at the nanometric size, which for food application can be considered to be below 200 nm, where, due to the subcellular size, emulsion droplets exhibit improved properties in delivering active biomolecules (Huang et al., 2010), significantly depends on emulsifier type and concentration. For a 10% oil phase, it is required a concentration higher than 10 g/L of modified starch, pea proteins, Tween 80 and soy lecithin, to obtain a mean droplet size below 200 nm. In contrast, emulsions with a mean droplet size below 200 nm were obtained with SDS and sugar ester concentration of 10 g/L, thanks to the lower O/W interfacial tension and faster kinetics of adsorption at the O/W interfaces than other emulsifiers (Figure IV.2).

IV.3.3 Effect of homogenization chamber geometry on mean droplet size

Figure IV.5 comparatively reports the emulsification curves (*Z-diameter* vs. energy density) obtained in the four homogenization chamber geometries tested for different emulsifiers (modified starch, pea proteins, Tween 80 and SDS) at the concentration of 10 g/L.

Very small differences were observed among the different chamber geometries, with the emulsification process being primarily ruled by the energy density and by the emulsifier properties. The geometry of the homogenization chamber contributed to the efficiency of the emulsification process in a less significant but still measurable way.

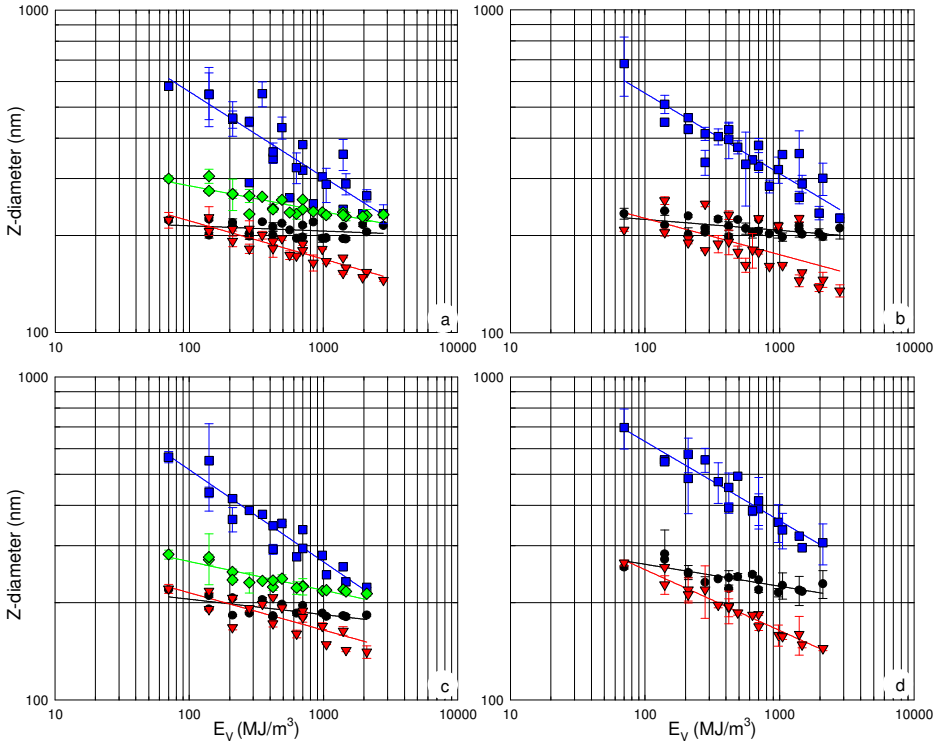

Figure IV.5 *Dependence of the mean droplet size, Z-diameter, of the emulsion on the energy density, E_V, for different geometries of the homogenization chamber: Z5 (a), Z5-cf (b), Z8 (c) and SFP (d). Experimental data: pea proteins (■), modified starch (◆), SDS (▼) and Tween 80 (●) and C_{em} = 10 g/L. Experimental data are fitted with eq. (IV.1) (solid lines).*

From Figure IV.5 it is evident that the SFP geometry performed worse, while Z8 geometry exhibited a slightly better performance than the other geometries for all the tested emulsifiers. In addition, no significant difference could be observed between the standard flow and counterflow configuration (Z5 and Z5-cf).

This is even more evident when considering the polydispersity index, *PDI,* of the produced nanoemulsions (Figure IV.6).The performance of the Z8 geometry is without any doubt better, followed by the Z5 and Z5-cf. In contrast, the performance of the SFP configuration was the poorest, with all the produced emulsions exhibiting a PDI always higher than 0.2, and above 0.3 at lower energy density, for all the tested emulsifiers.

These results suggest that in the interaction chamber of the SFP configurations the fluid-dynamic stresses are highly inhomogeneous, with

regions dominated by highly turbulent regimes alternating to regions characterized by milder conditions, where droplets are not efficiently disrupted.

It is also interesting to highlight that, when considering the mean droplet diameter, SDS performed better than Tween 80. Nevertheless, in terms of polydispersity index, SDS was less efficient than Tween 80 and exhibited a performance comparable to that of modified starch. Probably, the minimum *Z-diameter* significantly depends on the emulsifier effect on interfacial tension (σ_f), while the polydispersity index is affected mainly by the kinetics of surface adsorption of the emulsifier.

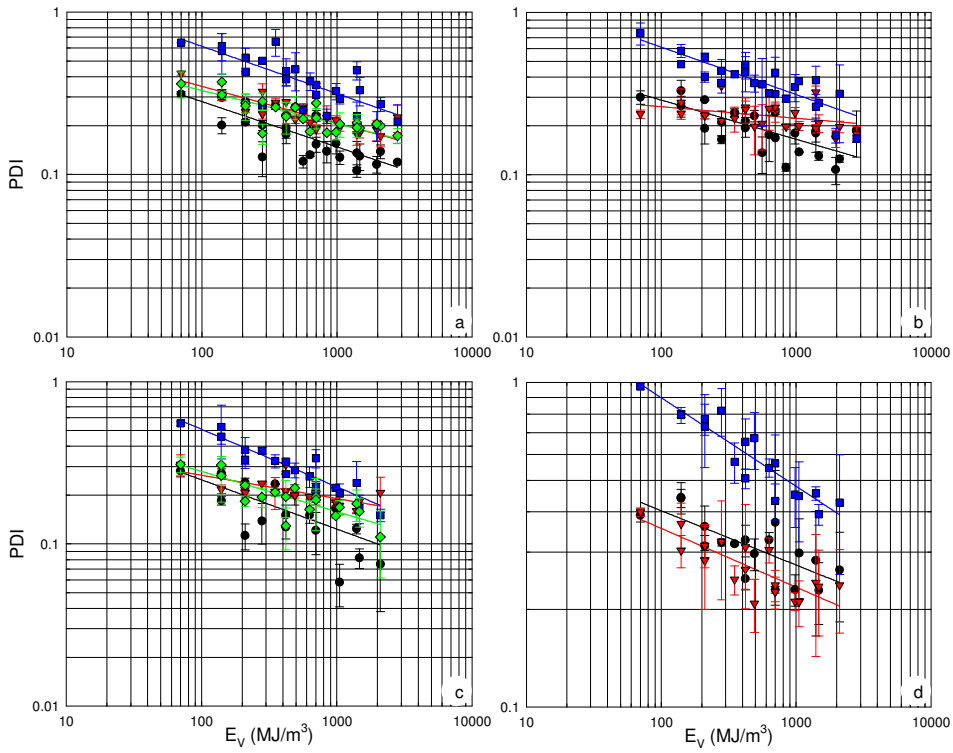

Figure IV.6 *Dependence of the polydispersity index, PDI, of the emulsion on the energy density, E_V, for different geometries of the homogenization chamber: Z5 (a), Z5-cf (b), Z8 (c) and SFP (d). Experimental data: pea proteins (■), modified starch (◆), SDS (▼) and Tween 80 (●) and C_{em} = 10 g/L. Experimental data are fitted with eq. (IV.6) (solid lines).*

IV.4 Discussion

According to the results reported in Figures IV.3-6, several factors contribute to regulate the efficiency of the HPH-based emulsification process. Therefore, a sensitivity analysis was conducted, based on a statistical approach previously tested on different problems (Cimino et al., 2008, Donsi et al., 2009), in order to define the dependence of the kinetic parameters of the emulsification process (*C* and *b*, according to eq. (IV.1)) on the emulsifier properties and concentration, as well as on the fluid-dynamic conditions.

The values of *C* and *b*, determined by the fitting of the data of Figures IV.3-5, are reported in Table IV.2, with the exception of those cases where a negative value of *b* was obtained, corresponding to the increase of the mean droplet size with the energy density (i.e. pea proteins, Tween 80 and soy lecithin at low concentration).

The emulsifier interfacial and dynamic properties were instead expressed through σ_f, τ_1 and τ_2, which resulted, from a preliminary analysis, to be the key determinants of the efficiency of the emulsification process (Table IV.1).

The fluid-dynamic parameters that are more likely to contribute to droplet disruption are the shear and elongational stresses, turbulence and cavitation (Stang et al., 2001, Floury et al., 2004b, Kleinig and Middelberg, 1998, Donsi et al., 2009).

At the entrance of the homogenization valve gap, emulsion droplets are subjected to a very intense elongational flow. The consequent extensional stresses may exceed the mechanical resistance of the droplet (Floury et al., 2002a), inducing a critical deformation, followed by droplet disruption in the turbulent region immediately downstream of the elongational flow (Stang et al., 2001), where a fluid jet is formed.

The balance between the elongational stresses and the droplet resistance can be expressed by the Weber number (*We*), defined in eq. (IV.7).

$$We = \frac{\rho_{em} \alpha^2 d_{em}^3}{4\sigma} \qquad \text{(IV.7)}$$

Fluid acceleration α (s^{-1}) is calculated from average fluid velocity in the gap u_{gap}, divided by the length over which acceleration occurs (Floury et al., 2004a), which was considered to be 10 times the orifice/gap size.

Turbulence is an important mechanism of droplet disruption especially for low-viscosity process media, due to the inertial forces generated in the highly turbulent region, located just at the exit of the gap (Floury et al., 2004b).

Turbulence in such region can be expressed through the Reynolds number (*Re*), defined in eq. (IV.8).

$$\mathrm{Re} = \frac{\rho_{em} u_{gap} d_{or}}{\eta_{em}} \qquad \text{(IV.8)}$$

For the SFP geometry, d_{or} is substituted by the gap opening h in eq. (IV.8).

In the case of viscous media, the primary disruption mechanisms is represented by shear stress in laminar flow (Kleinig and Middelberg, 1998, Middelberg, 1995, Stang et al., 2001, Floury et al., 2004b).

The importance of the shear stresses is expressed through the capillary number (*Ca*), as the ratio of the shear stress and the droplet resistance (Floury et al., 2004b), as shown in eq. (IV.9).

$$Ca = \frac{\eta_{em} \alpha d_{em}}{\sigma} \qquad \text{(IV.9)}$$

Another mechanism of droplet disruption may be represented by cavitation, which occurs in turbulence regions, due to fluid velocity and pressure fluctuations favoring the formation and collapse of vapor bubbles.

The cavitation number (*K*) can be expressed as the ratio between the difference of a local absolute pressure downstream of the homogenizing valve (P_2) from the vapor pressure (P_v) at the local temperature ($T_h = 4\ °C + 0.18 \cdot \Delta P_h$) (Donsi et al., 2009), and the specific kinetic energy, which depends on the velocity through the gap, eq. (IV.10) (Kleinig and Middelberg, 1998).

$$K = \frac{P_2 - P_v}{\frac{1}{2}\rho_{em} u_{gap}^2} \qquad \text{(IV.10)}$$

Preliminary data analysis showed that in the cases considered in the present study, shear stresses and cavitation do not significantly affect the emulsification process.

Therefore, the sensitivity analysis was set to take into account only the *We* and *Re* numbers as fluid-dynamic parameters, together with the emulsifier interfacial and dynamic properties σ_f, τ_1 and τ_2, as well as the emulsifier concentration C_{em}.

Table IV.2 collects all the dependent and independent variables used in the sensitivity study, together with the measured values of viscosity (η_{em}) and density (ρ_{em}) of the homogenized samples, as well as the mean droplet size of the primary emulsion $d_{em,0}$ (produced by high speed homogenization), used in the calculations of *We* and *Re*. The *We* and *Re* reported for each

emulsifier type and concentration are the average of the values calculated at the different pressure levels.

Table IV.2 *Dependent and independent variables used in the sensitivity analysis.*

Emulsifier	C_{em} (g/L)	HPH	$d_{em,0}$ (nm)	ρ_{em} (kg/m^3)	η_{em} (mPa·s)	*We*	*Re*	*C* (nm)	*b*
Modified starch	10	Z5	720	988	3.08	$1.66 \cdot 10^{-5}$	2880	412	0.080
	10	Z8	720	988	3.33	$1.62 \cdot 10^{-6}$	1940	404	0.090
	2.0	Z5	1700	988	2.63	$1.59 \cdot 10^{-4}$	3340	455	0.010
	50	Z5	560	988	5.39	$1.07 \cdot 10^{-5}$	1740	476	0.130
Pea proteins	10	Z5	2600	988	3.09	$1.29 \cdot 10^{-3}$	2880	1890	0.265
	10	Z5-cf	2600	988	3.09	$1.25 \cdot 10^{-3}$	2880	1740	0.249
	10	Z8	2600	988	3.31	$1.20 \cdot 10^{-4}$	1940	1919	0.285
	10	SFP	2600	988	3.31	$4.48 \cdot 10^{-4}$	107	1954	0.245
	50	Z5	1170	988	5.40	$1.41 \cdot 10^{-4}$	1740	954	0.202
SDS	2.0	Z5	12500	984	2.54	$2.54 \cdot 10^{-1}$	3450	433	0.122
	10	Z5	8990	984	2.66	$1.36 \cdot 10^{-1}$	3310	383	0.119
	10	Z5-cf	8990	984	2.66	$1.37 \cdot 10^{-1}$	3310	380	0.113
	10	Z8	8990	984	2.83	$1.31 \cdot 10^{-2}$	2250	365	0.116
	10	SFP	8990	984	2.83	$4.91 \cdot 10^{-2}$	124	602	0.188
	50	Z5	5380	984	3.23	$2.92 \cdot 10^{-2}$	2770	357	0.140
Tween 80	10	Z5	550	986	2.91	$2.13 \cdot 10^{-5}$	3230	231	0.016
	10	Z5-cf	550	986	2.73	$2.13 \cdot 10^{-5}$	3230	262	0.034
	10	Z8	550	986	2.91	$2.05 \cdot 10^{-6}$	2190	255	0.048
	10	SFP	550	986	2.91	$7.65 \cdot 10^{-6}$	121	360	0.068
	50	Z5	0.999	984	3.23	$3.00 \cdot 10^{-3}$	2770	336	0.142
Sugar ester	2.0	Z5	540	986	2.63	$2.75 \cdot 10^{-5}$	3350	444	0.014
	10	Z5	260	986	2.73	$3.07 \cdot 10^{-6}$	3230	357	0.155
	50	Z5	315	986	3.23	$5.45 \cdot 10^{-6}$	2770	436	0.129
Soy lecithin	50	Z5	330	988	3.78	$1.58 \cdot 10^{-6}$	1950	427	0.092
Mean value	19					$2.60 \cdot 10^{-2}$	2400	660	0.127

The statistical approach used to critically analyze the data was a simple linearized model, reported in eqs. (IV.11) and (IV.12) for *C* and *b*, respectively.

$$\frac{\Delta C}{\overline{C}} = m_1 \frac{\Delta C_{em}}{\overline{C_{em}}} + m_2 \frac{\Delta \sigma_f}{\overline{\sigma_f}} + m_3 \frac{\Delta \tau_1}{\overline{\tau_1}} + m_4 \frac{\Delta \tau_2}{\overline{\tau_2}} + m_5 \frac{\Delta We}{\overline{We}} + m_6 \frac{\Delta \mathrm{Re}}{\overline{\mathrm{Re}}} \qquad \text{(IV.11)}$$

$$\frac{\Delta b}{\overline{b}} = n_1 \frac{\Delta C_{em}}{\overline{C_{em}}} + n_2 \frac{\Delta \sigma_f}{\overline{\sigma_f}} + n_3 \frac{\Delta \tau_1}{\overline{\tau_1}} + n_4 \frac{\Delta \tau_2}{\overline{\tau_2}} + n_5 \frac{\Delta We}{\overline{We}} + n_6 \frac{\Delta \mathrm{Re}}{\overline{\mathrm{Re}}} \qquad \text{(IV.12)}$$

In the multilinear model of eqs. (IV.11) and (IV.12), the differential values of the kinetic parameters ΔC and Δb with respect to their mean values ($\overline{C}$, $\overline{b}$) were calculated as an incremental variation of the selected independent variables Δx_i with respect to their mean values $\overline{x}$, which are reported in the last row of Table IV.2. By fitting the data reported in Table IV.2, the regression coefficients m_i and n_i were calculated.

The coefficients m_i and n_i, reported in Figure IV.7a for each corresponding independent variable, represent the percentage gain or loss in *C* and *b* with respect to their own averages as a consequence of the variation of each independent variable.

The parity plot and the specific coefficients obtained by the linear regression are reported in Figure IV.7b. The linearized expressions of eqs. (IV.11) and (IV.12) are able to satisfactorily reproduce all the experimental data with regard to both *C* ($R^2 = 0.943$) and *b* ($R^2 = 0.847$).

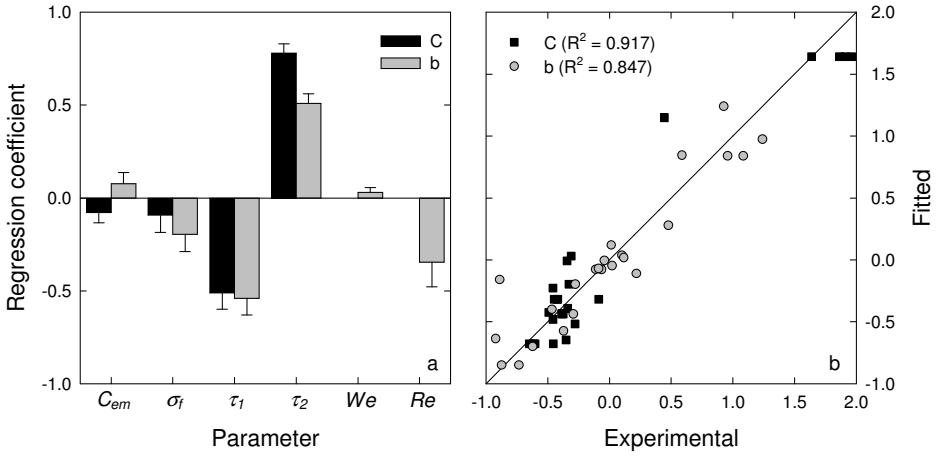

Figure IV.7 *Values of the regression coefficients of the different parameters from linearization of experimental data of HPH-emulsification (eqs. (IV.11) and (IV.12)) (a), and corresponding parity plot, reporting fitted vs. experimental values (b).*

The results of Figure IV.7a should be analyzed keeping in mind that a faster disruption kinetics is characterized by a low C value and a b value tending to 1 (Stang et al., 2001).

Figure IV.7a shows that the increase in the concentration of emulsifier is highly beneficial to the process of emulsification, with increasing C_{em} causing the decrease of C and the increase of b. Despite previous results showed that a small but measurable effect on disruption kinetics was caused by a viscosity increase due to large macromolecules (with molecular mass >> 100 kDa) (Stang et al., 2001), the increased viscosity of the emulsion, deriving from the increase of concentration of pea proteins and modified starch (Table IV.2), apparently did not affect the disruption kinetics. This is especially remarkable for pea proteins, whose molecular mass was previously shown to be in the range 49-80 kDa.

The interfacial properties of the emulsifier, which are lumped in the asymptotic value of the interfacial tension σ_f, exhibit a contrasting effect on the disruption kinetics: both regression coefficients are in fact negative. Nevertheless, it must be pointed out that the impact of a variation of σ_f on C is less significant than on b, meaning that the net impact of a good emulsifier (low σ_f) is a faster disruption kinetics.

The effect of the dynamic properties of the emulsifier was evaluated through the characteristic times τ_1 and τ_2 of adsorption at the O/W interface measured during the pendant drop experiments, adimensionalized by their respective mean values. Despite the kinetics of adsorption at the O/W interface in the pendant drop experiments can be significantly different from the kinetics of adsorption on the smaller emulsion droplets formed in the fluid dynamic field occurring in the homogenization chambers, a clear dependence of C and b values on adimensional τ_1 and τ_2 was observed. The decrease of the characteristic time of molecular adsorption and penetration in the oil phase (τ_1) causes the increase of both C and b, while the reduction of the characteristic time of reorganization at the interface (τ_2) determines the decrease of both C and b. Despite the values of the regression coefficients corresponding to τ_1 are comparable, a fractional variation of b has a significantly higher impact on the kinetics of disruption than a fractional variation of C of similar amplitude. On the other side, τ_2 has a lower impact, due to the main effect on C (lower τ_2 values contributes to reduce C) and a contrasting effect on b. Moreover, the regression coefficients corresponding to τ_1 and τ_2 are significantly higher than the regression coefficients of the other parameters considered, suggesting that the dynamic properties of the emulsifiers are the key determinants of the HPH-assisted disruption for the production of food nanoemulsions.

The results of Figure IV.7a also show that more intense elongational stresses contributes to accelerate the disruption kinetics, with lower C values and higher b values corresponding to higher We numbers. Nevertheless, the values of the corresponding regression coefficients are very small in

comparison to the other parameters, implying that the recoalescence stage is probably the limiting factor of the emulsification process.

The effect of *Re* number is contrasting, with increasing *Re* causing the decrease of *C*, as well as the decrease of *b*. Probably, a high *Re* number may contribute to the disruption efficiency, but is also responsible of a higher recoalescence degree in the homogenization chamber, due to the increased frequency of inter-droplet collisions.

From the sensitivity analysis it is possible to conclude that emulsifier interfacial and dynamic properties rules the disruption process when food emulsifiers are used and the emulsification process is carried out at the nanometric scale.

These results are quite different from the conclusions reached by Stang and coworkers, who showed that in a disruption-dominated HPH emulsification process, conducted with fast-adsorbing emulsifiers, the kinetics of disruption can be described by the power law of eq. (IV.1), with *b* values of about 0.6 for low-viscosity disperse phase (such as the case of sunflower oil) (Stang et al., 2001).

In contrast, in a stabilization/coalescence-dominated process, *b* values are always << 0.6 (Table IV.2), because the food-grade emulsifiers are not as fast as required to prevent completely recoalescence of newly formed droplets, as well as because in the reported experiments, nanometric size emulsions were obtained by multiple HPH passes at different pressure levels. In particular, recoalescence phenomena become more and more dominating when the emulsion droplet size is below 1 μm, such as for all the data reported in Figures IV.3-5.

In general, the production of food nanoemulsions by HPH requires the use of food-grade emulsifiers at a concentration as high as possible, compatibly with the product quality requirements and cost restrictions. Moreover, the homogenization chamber geometry should be able to ensure efficient droplet disruption, with high elongational stresses coupled with elevated turbulence, as well as a homogeneous volume of interaction downstream of the valve gap, where emulsifier adsorption at the droplet interface can occur uniformly to guarantee a low polydispersity index of the emulsion size distribution.

IV.5 Conclusions

High pressure homogenization processing for production of O/W nanometric emulsion is a process controlled by disruption efficiency achieved in the homogenization valve and by capability of the emulsifiers used to prevent recoalescence phenomena of newly formed droplets. For food application, the limiting stage is represented by the emulsifiers, whose requisites of food compatibility and use in limited amounts to minimize the

product quality, pose some limitations to their interfacial and dynamic properties.

The reported results showed that different emulsifiers, ranging from small molecules to biopolymeric macromolecules, can be characterized, by simple pendant drop measurements, in terms of interfacial properties and characteristic times of adsorption. These characteristics can be well correlated to the efficiency of the emulsification process.

Moreover, the geometry of the homogenization chamber plays a significant role, not that much in controlling the minimum mean droplet size achievable for a defined energy density delivered to the product, but especially in minimizing the width of the droplet size distributions. Homogenization chambers, where non-uniform flow regimes are established, are likely to produce wide particle size distributions that, as well as mean droplet diameters exceeding the nanometric size, are not acceptable for different applications of nanoemulsions in foods, such as the delivery of bioactive compounds.

Chapter V
Physicochemical stability of nanoencapsulated bioactives

In this chapter the physicochemical stability of some bioactive compounds, such as resveratrol, grape marc polyphenols and curcumin, encapsulated in O/W food-grade nanoemulsions of subcellular size, produced by high pressure homogenization, was evaluated under accelerated ageing conditions (high temperature, UV light exposure and high/low pH).

V.1 Nanoencapsulation of resveratrol

Resveratrol, a polyphenolic compound that can be found in red grapes, peanuts, as well as a variety of other plant sources, is one of the natural compounds that have been intensively investigated in recent years for its health-beneficial properties, and for potential applications in the fields of pharmaceutics, nutraceuticals and functional foods.
Resveratrol is well known for its high antioxidant activity and is considered as a key component for the health benefits of red wine. Chemically, resveratrol can be one of the two geometrical isomers, *trans*-resveratrol and *cis*-resveratrol, however, *trans*-resveratrol is the natural form of isomer and the more stable and the most active form (Filip et al., 2003).
Resveratrol is highly soluble in alcohols, whereas only soluble in trace amounts in aqueous or lipid phase. Its solubility was reported to be 0.023 mg/ml in drinking water (Asensi et al., 2002) and about 0.18 mg/ml in coconut oil (Hung et al., 2006). In addition, resveratrol is a very reactive molecule, very susceptible to react with dissolved oxygen, producing different degradation products, as well as very easily degraded by sunlight (Vian et al., 2005). The physicochemical properties of resveratrol, particularly its high reactivity and low solubility in aqueous and lipid phases,

have been limiting factors for its bioavailability and efficacies of the desired health-beneficial effects.

Therefore, exploitation of resveratrol as a functional food and nutraceutical ingredient or pharmaceutical compound is only feasible when encapsulated in a delivery system, which is capable of stabilizing and protecting it from degradation, while preserving its biological activities and enhancing its bioavailability. However, until now, only few studies have addressed the suitability of delivering encapsulated resveratrol to the site of action and the main research focus has been its biological activity, especially in synergy with the consumption of other diet/beverage components (Narayanan et al., 2009).

Encapsulation of resveratrol in delivery systems of micrometric size has been studied as a means to improve resveratrol stability and to control its release. In particular, polymeric microspheres have been used to improve resveratrol stability during long-term storage (Nam et al., 2005), and to improve the efficacies of a topical delivery (Hung et al., 2008) and a controlled-release formulation during oral application (Peng et al., 2010). Encapsulation in *Saccharomyces cerevisiae* cells has also been reported as an alternative strategy to significantly improve the release and stability of resveratrol (Shi et al., 2008).

On the contrary, encapsulation of resveratrol in delivery systems of nanometric size has been found to contribute even more significantly to the improvement of its cell uptake. For examples, nanometric carriers for pharmaceutical applications were designed using lipospheres to efficiently transport resveratrol into the cardiovascular system (Fang et al., 2007), while biodegradable polymeric nanoparticles (Shao et al., 2009) and liposomes were developed to enhance resveratrol chemopreventive efficacy (Narayanan et al., 2009). More recently, polymeric micelles have been used to enhance the ability of resveratrol to protect cells from oxidative stress and apoptosis (Lu et al., 2009), and solid lipid nanoparticles to increase the uptake of resveratrol in keratinocytes cells (Teskac and Kristl, 2010). In addition, cyclodextrins have been used as a carrier molecule to increase both bioavailability and stability of resveratrol through the formation of inclusion complexes (Lucas-Abellan et al., 2007).

Most of the above nanoparticulate carriers are based on hydrophobic interactions of resveratrol either with functional groups of specific molecules, such as biopolymers or cyclodextrins, or with amphiphilic molecular assemblies, such as liposomes or polymeric micelles. In all this cases, the ratio of the encapsulating functional molecules to resveratrol is very high, on one side strongly promoting its solubilisation in aqueous phase, but on the other side severely limiting the application in food, due to taste, regulations or cost constraints. Among the cited nanometric carriers, only solid lipid nanoparticles are suitable for food application, due to the high loading capacity and low emulsifier content. Nevertheless, the high cost

of production, related to the high processing temperature and pressure required, is still a limit to their full exploitation.
In food applications, an optimal delivery system of resveratrol would include a formulation containing all natural ingredients, which has minimal impact on the organoleptic properties of the food product, and is able to preserve resveratrol in its most active form during the different phases of food transformation and storage and to ensure high bioavailability upon ingestion.
Oil in water (O/W) nanoemulsions are ideal candidates for encapsulation of resveratrol, because of the easy fabrication by high-throughput processes (i.e. high pressure homogenization), the possibility of using all natural ingredients with low concentrations of emulsifiers (Donsi et al., 2010a, Donsi et al., 2011c, Donsi et al., 2011a), and the easy dispersibility in aqueous-based food matrices.
Since nanoemulsions have never been reported for the encapsulation of resveratrol because of the issues of formulation, stability and cell absorption, in this section is presented the contribution for the development of efficient nanoemulsion-based delivery systems for resveratrol. In particular, the main goal of the investigation activity is the fabrication of delivery systems, with requisites of (a) formulation with natural ingredients, (b) high physical stability of the emulsions and chemical stability of the most active form of resveratrol (*trans*-resveratrol) under conditions simulating the transformation and storage of the final product.

V.1.1 Materials and methods

V.1.1.1 Chemicals

Resveratrol, extracted from grape skin (purity > 98%), was a kind gift from Organic Herb Inc, China. Emulsion formulation was based on peanut oil (Sagra, Lucca, Italy) as organic phase, and the combination of lipophilic and hydrophilic emulsifiers. Lipophilic emulsifiers were soy lecithin Solec IP (a kind gift from Solae Italia s.r.l., Milan, Italy), soy lecithin Lecinova (Nutrition & Santè, Varese, Italy) and glycerol monooleate (Sigma-Aldrich s.r.l., Milan, Italy). Hydrophilic compounds were sugar ester P1670 (a kind gift from Prodotti Gianni, Milan, Italy), defatted soy lecithin Solec FS-B (a kind gift from Solae Italia s.r.l., Milan, Italy) and polysorbate Tween 20 (Sigma-Aldrich s.r.l., Milan, Italy). Bidistilled water was used as continuous phase.

V.1.1.2 Fabrication of nanoemulsions loaded with resveratrol

Resveratrol (0.01 wt%) was encapsulated in peanut oil-based nanoemulsions, produced by high pressure homogenization. A preliminary study was carried out to optimize the formulation by constructing a pseudo-ternary phase diagram of kinetic stability, which was used to determine the

optimal fractions of the different emulsion ingredients, as previously described chapter III.

The tested formulations had the following composition: 0.01°wt% resveratrol, 0.2°wt% ethanol, 1°wt% lipophilic soy lecithin Solec IP, 0.5°wt% defatted soy lecithin Solec FS-B, 6°wt% peanut oil, 92.29°wt% water (R/LSL-DSL); 0.01°wt% resveratrol, 0.2°wt% ethanol, 2.1°wt% soy lecithin Lecinova, 27.9°wt% peanut oil, 69.79°wt% water (R/LEC); 0.01°wt% resveratrol, 0.2°wt% ethanol, 1°wt% lipophilic soy lecithin Solec IP, 0.3°wt% sugar ester, 9°wt% peanut oil, 89.49°wt% water (R/LSL-SE); 0.01°wt% resveratrol, 0.2°wt% ethanol, 1.5°wt% polysorbate Tween 20, 1.5°wt% glycerol monooleate, 7°wt% peanut oil, 89.79°wt% water (R/T20-GMO).

Since the oil phase alone did not increase sufficiently the solubility of resveratrol, a small amount of ethanol (ethanol: resveratrol weight ratio was 20) was used to dissolve resveratrol crystals prior to mixing at room temperature with peanut oil and the eventual lipophilic emulsifier. The concentration of ethanol in oil was kept at 0.024 g/g, which is significantly lower than the equilibrium solubility of ethanol in different oils, which was reported to range at 25 °C from 0.125 g/g for canola oil to 0.147 g/g for corn oil (da Silva et al., 2010).

The lipid phase containing resveratrol was subsequently dispersed in the aqueous phase containing the hydrophilic emulsifier by high speed homogenization using an *Ultra Turrax T25* blender (IKA Labortechnik, *Jahnke und Kunkel, Germany*) at 24000 rpm for 4 min, to obtain a primary emulsion. The primary emulsion was then disrupted to the nanometric size in a Nano DeBEE Electric Bench-top laboratory high pressure homogenizer (BEE International, USA), by means of 10 passes at 300 MPa. The operating temperature was maintained at 10 °C, by initial conditioning of the primary emulsion in a thermostatic bath and by rapidly cooling the heat generated by friction with a heat exchanger, fitted immediately downstream of the homogenization valve. All formulations tested were prepared in triplicate.

V.1.1.3 Fluorescence spectrum of nanoencapsulated resveratrol

The fluorescence emission spectra of resveratrol water solution and nanoencaspsulated resveratrol were determined using a Jasco FP-8200 fluorescence spectrofluorometer (Jasco Europe, Milano). The excitation wavelength was set at 280 nm and the corresponding emission spectra were recorded in the range of 320-500 nm. The slit widths for excitation and emission were set both at 5 nm.

V.1.1.4 Physical stability

The physical stability of nanoencapsulated resveratrol was evaluated in terms of evolution of the mean droplet size of the nanoemulsions and of the

creaming volume over time under accelerated ageing conditions. For each formulation, three independent samples (15 ml) were stored vertically in plastic tubes at different temperatures (4, 30 and 55 °C) in dark condition, with observations being carried out for 4 weeks.

The droplet size distribution was determined by photon correlation spectroscopy (PCS) at 25 °C (HPPS, Malvern Instruments, UK). The mean droplet size (*Z-diameter*) was determined by Cumulant analysis of the intensity-intensity autocorrelation function, G(q,t) (Stepanek, 1993). Prior to measurements, the samples were diluted with bidistilled water to a suitable concentration.

The value of the creaming volume percentage *C* was computed for each nanoemulsion using eq. (V.1) (Roland et al., 2003):

$$C = 100\frac{(V_t - V_s)}{V_t} \qquad \text{(V.1)}$$

where V_t (ml) is the total volume of the sample and V_s (ml) is the volume of the lower phase layer (serum). According to eq. (V.1), the value of *C* tending to 100 is an indication of a stable emulsion. Physical stability tests were conducted in triplicates.

V.1.1.5 Chemical stability

The chemical stability of nanoencapsulated resveratrol was also evaluated under accelerated ageing conditions, by determining the kinetics of degradation upon UV light exposure and at three different storage temperatures (4, 30 and 55 °C).

For UV light stability, samples (20 ml) of each nanoemulsion containing resveratrol were exposed to a laboratory UV-C lamp (280-100 nm) at room temperature for 2 h. Aliquots were sampled at predetermined time points (10, 30, 60 and 120 min) for quantitative analysis.

For thermal stability, samples (15 ml) of resveratrol nanoemulsion were stored vertically in open test tubes in dark condition and aliquots were sampled each week for 4 weeks for quantitative analysis.

Quantitative analysis was conducted by extracting resveratrol from the emulsion and by using HPLC. One ml of resveratrol nanoemulsion was mixed in a test-tube with 400 µl of carbon tetrachloride and 400 µl of ethanol, by agitation on a vortex mixer for 15 s. The separation of the phases was improved by centrifugation at 6500 rpm for 5 min at 10 °C. The lighter phase, which contains resveratrol, was recovered with a Pasteur pipette and the heavier phase was then extracted twice with 500 µl of ethanol. Anhydrous sodium sulphate was added to the organic phase to remove any traces of water, prior to concentration under reduced pressure (Rotavapor) at 36 °C and the residue was redissolved in 1 ml of ethanol. The resveratrol extract was then injected in the HPLC system, consisting of a Waters 1525

Binary HPLC pump and a UV-Vis 2487 Waters Dual Absorbance Detector. A RP C18 Spherisorb® (Waters, 5 µm, 4.6 x 250 mm) column was used, and the separation was done using an isocratic mobile phase of 45% methanol in water (v/v) which was adjusted to pH 2.6 with acetic acid. The flow rate was 0.8 ml/min and the injection volume was 10 µl. The UV/visible detector was set at 306 nm for *trans*-resveratrol and at 280 nm for *cis*-resveratrol.

Quantification of *trans*-resveratrol was based on a calibration curve generated with serial dilutions (0.1 and 100 mg/l) of the stock solution of 200 mg/l in ethanol. The calibration curve of *cis*-resveratrol was obtained using the standard solutions of *trans*-resveratrol exposed to daylight for 1 h, because of the unavailability of commercial standard. According to a previously reported method (Vian et al., 2005), the concentrations of *cis*-resveratrol were assigned on the basis of the decreased levels of intensity of the *trans*-resveratrol peak which were proportional to the area of the *cis*-resveratrol peak.

The effect of encapsulation on the kinetics of degradation under UV light and at different temperatures was evaluated in terms of retention percentage, θ_{trans}, shown in eq. (V.2), and of yield of *cis*-resveratrol with respect to the initial *trans*-resveratrol content, θ_{cis}, shown in eq. (V.3) (Shi et al., 2008).

$$\theta_{trans} = \frac{c_{trans}(t)}{c_{trans}(t_0)} \tag{V.2}$$

$$\theta_{cis} = \frac{c_{cis}(t)}{c_{trans}(t_0)} \tag{V.3}$$

The chemical stability of encapsulated resveratrol was compared with unencapsulated resveratrol, which was dissolved in ethanol (ethanol: resveratrol weight ratio was 20) and then in water until the same resveratrol concentration of nanoemulsions was reached. Chemical stability tests were conducted in triplicates.

V.1.2 Results

V.1.2.1 Formulation of stable nanoemulsions

Resveratrol was encapsulated in peanut oil-based nanoemulsions at a final concentration of 0.01% by weight. The resveratrol concentration used was preliminary chosen to be 10 times higher than the therapeutic blood concentration, which is at least 10 mg/l (Yu et al., 2003).

The percentage of each ingredient and the formulation of the nanoemulsion-based delivery systems were largely determined according to

the use of the lipophilic and hydrophilic emulsifiers with the ultimate goal of improving resveratrol entrapment in the lipid phase by hydrophobic interactions, thus reducing the extent of localization of resveratrol at the O/W interface, where it can be easily degraded (Fang et al., 2007).

Resveratrol localization can be determined by investigating the extent of hydrophobic interactions between resveratrol and emulsion constituents (lipid phase and emulsifiers) through fluorescence spectroscopy.

Considering that resveratrol itself is a fluorescent compound, and the fact that the fluorescence spectrum of a compound is usually affected by its microenvironment (Hailong and Qingrong, 2010), the comparison of the fluorescent emission spectrum of resveratrol in pure water with that of resveratrol in nanoemulsion shows that the characteristic emission peak of resveratrol is shifted from 400 nm in water to 386 nm when resveratrol was encapsulated in peanut oil-based nanoemulsion (Figure V.1). This result confirms that microenvironment of resveratrol is changed after encapsulation, supporting the hypotheses of its entrapment in the nanoemulsion lipid phase.

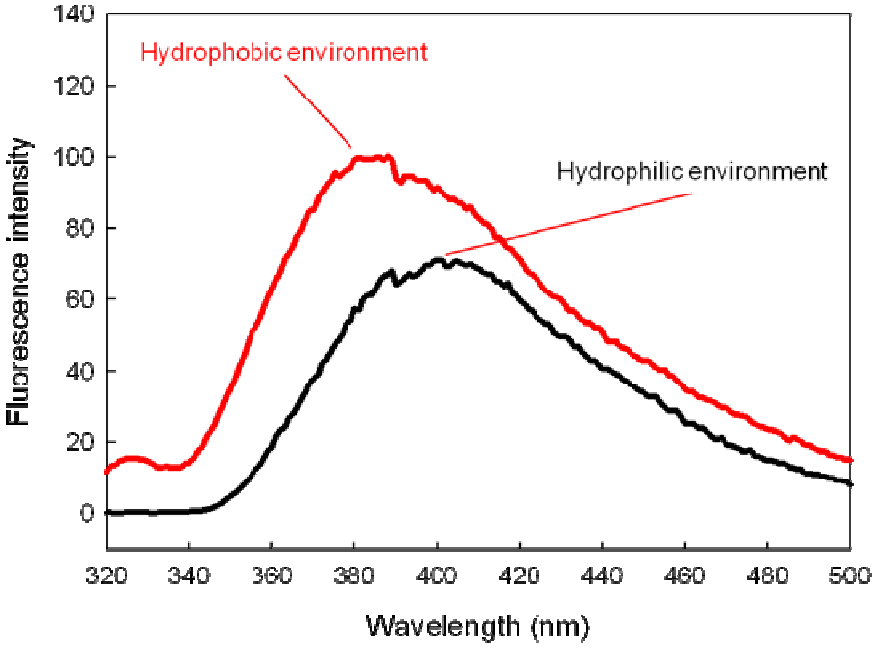

Figure V.1 *Fluorescence emission spectra of resveratrol dissolved in water and encapsulated resveratrol into peanut oil-based nanoemulsion.*

V.1.2.2 Physical stability

The physical stability of the resveratrol-encapsulating nanoemulsions was evaluated in terms of the evolution of their mean droplet diameter under accelerated ageing conditions at different storage temperatures (4, 30 and 55 °C) for 30 days. Both lecithins-based nanoemulsions, R/LEC and R/LSL-DSL, characterized by an initial mean droplet diameter of 270 and 230 nm, respectively, and sugar ester-based nanoemulsion R/LSL-SE, with an initial mean droplet diameter of 160 nm, exhibited no significant variations of the *Z-diameters* at all storage temperatures (Figure V.2b, d and f). On the contrary, the nanoemulsion R/T20-GMO, which exhibited smaller initial mean droplet diameter (90 nm), was stable only at low temperatures (4 and 30 °C), while at 55 °C underwent significant instability phenomena, highlighted by a drastic increase of *Z-diameter* already at day 14 (Figure V.2f).

The different physical stability of the nanoemulsions tested could be related to the different emulsifiers used, with the respective interfacial properties depending on the kinetics of adsorption at the O/W interface as well as on the subsequent molecular reorganization at the interface (Donsi et al., 2011b). Molecules with high mobility and fast adsorption kinetics, such as polysorbate, significantly contribute to reduce recoalescence phenomena during high pressure homogenization, because of the extremely short times of coverage of the newly formed droplet surfaces. On the other side, at increasing temperature, the muted thermodynamic conditions may induce the displacement of emulsifier molecules from the O/W interface. Emulsifiers with higher molecular mobility will therefore exhibit higher instability and coalescence phenomena, as observed for polysorbate-based nanoemulsions (R/T20-GMO).

The evolution of the creaming volume percentage *C* over time was coherent with the droplet size measurements. *C* remained constant at about 100% for all nanoemulsions at 4 °C (Figure V.2a), decreased by 10% at most after 30 days for all the formulations at 30 °C, except for R/T20-GMO which remained completely stable (Figure V.2c). This parameter was reduced by 30% for R/LEC and R/LSL-DSL and by 10% for R/T20-GMO and R/LSL-SE after 30 days at 55 °C (Figure V.2e).

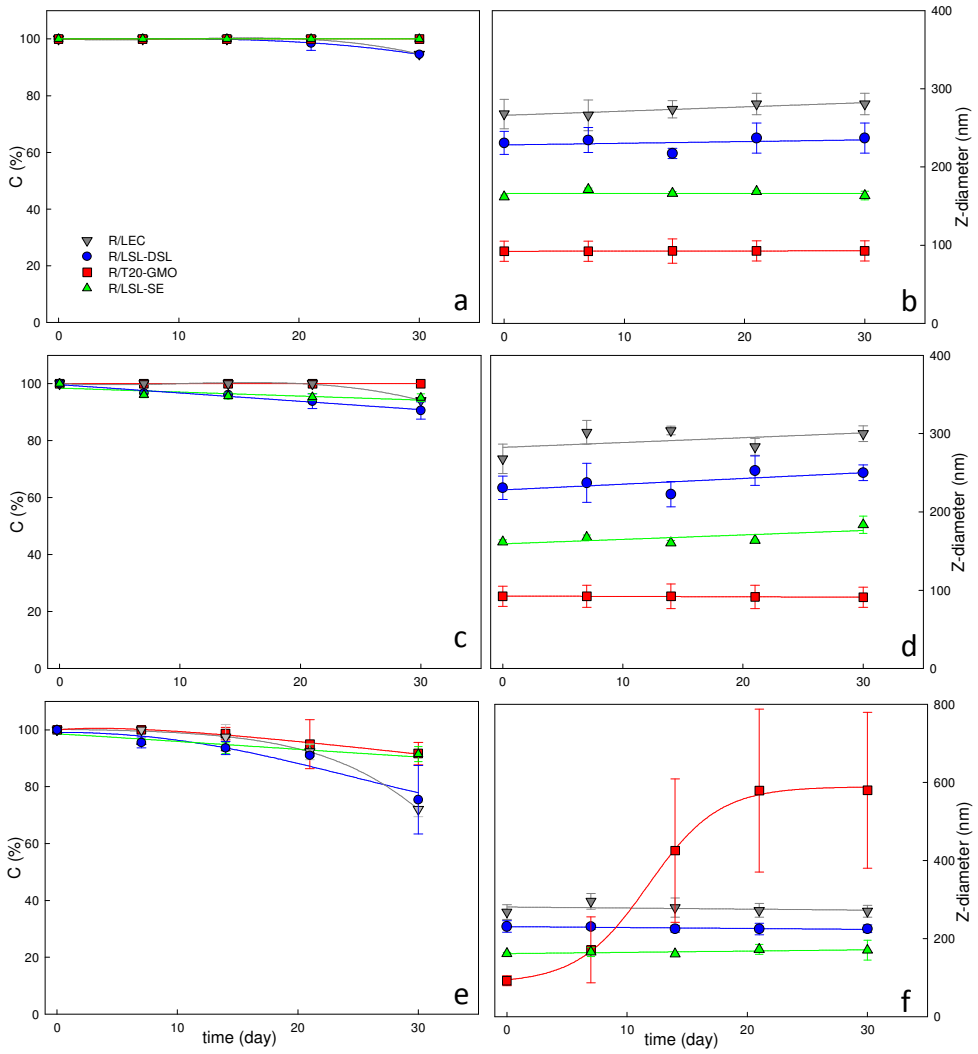

Figure V.2 *Evolution of the creaming volume percentage, C, (a, c and e) and of the mean droplet diameter, Z-diameter, (b, d and f) of the resveratrol-encapsulated nanoemulsions stored at 4 °C (a, b), 30 °C (c, d) and 55 °C (e, f) for 30 days.*

V.1.2.3 Chemical stability

The chemical stability of the encapsulated resveratrol was evaluated for the retention percentage of *trans*-resveratrol, θ_{trans}, and the formation yield of *cis*-resveratrol, θ_{cis}, under different storage conditions.

Preliminary studies showed that *trans*-resveratrol, which is extremely photosensitive and susceptible to oxidative degradation, remained stable during the nanoencapsulation process. In fact, the typical HPLC chromatograms of unencapsulated and nanoencapsulated resveratrol had the same retention time at about 8 min under the same chromatographic conditions used in this study. In addition, the UV-Vis spectra of the unencapsulated and nanoencapsulated resveratrol exhibited the same pattern, with the absorption maximum at 306 nm, in agreement with previous results (Vian et al., 2005). The same HPLC retention time and UV-Vis spectrum suggested that no chemical changes occurred during the nanoencapsulation process.

The exposure of unencapsulated resveratrol to UV-C light showed the formation of the *cis*- form of resveratrol. In fact, the area of *trans*-resveratrol decreased and a new peak appeared, with its area increasing with the exposure time. More specifically, the UV-Vis spectrum of the new peak was consistent with that of *cis*-resveratrol, with the absorption maximum at 280 nm (Vian et al., 2005). Therefore, the new peak can be ascribed to *cis*-resveratrol, formed from *trans*-resveratrol due to UV light exposure, as previously reported (Shi et al., 2008). It must be pointed out that in this study the formation of *cis*-resveratrol was used as a qualitative instead of a quantitative indicator of *trans*-resveratrol oxidation.

Figure V.3 reports the evolution of θ_{trans} (Figure V.3a) and of θ_{cis} (Figure V.3b) of unencapsulated and nanoencapsulated systems. The *trans*-resveratrol was significantly degraded ($\theta_{trans} \approx 45\%$) after a 2 h exposure to UV-C light. Concurrently θ_{cis} increased up to 0.04%, with trace amounts of *cis*-resveratrol appearing already after 10 min of UV-C light exposition.

Nanoencapsulated resveratrol was more stable under the UV-C light compared to the unencapsulated compound, with a slower rate of degradation of *trans*-resveratrol and less formation of *cis*-resveratrol (Figure V.3a and b). In particular, for R/LSL-SE and R/LEC only a limited degradation of *trans*-resveratrol was observed, with θ_{trans} being reduced to 83% and 92% respectively, and no formation of *cis*-resveratrol being detected over the exposure time. R/T20-GMO system exhibited a comparable *trans*-resveratrol degradation (≈ 82%), but detectable *cis*-resveratrol ($\theta_{cis} \approx 0.03\%$) after 2 h of light exposure. R/LSL-DSL was the least stable system which exhibited a reduction of the θ_{trans} value ≈ 65% and a sustained increase of θ_{cis} value, which was however slower than that of the unencapsulated resveratrol.

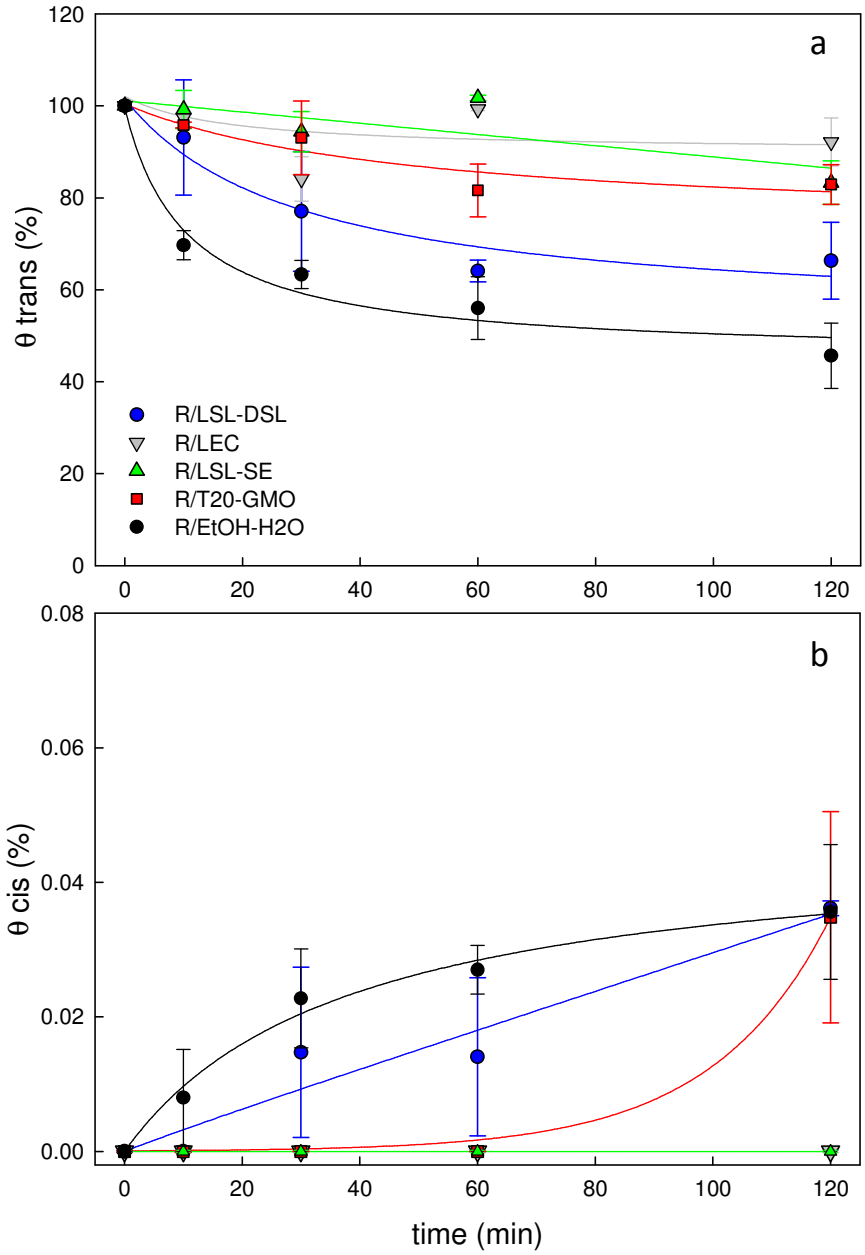

Figure V.3 *The retention percentage of trans-resveratrol, θ_{trans}, (a) and cis-resveratrol yield, θ_{cis}, (b) under UV-C light exposure.*

Figure V.4 shows the kinetics of degradation of unencapsulated and nanoencapsulated resveratrol at three different storage temperatures (4, 30 and 55 °C). In all cases *cis*-resveratrol was never detected.

Under refrigerated conditions (4 °C) and at 30 °C nanoencapsulated resveratrol remained extremely stable for all the formulations, with a reduction of θ_{trans} value ≈ 70% being observed only for R/LSL-DSL after 30 days (Figure V.4a and b).

On the contrary, the unencapsulated resveratrol exhibited a different behaviour, with active resveratrol being better preserved at higher temperatures. In particular, a severe chemical degradation occurred at 4°C, which reduced the θ_{trans} value to ≈ 50% after 30 days (Figure V.4a), while θ_{trans} value was substantially stable at 30 °C (Figure V.4b) and at 55 °C (Figure V.4c). This can be explained by increased oxidative degradation due to the higher solubility of oxygen in water at lower temperatures. Therefore, the observed stable behaviour of the encapsulated compound at lower temperature means that the nanoencapsulation process prevented the chemical degradation of resveratrol, effectively protecting it from contact with oxygen molecules dissolved in the water.

Trans-resveratrol in all nanoemulsion formulations degraded significantly after 30 days at 55°C (Figure V.4c), which can be explained by its interaction with the emulsion ingredients and the destabilization of the nanoemulsion as shown in Figure V.2f.

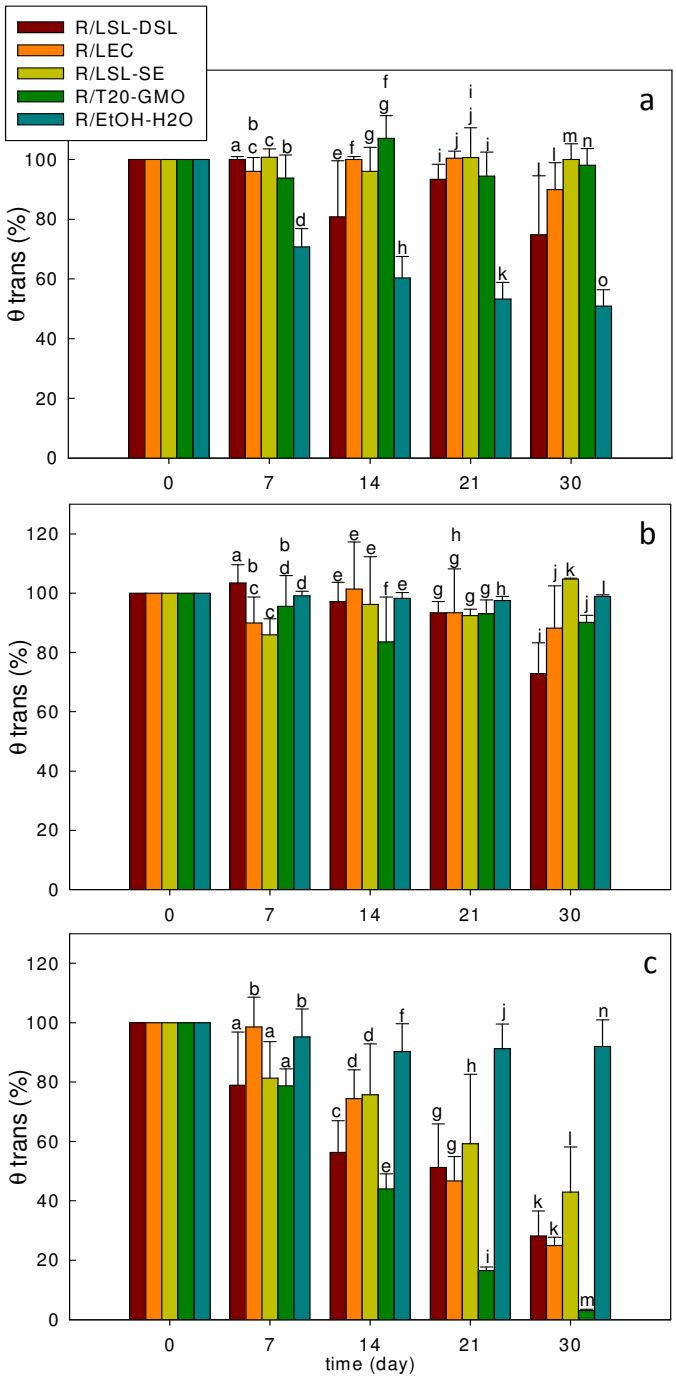

Figure V.4 *The retention percentage of trans-resveratrol, θ_{trans}, at 4 °C (a), 30 °C (b) and 55 °C (c) for 30 days. Different letters in the same day indicate statistically (Student t-test) significant differences ($p<0.05$).*

V.2 Nanoencapsulation of grape marc polyphenols

The increase in demand for processed crop products has substantially increased the amount of waste produced during food processing, giving consequently impulse to the search of possible solutions for waste recovery. For example, in the wine industry, vast amounts of grape marc is produced as a waste: every 100 kilograms of grape-vine generates approximately 20-25 kilograms of grape marc. Grape marc has a heavy environmental impact for the high content of phenols that considerably increase chemical and biochemical oxygen demands (Spigno and De Faveri, 2007), making its disposal an increasing environmental problem. The industrial exploitation of this by-product was oriented to its use as animal feed (Vaccarino et al., 1992), as organic fertilizer (Ferrer et al., 2001), or in harvesting yeast cells (Lo Curto and Tripodo, 2001). More attractive are instead those options with higher added value, involving the extraction and recovery of bioactive plant constituents from grape seeds and skins (Bonilla et al., 1999, Negro et al., 2003, Amendola et al., 2010), such as anthocyanins to be used as natural dyes (Vatai et al., 2009), as well as polyphenols to be used as a low-cost natural source of antioxidants for the pharmaceutical, nutraceutical and food industries. The exploitation of grape marc wastes as a source of antioxidant compounds can also greatly contribute to reduce their production costs while increasing the margin profit (Spigno and De Faveri, 2007).

Recovery of antioxidant compounds from grape marc is mainly carried out by organic solvent extraction, with the extraction yield being increased by non-conventional techniques, such as ultrasound-assisted extraction (UAE) (Ghafoor et al., 2009, Palma and Barroso, 2002), microwave-assisted extraction (MAE) (Li et al., 2011), as well as high pressure and temperature extraction (HPTE) (Casazza et al., 2010b).

The polyphenols are generally characterized by scarce solubility in water, which severely limit their use in pure form as bioactive compounds in functional foods, because of insufficient solubility in the GI tract and low permeability to pass through the intestinal wall (Haslam, 1996).

Consequently, their effective oral delivery requires the encapsulation in nanometric size carriers, such as O/W nanoemulsions or solid lipid nanoparticles.

The aim of this section is to show how polyphenolic compounds, recovered from grape marc, can be exploited as natural antioxidants for possible use in functional foods and nutraceutical products, by means of their encapsulation into nanoemulsion based delivery systems. Based on these premises, the polyphenols nanoencapsulation will be carried out using solely food-grade solvents and ingredients. The delivery systems will be validated by evaluating the stability of the extracts under accelerated storage.

V.2.1 Materials and methods

V.2.1.1 Chemicals

Skins and seeds of Pinot Noir cultivar from white-vinification (a kind gift from a company located in Trentino region, Italy) were used for the extraction of polyphenols.

Emulsion formulations were based on sunflower oil (Sagra, Italy) or palm oil (Fluka, Germany) as organic phase, and the combination of lipophilic and hydrophilic emulsifiers. Defatted soy lecithin Solec FS-B (a kind gift from Solae Italia s.r.l., Italy) was used as hydrophilic emulsifier, while soy lecithin Solec IP (a kind gift from Solae Italia s.r.l., Italy) and glycerol monooleate (Sigma-Aldrich, Germany) as lipophilic emulsifiers. Bidistilled water was used as continuous phase.

V.2.1.2 Extraction of grape marc polyphenols

Grape marc (skins and seeds) were separated from stalks manually and then by means of sieves. After that, the samples were washed in order to eliminate the possible rest of the pomace. The samples were oven-dried at 65 °C to a constant moisture of about 4-5 % (D-82152, MMM Medcenter, München, Germany) (Fiori et al., 2009). Samples were then ground with the help of a laboratory mixer to obtain a homogeneous powder for extraction with a particle size of 0.80 ± 0.05 mm.

Dried and ground samples were extracted by methanol with a constant solid liquid ratio of 1:5. Extraction tests were performed in a high pressure high temperature reactor (HPTE) model 4560 (PARR Instrument Company, Moline, IL, USA). Grape marc was extracted at 150 °C for 150 min of contact time following the method previously described (Casazza et al., 2011).

After the reaction, the alcoholic extracts were centrifuged by a PK 131 centrifuge (ALC, Alberta, Canada) at 6000 xg for 10 min and the supernatant was subjected to quantitative analysis.

The supernatants were then subject to total polyphenol analysis, using the Folin-Ciocalteau assay as described previously (Casazza et al., 2010a).

The single phenolic compound analysis was carried out using a HPLC (1100 Series, Hewlett Packard, Palo Alto, CA, USA) equipped with a C18 reverse-phase column (201TP54, Vydac, Hesperia, CA, USA) coupled with a UV-Vis detector. The mobile phase was water/acetic acid (99:1 %, v/v) and methanol/acetonitrile (50:50 %, v/v), following a previously described method (Aliakbarian et al., 2011).

V.2.1.3 Encapsulation of grape marc polyphenols at the nanoscale

Grape marc polyphenols were encapsulated in nanoemulsion-based delivery systems by high pressure homogenization (HPH) technique. First of all the grape marc polyphenols in methanol were dispersed in the lipid and lipophilic emulsifier phase on a hot plate at a temperature of 60 °C to obtain the melting of the lipid (in the case of palm oil), as well as the evaporation of the methanol. Subsequently, the primary emulsions were prepared mixing the lipid and water phases by high shear homogenization (HSH) using an Ultra Turrax T25 (IKA Labortechnik, Jahnke und Kunkel, Germany) at 16800 rpm for 3 min at 60 °C. The emulsion droplets embedding the polyphenolic compounds were finally reduced to nanometric size by high pressure homogenization in a Nano DeBEE Electric Bench-top Laboratory homogenizer (BEE International, USA) at 200 MPa for 10 passes, maintaining the temperature during processing always at about 60 °C through heat exchange downstream of the homogenization valve and thermal conditioning of the inlet tank. All formulations were prepared in duplicate.

V.2.1.4 Physical stability

The physical stability of nanoencapsulated grape marc polyphenols was evaluated in terms of evolution of the mean droplet size of the nanoemulsions and of the creaming volume over time under accelerated ageing conditions according to the method described in the section *V.1.1.4*.

V.2.1.5 Chemical stability

The chemical stability of nanoencapsulated grape marc polyphenols was evaluated by recording the evolution of the ultraviolet–visible (UV–Vis) absorption spectra of the encapsulated polyphenols, at three different storage temperatures (4, 30 and 55 °C) for 14 days. The UV-Vis measurements were performed in the range of 250-450 nm using a V-650 UV-Vis spectrophotometer (Jasco Instruments, USA). Prior to measurements, the samples were diluted with bidistilled water to a suitable concentration. Chemical stability tests were conducted in duplicates.

V.2.3 Results

V.2.3.1 Composition of the polyphenols in the grape marc extracts

The poliphenolic compounds were extracted from grape marc using high pressure and temperature extraction (HPTE) with methanol as solvent to obtain improved extraction yield and antioxidant power of the extracts in comparison to conventional methods, as previously discussed (Casazza et al., 2010a).

The polyphenol concentration in the extract was 51.2 mg of gallic acid equivalent per g of dried marc, while the concentration in the methanolic extract was 12.29 $mg/ml_{methanol}$.

The content of the main phenolic compounds contained in the extracts is reported in Table V.1 per gram of dry extracts and per milliliter of extracting solvent. The most abundant phenolic compound is syringic acid (3.09 mg/g_{DW}), followed by catechin, gallic acid and quercetin. *Trans*-resveratrol was detected only in trace amounts (0.39 mg/g_{DW}).

Table V.1 *Total polyphenols and main phenolic compounds content (mg/g_{DW}) and concentration ($mg/ml_{methanol}$) in skin extract obtained by HPTE and analyzed with Folin-Ciocalteau and HPLC.*

	TP[1]	Single phenolic compounds								
		GA[2]	HMF[3]	PA[4]	CA[5]	VAA[6]	SA[7]	CUA[8]	RSV[9]	QE[10]
Extraction yield (mg/g_{DW})	51.20	1.44	0.16	0.46	2.67	0.18	3.09	0.16	0.39	1.21
Concentration ($mg/ml_{methanol}$)	12.29	0.35	0.04	0.11	0.64	0.04	0.74	0.04	0.09	0.29

[1] Total polyphenols; [2] gallic acid; [3] 5-hydroxymethylfurfural; [4] protocatecuic acid; [5] catechin; [6] vanillic acid; [7] syringic acid; [8] cumaric acid; [9] *trans*-resveratrol; [10] quercetin.

The total amounts of individual phenolic compounds quantified by HPLC (9.76 mg/g_{DW}) was significantly lower than the value of total polyphenols measured by the Folin–Ciocalteau colorimetric method (51.2 mg_{GAE}/g_{DW}), because of the low selectivity of the Folin–Ciocalteu reagent, that reacts positively with different antioxidant compounds (phenolic and non-phenolic substances) (Que et al., 2006).

V.2.3.2 Physicochemical stability of the nanoencapsulated polyphenolic extracts

Grape marc polyphenols were encapsulated at a final concentration of 0.1% (w/w) in sunflower oil and palm oil-based nanoemulsions.

The polyphenolic compounds were encapsulated in the core of the tested nanoemulsion by using a dual-emulsifier formulation, which was previously tested in the nanoencapsulation of resveratrol (Sessa et al., 2011). In particular, the addition of a lipophilic emulsifier such as glycerol monooleate or soy lecithin to the lipid phase improves the hydrophobic interactions and

hydrogen bonding with the polyphenolic compounds, which are scarcely soluble both in lipid and in aqueous phase. The hydrophilic emulsifier (defatted soy lecithin) contributed not only to the stabilization of the lipid droplets in the continuous aqueous phase, but also to limit the localization of polyphenols at the oil/water interface, thus improving the encapsulation in the lipid phase by hydrophobic interactions.

Table V.2 reports the compositions of those formulations that resulted to be stable. The total lipid phase, consisting of the oil and of the lipophilic emulsifier, was always kept at a fixed concentration of 10% (w/w), varying the type of oils and emulsifiers used.

Table V.2 *Composition, mean droplet size (Z-diameter) and polidispersity index (PDI) of the stable delivery systems of the grape marc polyphenols.*

Delivery systems	Composition	Z-diameter (nm)	PDI
SO/GMO-DSL	0.1% grape marc polyphenols 1% glycerol monooleate 0.5% defatted soy lecithin 9% sunflower oil 89.4% water	176 ± 2	0.130 ± 0.07
SO/LSL-DSL	0.1% grape marc polyphenols 1% lipophilic soy lecithin 0.5% defatted soy lecithin 9% sunflower oil 89.4% water	219 ± 4	0.190 ± 0.03
PO/GMO-DSL	0.1% grape marc polyphenols 1% glycerol monooleate 0.5% defatted soy lecithin 9% palm oil 89.4% water	1330 ± 124	0.980 ± 0.09
PO/LSL-DSL	0.1% grape marc polyphenols 1% lipophilic soy lecithin 0.5% defatted soy lecithin 9% palm oil 89.4% water	178 ± 2	0.140 ± 0.03

The physical stability of encapsulated grape marc polyphenols was evaluated in terms of the evolution over time of the mean droplet diameter, *Z-diameter*, and the creaming volume percentage, *C*, under accelerated ageing conditions.

The sunflower oil-based nanoemulsions, SO/GMO-DSL and SO/LSL-DSL, characterized by an initial mean droplet diameter of 175 and 220 nm respectively, showed no significant ($p < 0.05$) variation of *Z-diameter* at all storage temperatures (Table V.3). The good physical stability of these formulations was confirmed by the evolution of the creaming volume percentage, which exhibited at all tested temperatures a decrease below 5% (Figure V.5a and b).

Unlike the sunflower oil-based nanoemulsions, the palm oil-based systems, PO/LSL-DSL and PO/GMO-DSL, exhibited different trends of physical stability under accelerated ageing. PO/LSL-DSL, characterized by an initial mean droplet size of 180 nm, showed a slight increase of the *Z-diameter* until 250 nm over the 14 days of storage at all the tested temperatures (Table V.3). In contrast, PO/GMO-DSL, formulated with glycerol monooleate as lipophilic emulsifier, was characterized by an initial mean droplet diameter, as measured immediately after HPH treatment, in the micrometric range (1300 nm), probably due to the formation of aggregates of the solid fat droplets. This hypothesis is confirmed by the evolution of the *Z-diameter* over storage time: while at lower temperatures a micrometric mean droplet size is always observed, when the temperature is increased above the melting temperature of the palm oil (i.e. for storage temperature of 55 °C), the mean droplet size decreases to values similar to the other tested systems (around 200 nm), as shown in Table V.3.

This phenomenon can be attributed to the break-down of the droplet aggregates when the storage temperature is higher than the melting point of the lipid phase. The evolution of the creaming volume percentage, *C*, over time was coherent with the droplet size measurements. For PO/LSL-DSL, *C* remained constant at about 100% at 4 and 30 °C and decreased slightly at about 88% at 55 °C (Figure V.5d). On the contrary, for PO/GMO-DSL *C* was constant only at 4 °C, while a decrease of *C* by 20 and 25% was measured at 30 and 55 °C respectively (Figure V.5c), in accordance with an unstable behaviour observed in the particle size measurements.

Table V.3 *Evolution of the mean droplet diameter (Z-diameter) of the encapsulated grape marc polyphenols in sunflower oil-based (SO/GMO-DSL and SO/LSL-DSL) and palm oil-based (PO/GMO-DSL and PO/LSL-DSL) delivery systems, stored at 4, 30 and 55 °C for 14 days. Different lowercase letters in the same day indicate statistically (Student t test) significant differences (p<0.05). Different capital letters at a fixed storage temperature indicate statistically (Student t test) significant differences (p<0.05).*

Delivery system	Time (day)	Z-diameter (nm)		
		4 °C	30 °C	55 °C
SO/GMO-DSL	0	176 ± 2 a, A	176 ± 2 a, D	176 ± 2 a, G
	1	183 ± 3 b, B	185 ± 10 b, E	180 ± 1 b, H
	3	184 ± 4 c, B	178 ± 1 d, D F	189 ± 8 c, I L
	6	183 ± 5 e, B C	182 ± 5 e, E F	192 ± 11 f, I
	10	178 ± 1 g, A C	175 ± 1 h, D	185 ± 1 i, L
	14	181 ± 2 l, B C	181 ± 1 l, E	192 ± 2 m, I
SO/LSL-DSL	0	219 ± 4 a, A	219 ± 4 a, F	219 ± 4 a, L
	1	231 ± 11 b, B C	326 ± 6 c, G	256 ± 21 d, M
	3	254 ± 19 e, D	227 ± 2 f, H	248 ± 15 e, M N
	6	239 ± 9 g, B E	225 ± 2 h, H	238 ± 20 g, N P
	10	247 ± 31 i, D E	216 ± 1 l, F	273 ± 7 m, O
	14	225 ± 2 n, C	232 ± 2 o, I	229 ± 2 o, P
PO/GMO-DSL	0	1330 ± 124 a, A	1330 ± 124 a, G	1330 ± 124 a, O
	1	19400 ± 8000 b, B	1530 ± 523 c, H	1670 ± 85 d, P
	3	13600 ± 976 e, C	1120 ±199 f, I	220 ± 34 g, Q
	6	13900 ± 3010 h, D	971 ± 175 i, L	199 ± 2 l, R
	10	18300 ± 2480 m, E	2610 ± 1030 n, M	208 ± 4 o, Q
	14	17800 ± 1630 p, F	5720 ± 3800 q, N	190 ± 3 r, S
PO/LSL-DSL	0	178 ± 2 a, A	178 ± 2 a, F	178 ± 2 a, L
	1	188 ± 7 b, B	187 ± 7 b, G	213 ± 20 c, M
	3	184 ± 2 d, B	207 ± 33 e, H	248 ± 42 f, N
	6	226 ± 28 g, C	243 ± 23 h, I	215 ± 34 g, M
	10	241 ± 3 i, D	180 ± 1 l, F	296 ± 8 m, O
	14	246 ± 3 n, E	197 ± 2 o, H	251 ± 10 n, N

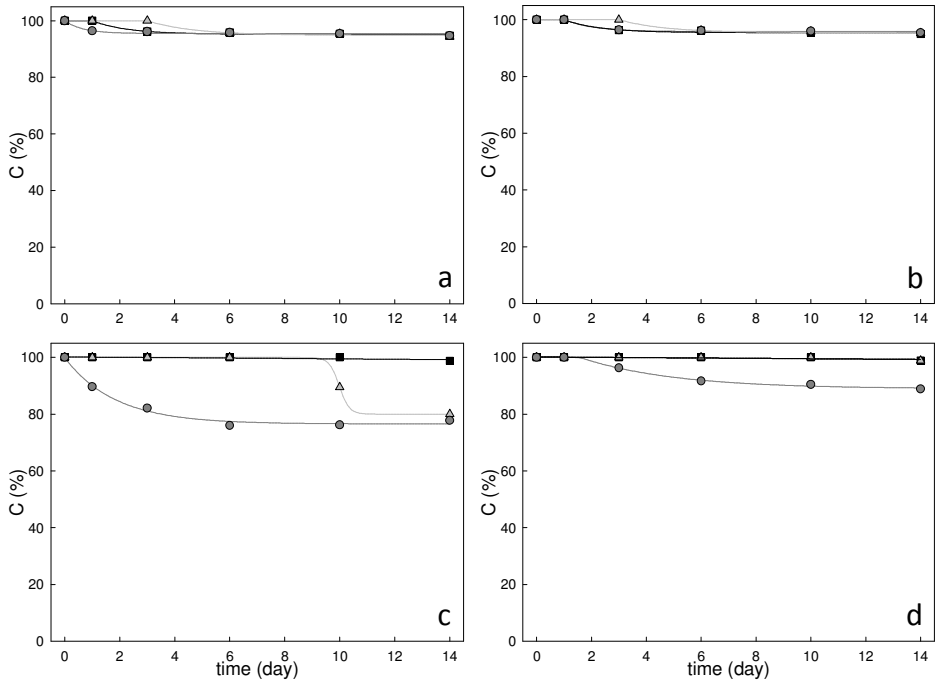

Figure V.5 *Evolution of the creaming volume percentage, C, of the encapsulated grape marc polyphenols into different delivery systems: (a) SO/GMO-DSL, (b) SO/LSL-DSL, (c) PO/GMO-DSL and (d) PO/LSL-DSL. Storage temperatures were 4 °C* (■)*, 30 °C* (△) *and 55 °C* (●).

The chemical stability of the nanoencapsulated grape marc polyphenols was evaluated monitoring the evolution of their UV-Vis absorption spectra over 14 days of storage at different temperatures (4, 30 and 55 °C), with the results being reported in Figure V.6. It must be highlighted that the chemical stability of the different systems reproduced the same trends observed for the physical stability. The SO/GMO-DSL and SO/LSL-DSL systems were able to efficiently protect the grape marc polyphenols from degradation over 14 days at all the storage temperatures (Figure V.6.1a, 2a, 3a and Figure V.6.1b, 2b, 3b). In contrast, the palm oil-based systems were less efficient, with a slight decrease of the absorbance peak being measured after 14 days for PO/LSL-DSL and a much more significant decrease already after 3 days for PO/GMO-DSL, suggesting the release of the encapsulated compounds and subsequent degradation (Figure V.6.1d, 2d, 3d and Figure V.6.1c, 2c, 3c). The unstable behaviour of grape marc polyphenols nanoencapsulated in the formulation PO/GMO-DSL is in agreement with the observed physical instability of the system.

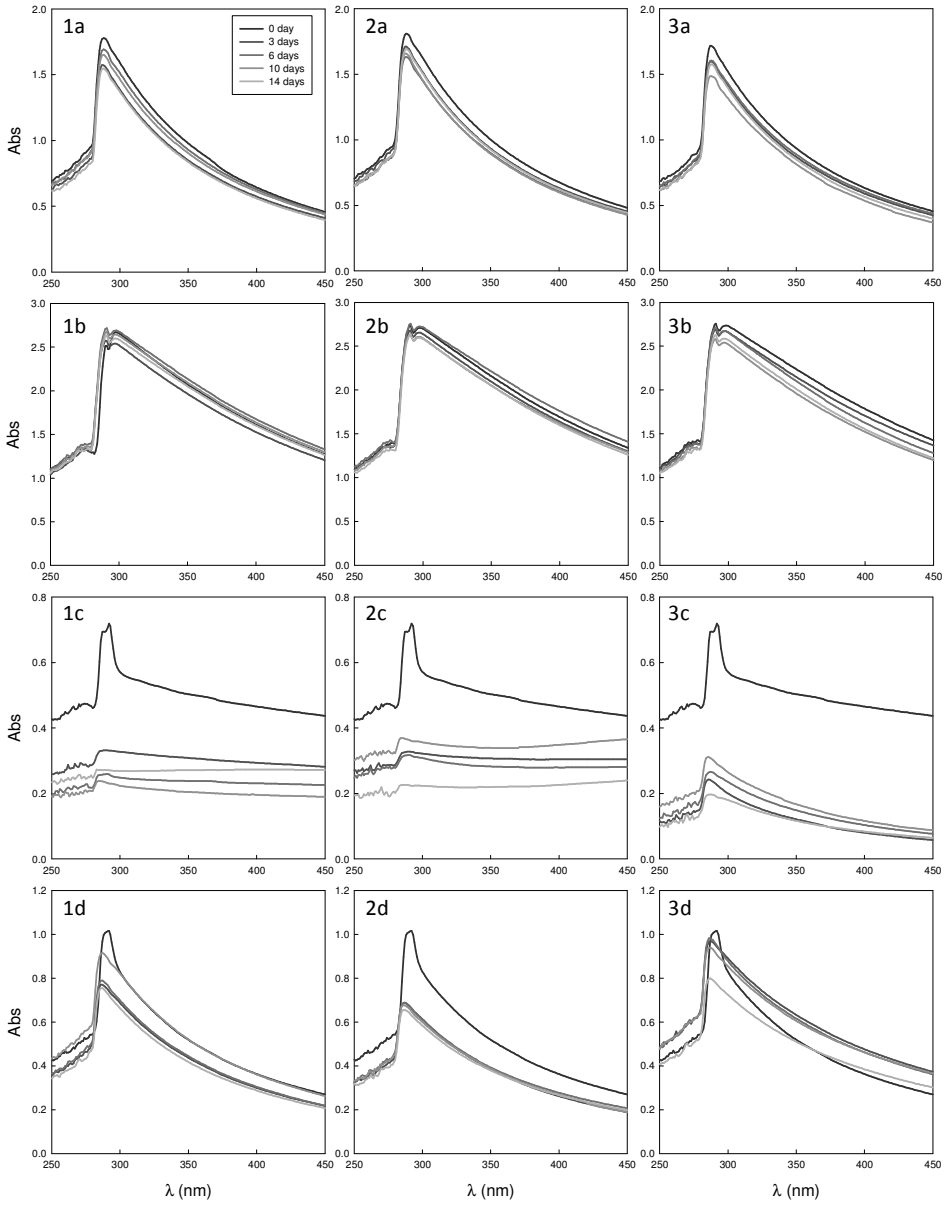

Figure V.6 *The UV-Vis absorption of the encapsulated grape marc polyphenols into different nanoemulsions: a) SO/GMO-DSL, b) SO/LSL-DSL, c) PO/GMO-DSL and d) PO/LSL-DSL, after storage at 1) 4 °C, 2) 30 °C and 3) 55 °C for 14 days.*

V.3 Encapsulation of curcumin

Curcumin (diferuloylmethane), the yellow pigment in turmeric and curry, is extensively used in the food and chemical industry as a colouring, flavouring and preservative agents. It has also been found to exhibit anti-oxidative (Sharma et al., 1994) and anti-inflammatory properties in clinical trials (Lin et al., 1997). During the past decades, many research reports indicated that curcumin can induce apoptosis and suppress the formation of procarcinogens through various mechanisms (Chauhan, 2002). Curcumin possesses not only chemopreventive but also anti-cancer activities (Huang et al., 1994, Huang et al., 1997). Curcumin has been considered by the National Cancer Institute (NCI) as the third generation of cancer chemopreventive agent in America.

Curcumin with its polyphenolic structure is water insoluble and scarcely dissolved in the organic phase. Previous studies addressing the absorption and metabolism of curcumin after oral administration showed its poor bioavailability in vivo (Ravindranath and Chandrasekhara, 1981). Curcumin, however, is unstable at neutral-basic pH values and in serum-free medium, and is degraded to vanillin, ferulic acid, feruloyl methane and trans-6-(40-hydroxy-30-methoxy-phenyl)-2,4-dioxo-5-hexenal (Huang et al., 1994).

Lin and coworkers have investigated the stability and characterization of a curcumin-encapsulated O/W microemulsion system using food-acceptable components, lecithin and Tween 80 as the surfactants and ethyl oleate as the oil phase (Lin et al., 2009). The formulations tested resulted stable for 2 months with an average diameter of 72 nm.

Tiyaboonchai and co-workers have investigated the stability of curcumin in microemulsion and solid lipid nanoparticles (SLNs) (Tiyaboonchai et al., 2007). However, the high dose of ethanol used in the formulation and the submicron size of SLNs (about 450 nm) calls for the improvement of the procedure.

Solid lipid nanoparticles have attracted much interest over the past years as potential drug delivery systems because of their ease of preparation and long-term stability. Furthermore, the choice of the surfactant is critical for the formulation of the curcumin-based delivery systems. Lecithin, which has two long hydrocarbon chains, is a major component of lipid bilayers of cell membranes and a natural, biological amphiphilic compound. Moreover, it is in many respects regarded as an ideal biological surfactant because it is biodegradable.

The main aim of this study was to find stable O/W emulsions containing curcumin encapsulated with food-acceptable ingredients, such as soy lecithin and sugar ester, to protect curcumin from chemical degradation.

V.3.1 Materials and methods

V.3.1.1 Chemicals

Curcumin (85% pure, with 11% demethoxycurcumin and 4% bisdemethoxycurcumin as impurities) was obtained from Sabinsa Corporation (Piscataway, NJ) and used without further purification.

The submicron emulsion were prepared using stearic acid (Sigma-Aldrich s.r.l., Milan, Italy) as lipid phase and soy lecithin Solec IP (a kind gift from Solae Italia s.r.l., Milan, Italy) and sugar ester P1670 (a kind gift from Prodotti Gianni, Milan, Italy as lipophilic and hydrophilic emulsifiers.

V.3.1.2 Fabrication of encapsulated curcumin into emulsion

Curcumin (0.1% w/w) was dispersed in the lipid and lipophilic emulsifier phase on a hot plate at a temperature of 70 °C to obtain the melting of the lipid. Subsequently, the primary emulsion was prepared mixing the lipid and water phases by high shear homogenization (HSH) using an Ultra Turrax T25 (IKA Labortechnik, Jahnke und Kunkel, Germany) at 16800 rpm for 2 min at 70°C. The emulsion droplets embedding curcumin were finally reduced to micrometric size by high pressure homogenization in a high pressure bench-scale homogenizer (nm-GEN 7400 series by Stansted Fluid Power, UK) at 200 MPa for 10 passes, maintaining the process temperature above the lipid melting temperature (70 °C), in order to produce a hot emulsion, whose rapid cooling will generate solid lipid particles.

It was tested the formulation which proved to be the most stable by the construction of the pseudo ternary phase diagram, described in detail in Chapter III, and having the following composition: 0.1% (w/w) curcumin, 2.4% (w/w) stearic acid, 3.73% (w/w) lipophilic soy lecithin, 1.87% (w/w) sugar ester and 91.9% (w/w) water.

V.3.1.3 Physicochemical stability of encapsulated curcumin

The physical stability was evaluated by measuring the variation of the mean droplet diameter over time under accelerated ageing conditions. The particle size distributions (PSD) were measured by wet laser diffraction (Mastersizer 2000, Malvern Instruments, Malvern, UK).

Moreover the chemical stability of encapsulated curcumin was measured recording the evolution of the UV–Vis absorption spectra at three different storage temperatures (4, 30 and 55 °C) and pH (3, 7 and 10) for 20 days. The UV-Vis spectra were obtained in the range of 360-460 nm using a V-650 UV-Vis spectrophotometer (Jasco Instruments, USA). (high temperature and high-low pH).

Each measurement was replicated three times.

V.3.3 Results

V.3.3.1 Physicochemical stability of curcumin emulsions

In this section, the physical and chemical stability of the encapsulated curcumin into submicron emulsion was examined in terms of the evolution of the mean droplet diameter and curcumin degradation over time under accelerated ageing conditions (high temperature and high-low pH).

The results, reported in Figure V.7, show that the emulsion, after a slight initial increase of the mean droplet diameter, probably due to the formation of aggregates of the solid fat crystals, was very stable when kept at refrigerated conditions (4 °C) and at room temperature (30 °C) for 20 days with averaged diameter of about 7 μm; on the contrary at high storage temperature (55 °C) the particle diameters gradually increased with the storage time. Moreover, after 10 days for the samples stored at 55 °C it has been observed the settling of curcumin at the bottom of the test-tube. When the temperature is increased around the melting temperature of the stearic acid (i.e. for storage temperature of 55 °C), coalescence and aggregation phenomena were favoured by the melting and subsequent break-down of solid lipid particles, causing an increase of the mean droplet diameter and also the release of curcumin from the capsules.

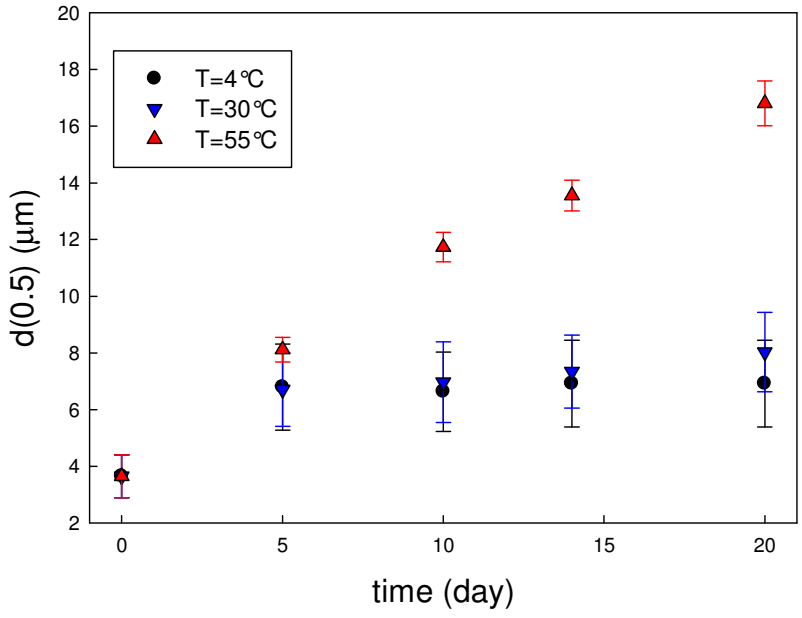

Figure V.7 *The evolution of the mean droplet diameter, d(0.5), of the curcumin-encapsulated emulsion under accelerated ageing conditions.*

An analogous behaviour was confirmed by the analysis of the chemical stability of the encapsulated curcumin. Figure V.8 shows the UV-Vis absorption curves of encapsulated curcumin into solid lipid particles, stored at different temperatures and pH. The results demonstrate that emulsions stored at 4 and 30 °C were more stable than emulsion at 55 °C with no degradation and release of the curcumin from the delivery system after 20 days. Moreover, the peaks of the absorbance at 420 nm remain quite constant at pH 3 and 7 over the storage time. At pH 10 the peak of the absorbance at 420 nm disappeared after only 4 days (Figure V.8f) and decreased rapidly in few hours due to a rapid degradation of encapsulated curcumin.

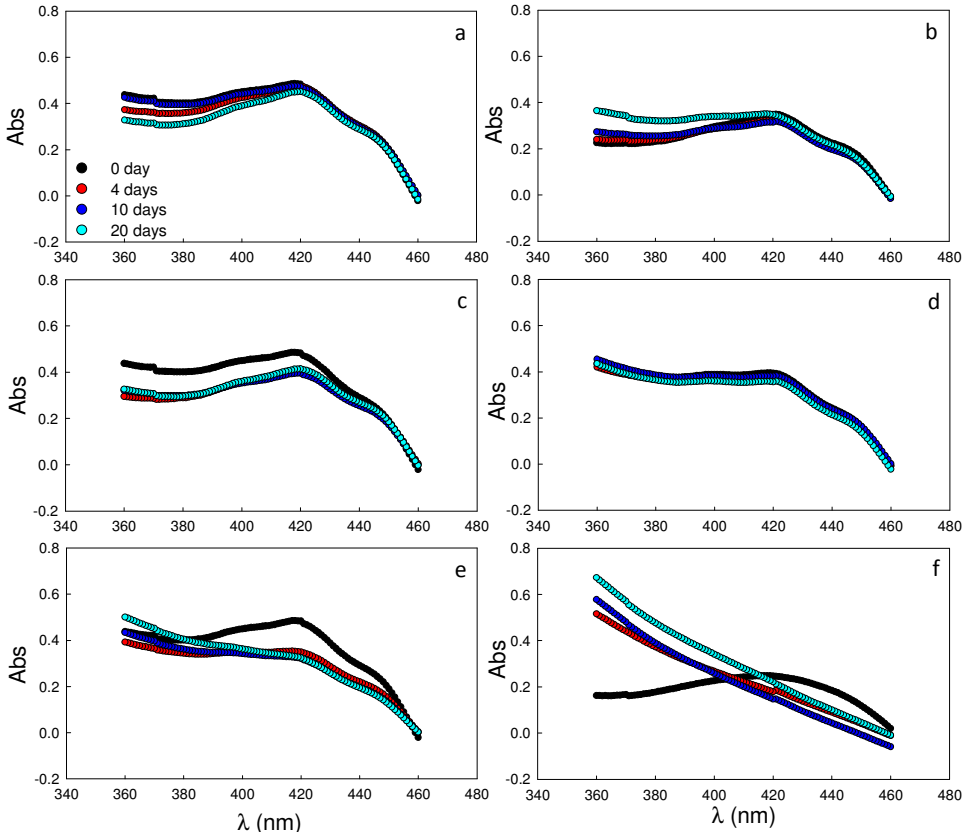

Figure V.8 *The evolution of the UV–Vis absorption curves of the curcumin-encapsulated emulsion after storage at different temperatures, (a) 4 °C, (c) 30 °C and (e) 55 °C) and different pH, (b) 3, (d) 7 and (f) 10, for 20 days.*

V.4 Conclusions

The design of nanoemulsion-based delivery systems with the use of a combination of hydrophilic (sugar ester, defatted soy lecithin, polysorbate 20) and lipophilic emulsifiers (defatted soy lecithin, glycerol monooleate) was able to encapsulate polyphenols, such as resveratrol and grape marc extracts, and disperse them in aqueous systems at a concentration at least 10 times higher than their therapeutic concentration.

Fluorescence spectroscopy studies have confirmed the hypothesis that the combined use of a hydrophilic and a hydrophobic emulsifier can better retain, through hydrophobic interactions, the scarcely water- and lipid-soluble polyphenols in the droplet core.

For the first time, a nanoencapsulation system based on nanoemulsions was developed for the delivery of resveratrol, while measurably increasing its physical and chemical stability in comparison with the unencapsulated compound. Accelerated ageing tests, conducted at different storage temperatures (from 4 to 55 °C) and under UV-C light showed that the formulation based on the combination of soy lecithin and sugar esters was the most physically and chemically stable, with the mean droplet size always lower than 180 nm under the different conditions tested.

Furthermore, the exploitation of polyphenols extracted from grape marc was evaluated by means of their encapsulation in nanoemulsions, formulated with only natural ingredients, using either a liquid (sunflower oil) or a solid (palm oil) lipid phase. Sunflower oil-based nanoemulsions resulted to be the most physically and chemically stable, with no significant variation of the mean droplet size and no degradation of the encapsulated compounds under the different conditions tested.

Finally, curcumin was encapsulated in stearic acid-based solid lipid particles, increasing solubility in aqueous systems more than 1600 times in comparison to its solubility in water. It was observed that the solid lipid core protects curcumin from chemical degradation at high temperatures and neutral pH. Further studies are needed to prevent the aggregation of solid lipid particles during the rapid cooling treatment after hot HPH in order to further reduce the mean droplet diameters.

The present study serves as a useful model for developing delivery systems of bioactive compounds, poorly water soluble and chemically unstable once extracted from plant tissues, for the nutraceutical and functional food industry.

Chapter VI
Bioavailability of nanoencapsulated bioactives

In this chapter the demonstration is given of how the nanoencapsulation of bioactive compounds, and in particular resveratrol, which is studied as model compound, can improve their bioavailability, protecting them from chemical degradation and avoiding a rapid metabolism. To this purpose, the gastric-intestinal digestion process was simulated *in vitro*. Furthermore, the transport of nanoencapsulated resveratrol through the intestinal wall was investigated through the *ex vivo* measurement of its transport rate through Caco-2 cell monolayers grown on permeable supports. These *in vitro* and *ex vivo* experiments were conducted in the laboratories of the Guelph Food Research Centre, Agriculture and AgriFood Canada.

Finally, the *in vitro* release of nanoencapsulated resveratrol was studied evaluating the possibility to use O/W nanoemulsions as delivery systems for a sustained release of the encapsulated bioactive compound.

VI.1 Resveratrol and its beneficial effects

Starting in 1990s and continuing to date, clinical studies have demonstrated several health-promoting activities of *trans*-resveratrol, such as anti-oxidizing (Orallo, 2006) and anti-atherosclerotic effects, inhibition of platelet aggregation (Olas and Wachowicz, 2005), beneficial effects on the cardiovascular system, reducing lipid peroxidation, improving vasodilatation and lowering blood pressure (Bradamante et al., 2004) and chemoprotective advantages against cancer proliferation (Jang et al., 1997).

The biological properties of resveratrol are attributed to its ability to inhibit the oxidation of human low-density lipoprotein and its suppression of cyclooxygenase-2 contribute to its anti-inflammatory and antioxidant effects (King et al., 2005). On the other hand, the chemopreventive effect of

resveratrol is due to the inhibition of quinone reductase 2 activity, which regulates the expression of cellular antioxidant and detoxification enzymes to improve cellular resistance to oxidative stress (Buryanovskyy et al., 2004). Furthermore, resveratrol increases the activity of SIRT (a member of the sirtuin family of nicotinamide adenine dinucleotide-dependent deacetylases), resulting in improved cellular stress resistance and longevity (Holme and Pervaiz, 2007).

However, the physicochemical properties of resveratrol, particularly its high reactivity and low solubility in aqueous and lipid phases, constituted also the limiting factors for its bioavailability and for the explication of the desired health-beneficial effects.

In a biological system, resveratrol is rapidly and extensively metabolized, probably due to its low water solubility, which reduces the dissolution-rate limited cell absorption (Wenzel and Somoza, 2005), thus reducing its oral bioavailability. In order for resveratrol to exert its beneficial effects, it must reach a concentration in the blood of at least 10 mg/l (Yu et al., 2003), which, for an average weight person, translates in the absorption of 50 mg of resveratrol.

The development of the therapeutic potential of resveratrol can only be applied in vivo if the limitations tied to its bioavailability can be overcome. Research is currently exploring different methods for enhancing resveratrol bioavailablility, including a) co-administration with inhibitors of resveratrol metabolism in order to prolong its presence in vivo, b) the use of resveratrol analogs possessing a better bioavailability, c) investigation of the potential activity of resveratrol metabolites, and d) design of drug delivery systems exploiting the advantages of nanotechnology (Amri et al., 2011).

Concerning the first approach, some authors have evaluated the opportunities for enhancing the pharmacokinetic parameters of resveratrol by partially inhibiting its glucuronidation via a co-administration with inhibitors, thereby slowing its elimination. For example, Johnson et al. (Johnson et al., 2011) used piperine, an alkaloid derived from black pepper, to inhibit glucuronidation and observed in vivo an increase in the serum resveratrol concentration.

There is also increasing interest in the second strategy, consisting in evaluating novel naturally-occurring and/or synthetic analogs of resveratrol possessing the same structural backbone but with chemical modifications resulting in superior efficacy. Kapetanovic and coworkers studied the naturally-occurring dimethylether analog of resveratrol, pterostilbene, and compared its bioavailability to that of resveratrol in healthy rats, which was resulted 3-4 fold higher (Kapetanovic et al., 2011).

There is speculation that resveratrol metabolites may retain some activity, making it necessary to lead further studies on the their beneficial effects. Among the numerous resveratrol metabolites, piceatannol significantly decreased dextran sulfate sodium which induces inflammatory injury and

regulated iNOS expression in the same way as resveratrol did in mouse colitis (Youn et al., 2009).

Finally, the design of drug delivery systems able to enhance resveratrol bioavailability is particularly promising. While conventional forms, such as tablets or capsules, are only mentioned in clinical studies evaluating resveratrol bioavailability in humans (Boocock et al., 2007), research is currently focused on exploring delivery systems in micrometric to nanometric range, as described in section V.1.

The aim of this chapter is to demonstrate how the O/W nanoemulsions, being able to protect bioactive compounds from chemical degradation, as demonstrated in chapter V, can be also efficient delivery systems for the oral administration of resveratrol, preserving it during the digestion process, favoring a sustained release and hence enhancing its bioavailability.

VI.2 Materials and methods

VI.2.1 Chemicals

Pepsin from porcine gastric mucosa, pancreatin from porcine pancreas, bile salts and phenylmethanesulfonyl fluoride (PMSF), were all purchased from Sigma-Aldrich (Oakville, ON, Canada).

Dulbecco's Modified Eagle Medium (DMEM), Hanks' Balanced Salt Solution (HBSS) and antibiotic-antimycotic (100x) were purchased from Gibco Life Technologies (Grand Island, NY). Fetal bovine serum (FBS) was obtained from Thermo Scientific HyClone (Logan, UT).

All other solvents were of HPLC grade and were purchased from Sigma-Aldrich (Oakville, ON, Canada).

VI.2.2 Production of nanoemulsions for resveratrol delivery

Resveratrol (0.01 wt%) was encapsulated in peanut oil-based nanoemulsions by high pressure homogenization, as described in section *V.1.1.2*.

The O/W nanoemulsions were produced using a combination of hydrophilic and lipophilic emulsifiers to enhance the entrapment of resveratrol into the lipid phase. Natural products, such as defatted soy lecithin, lipophilic soy lecithin and sugar ester, or synthetic compounds, such Tween 20 and glycerol monooleate, were used as emulsifiers.

The composition and the mean droplet diameter (*Z-diameter*) of the formulations tested were reported in Table VI.1.

Table VI.1 *Composition and mean droplet diameters, Z-diameter, of the nanoemulsions tested.*

Delivery systems	Composition	Z-diameter (nm)
R/LSL-DSL	0.01% resveratrol 0.2% ethanol 1% lipophilic soy lecithin 0.5% defatted soy lecithin 6% peanut oil 92.29% water	212 ± 4.9
R/LEC	0.01% resveratrol 0.2% ethanol 2.1% soy lecithin Lecinova 27.9% peanut oil 69.79% water	235 ± 1.5
R/T20-GMO	0.01% resveratrol 0.2% ethanol 1.5% Tween 20 1.5% glycerol monooleate 7% peanut oil 89.79% water	128 ± 2.3
R/LSL-SE	0.01% resveratrol 0.2% ethanol 1% lipophilic soy lecithin 0.3% sugar ester 9% peanut oil 89.49% water	138 ± 0.4

VI.2.3 In vitro gastrointestinal digestion

The digestion process was conducted according to the method proposed by Boyer and coworkers (Boyer et al., 2005) with some modifications. Briefly, for simulated gastric digestion, a sample of 6 ml of each nanoemulsion containing resveratrol was placed in a test tube with 3 ml of saliva and incubated in a water bath at 37 °C for 15 min. Saliva was collected in a sanitary manner to sterile tube 5 min after a volunteer had consumed 250 ml of milk. A sample of 3 ml of phosphate buffer saline was then added, the pH was adjusted to 2.0 by drop-wise addition of 1 M HCl and porcine pepsin was then added to a final concentration of 1.3 mg/ml. The sample was incubated in a water bath at 37 °C for 30 min. Aliquots of the digestion mixture were collected for HPLC analysis.

Then the pH was increased to 5.8 by drop-wise addition of 1 M $NaHCO_3$, to prepare for the simulated intestinal digestion. Pancreatin and bile salts were added to a final concentration of 0.175 and 1.1 mg/ml, respectively.

The pH was adjusted to 6.5 by drop-wise addition of 1 M $NaHCO_3$ and the digestate was incubated in a water bath at 37 °C for 2 h, before sample collection. The two different stages of digestion (gastric and intestinal) were stopped by adding PMSF to a final concentration of 0.174 mg/ml.

VI.2.4 Cell cultures

Caco-2 cells were obtained from the American Type Culture Collection (ATCC) (Rockville, MD). The cells were maintained at 37 °C in Dulbecco's Modified Eagle's Medium (DMEM), supplemented with 10% fetal bovine serum (FBS) and 1% antibiotic-antimycotic solution, in an atmosphere of 5% CO_2. The cells were seeded on PTFE filter inserts (0.4 μm, 6.5 mm diameter) of Transwell cell culture chambers (Corning Incorporated - Life Sciences, Lowell, MA, USA). Cells used were at passage 25-30. The cells were allowed to grow and differentiate to confluent monolayers for 14-21 days.

VI.2.5 Transport across filter-grown Caco-2 cell monolayers

Transport at 37 °C was determined across Caco-2 cell monolayers in the apical-to-basolateral direction according to Nature Protocols (Hubatsch et al., 2007). For cell culture experiments, Transwell-grown cell monolayers at days 19-21 after plating were used. Donor solutions containing 100 μl of encapsulated resveratrol in nanoemulsion-based delivery systems in 150 μl of medium were prepared. In the receiving compartment were added 750 μl of cell culture medium. Samples (30 μl) were taken from the receiver side at specified time intervals. The transport experiments were carried out over a time period of 6 h. The amount of the transported compound was determined by HPLC. At beginning and at the end of the transport experiments the integrity of the monolayer was checked by measurement of the transepithelial electrical resistance, *TEER*, using Millicell-ERS (Millipore Corporation, Billerica, MA, USA). The transport experiments were performed in triplicate at 37 °C in an incubator.

The cumulative amount, Q, transported at any time point is the sum of the amount of the transported compound in the receiver side and the amount of the compound contained in the samples removed at previous time points.

The cumulative amount was calculated with the following equation:

$$Q = c_n V_r + \sum_{i=1}^{n-1} c_i V_s \qquad \text{(VI.1)}$$

where Q is the cumulative amount of the resveratrol transported; c_n is the concentration of resveratrol determined at n^{th} sampling interval; V_r is the volume of the solution on the receiver side (750 μl) and V_s is the sampling

volume (30 µl); c_i was the resveratrol concentration determined at n-1 sampling interval. Plotting the cumulative amount transported (Q) versus time, the linear appearance rate (slope = $\Delta Q/\Delta t$) of resveratrol on the receiver side was determined. Then, the apparent permeability coefficient, P_{app} (cm/s), was calculated according to the following equation:

$$P_{app} = (dQ / dt)(1 / Ac_0) \quad \text{(VI.2)}$$

where $\Delta Q/\Delta t$ is the linear appearance rate of the compound on the receiver side (in mmol/sec); A is the surface area of the cell monolayers (in cm^2; 4.71 cm^2 for Transwells 24 mm in diameter); and c_0 is the initial concentration of the compound on the donor side (in mmol/cm^3).

VI.2.6 Cellular uptake

To check mass balance, the uptake of the compound in Caco-2 cells was determined. Immediately after performing transport studies, the transport medium was removed and the cells were washed with HBSS to stop further uptake and to remove unbound compound. Subsequently, the cells were scraped from the polycarbonate filters into 1 ml of 0.01 M HCl:methanol solution (50:50% v/v – pH:2.4). After sonication in water bath sonicator for 5 min, the samples were centrifuged at 8600 xg for 5min at 4°C. Samples were then analyzed by HPLC.

VI.2.7 In vitro release

Release profile of resveratrol from nanoemulsions was performed by a dialysis bag method using water as dissolution medium. A sample of 2 ml of resveratrol nanoencapsulated was placed into a pre-swelled 12 kDa molecular weight cutoff dialysis bags (20/32'' Visking tubing, Scientific Instument Centre Ltd, London, UK) with the two ends fixed by clamps. The bags were immersed in 200 ml of water and stirred at 100 rpm at 37°C. At predetermined time, samples of 5 ml were withdrawn from the release media and replaced with an equal volume of the corresponding fresh media to maintain a constant volume. The test solution was analyzed by HPLC and the cumulated amounts of resveratrol released from the nanoemulsions were calculated according to eq. (VI.3):

$$Q = \frac{c_n V_t + \sum_{i=1}^{n-1} c_i V_s}{c_0 V_b} \times 100 \quad \text{(VI.3)}$$

where Q was the cumulative amount of resveratrol released (%); c_n was the concentration of resveratrol (mg/l) determined at n^{th} sampling interval; c_i was the resveratrol concentration (mg/l) determined at n-1 sampling interval;

V_t and V_s were the volumes of the acceptor phase (200 ml) and of the sample withdrawn from the acceptor phase (5 ml) respectively; c_0 was the initial concentration of resveratrol in dialysis bag and V_b was the volume of the sample in dialysis bag (2 ml).

Experiments were performed at least three times.

VI.2.8 HPLC analysis

An HPLC system (Agilent Technology 1100 series, Palo Alto, CA) equipped with a quaternary pump, an inline degasser, a thermostatic autosampler, and a diode array detector (DAD) was used for the identification and quantification of resveratrol in the samples. A Phenomenex Luna C18(2) analytical column (250 × 4.6 mm i.d.; particle size, 5 μm) with a C18 guard column (Phenomenex, Torrance, CA) was used for the separation. The binary mobile phase consisted of methanol:acetic acid:water (45:5:50 v/v %) (solvent A) and 1.2 v/v % of acetic acid in methanol (solvent B), and the gradient program was as follows: 0% B to 10% B in 10 min, 10% B to 100% B in 2.5 min, 100% B for 2.5 min, 100%B to 100% A in 2.5 min and 100% A for 5 min.

The flow rate was 0.8 ml/min for a total run time of 22.5 min. The injection volume was 10 μl for all samples. The standard curve was constructed diluting resveratrol in methanol. The detector was set at 310 nm for *trans*-resveratrol and at 280 nm for *cis*-resveratrol. The excitation wavelength was set to 298 nm and the emission wavelength to 386 nm.

VI.3 Results

VI.3.1 In vitro digestion of nanoencapsulated resveratrol

The polyphenols are generally characterized by scarce solubility in water, which severely limits their use in pure form as bioactive compounds in functional foods, because of insufficient solubility in the GI tract and low permeability to pass through the intestinal wall (Haslam, 1996).

Although the biochemical changes in the digestive tract by enzymes and intestinal microflora makes them more soluble in water and suitable to be metabolized, this process is likely to affect their therapeutic properties (Scalbert and Williamson, 2000). For this reason, the use of a delivery system is necessary to protect the encapsulated bioactive compound during the digestion process by allowing to keep intact its health-beneficial properties up to the intestinal wall where it must be adsorbed.

In this section the chemical and physical stability of encapsulated resveratrol into different nanoemulsion-based delivery systems was evaluated during the digestion process conducted under conditions

simulating cumulatively the digestion activities of the stomach and the small intestine.

During the gastric and intestinal digestions, resveratrol remained chemically stable, with no significant changes in the quantity and quality of the encapsulated resveratrol. The HPLC analysis has confirmed the stability of the nanoencapsulated resveratrol with no additional peaks detected after digestion. It can be then speculated that resveratrol remains encapsulated in the lipid phase, is not metabolized in the gastrointestinal tract, and can therefore reach the colon in active form to be absorbed through the intestinal wall. Nevertheless, final proof of resveratrol being still encapsulated requires further experimental investigations.

However, several studies based on animal and human models have demonstrated that for unencapsulated resveratrol, only traces of its active form actually circulate in the plasma; resveratrol was found to be extensively glucuronidated and sulfated in gut and liver (Walle et al., 2004). Biliary excretion has been found to be an important elimination pathway for resveratrol and previous studies have shown that in rats at least 30% of the administered dose was eliminated via feces in the form of conjugated metabolites (Wenzel et al., 2005).

The integrity of the nanocapsules during digestion was assessed by measuring the variation of the mean droplet diameters after the different digestion phases (Figure VI.1).

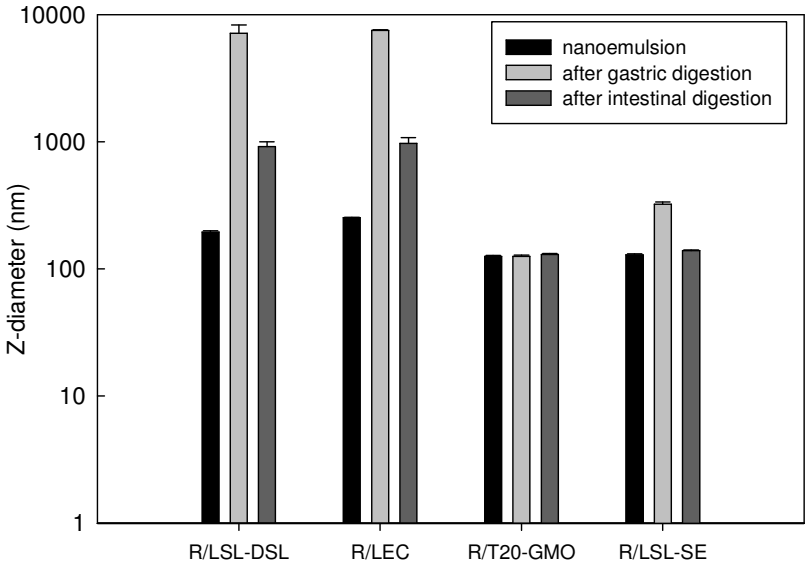

Figure VI.1 *Mean droplet diameter, Z-diameter, of the nanoemulsions encapsulating resveratrol before and after the* in vitro *digestion process.*

The R/T20-GMO and R/LSL-SE nanoemulsions were physically stable during gastric and intestinal digestion, without any variation of the *Z-diameter* being observed. The lecithins-based nanoemulsions, R/LEC and R/LSL-DSL, characterized by a higher initial mean droplet diameter in comparison to the previous formulations, appeared to be not as stable during gastric digestion, with a significant increase of the *Z-diameter*. Nevertheless, the following step of intestinal digestion determined the reduction of the mean droplet size due to the action of the bile salts, which emulsified the fat aggregates produced during gastric digestion.

VI.3.2 Transport through Caco-2 cell monolayers

Figure VI.2 shows the cumulative amount transported from the apical to the basolateral side across Caco-2 cell monolayers for encapsulated resveratrol into nanoemulsion-based delivery systems in comparison with the unencapsulated compound diluted in DMSO. The formulations R/T20-GMO and R/LSL-SE, with smaller particle size (128 and 138 nm respectively), show higher cumulative amount transported in comparison to the other formulations, confirming the importance of nanometric size to improve the passive transport mechanisms through the cell membrane. Furthermore, although these two formulations show a slight difference in the mean droplet diameters, R/LSL-SE shows an higher permeability due to the presence of soy lecithin, which, being a mixture of phospholipids similar to the phospholipid bilayer structure of the cellular membrane, favours the absorption and the entrapment of the oil droplets in the microvilli and their consequent transport through the cell membrane.

From the HPLC analysis of the samples in the basolateral side no new peaks were detected in addition to the peak of resveratrol, confirming the fact that resveratrol is not metabolized by the cells, not being detected its metabolites, because it was entrapped in the lipid phase and protected by the double layer of hydrophilic and lipophilic emulsifiers during transport through the Caco-2 cell monolayers. In fact, the analysis of the mean droplet diameters confirmed the hypothesis that resveratrol has been transported through the cell monolayers into the oil droplets, due to the fact that no variation of *Z-diameter* was observed after transport experiments, as showed in Figure VI.3.

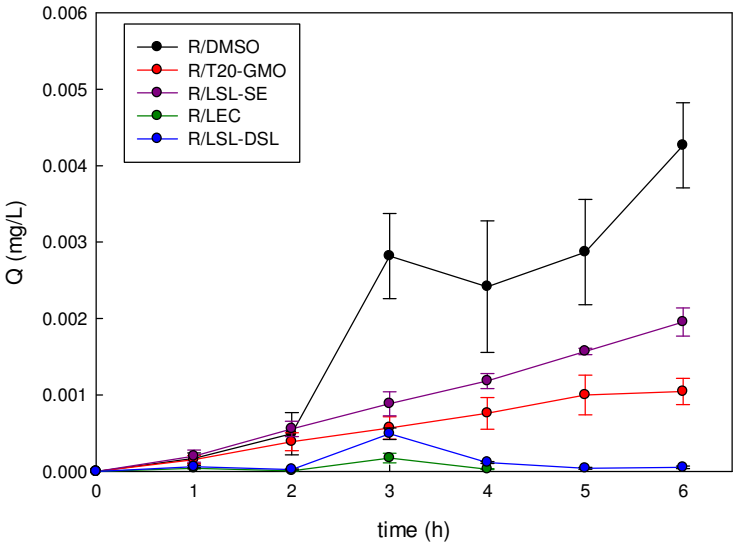

Figure VI.2 *Cumulative amount (Q) versus time (t) of unencapsulated resveratrol (R/DMSO) and nanoencapsulated resveratrol transported from the apical to the basolateral side across Caco-2 cell monolayers.*

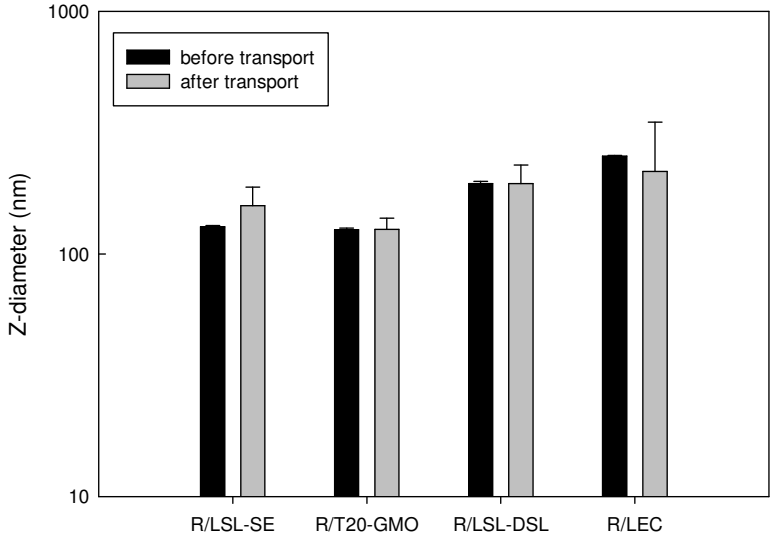

Figure VI.3 *Mean droplet diameter (Z-diameter) of the nanoemulsions encapsulating resveratrol before and after transport across Caco-2 cell monolayers.*

The transepithelial electrical resistance, *TEER*, was measured before and after the transport experiments to check the integrity of the monolayer. Generally, *TEER* values obtained are in the range of 1000-4000 Ohms for a 21 day culture and 1000-3000 Ohms for a 10 day culture. It is considered a failing well below 1000 Ohms. Table VI.2 shows that for all the samples tested the *TEER* values were higher than 1000 Ohm and remained constant after the transport experiments, confirming that the cell monolayers were not damaged during the tests.

Table VI.2 *Transepithelial electrical resistance measurements (TEER) of Caco-2 cell monolayers grown on permeable supports before and after transport experiments.*

Delivery systems applied to the cells	**TEER (Ohm)**	
	Befor transport	**After transport**
R/DMSO	1250 ± 130	1310 ± 170
R/LSL-SE	1293 ± 20	1297 ± 20
R/T20-GMO	1150 ± 14	1073 ± 50
R/LSL-DSL	1030 ± 40	1013 ± 10
R/LEC	1153 ± 30	1037 ± 70

The apparent permeability of nanoencapsulated resveratrol has been calculated plotting the cumulative amount transported (Q) versus time and extrapolating the linear appearance rate ($\Delta Q/\Delta t$) of resveratrol on the receiver side. It must be used the linear part of the graph to determine $\Delta Q/\Delta t$ and ignore any possible lag time and plateau regions that may exist. A lag phase in the beginning of the experiment may be caused by loading of the compound into the cells. This phenomenon may be significant for a compound that has high cellular uptake. A late plateau region may be caused by a significant decrease in the donor concentration of the compound, due to the fact that a large amount has been transported to the receiver side (Gao et al., 2001).

The apparent permeability of most compounds falls in a range of 1×10^{-7} to 1×10^{-5} cm/sec. A poorly transported compound, such as mannitol, usually exhibits a low P_{app} value of 1×10^{-7} cm/sec. In contrast, a well-transported compound, such as testosterone, has a P_{app} value of 1×10^{-5} cm/sec. An "average" compound will have a P_{app} value of 1×10^{-6} cm/sec (Gao et al., 2001). Figure VI.4 shows that for all the formulations tested the P_{app} value

falls in the range indicated. In particular, R/LSL-SE shows the higher P_{app} value and can be considered a very good formulation to increase the transport of resveratrol. In particular, it has been observed as expected that the apparent permeability decreases with the increase of the mean droplet diameters. On the other side, the unencapsulated resveratrol shows a P_{app} value higher than that of the nanoencapsulated resveratrol. This behaviour can be explained in terms of the different matrices used: the unencapsulated resveratrol was dissolved in a organic solvent (DMSO) and the nanoencapsulated resveratrol was entrapped in a aqueous system (O/W nanoemulsions). For the permeability test across Caco-2 cell monolayers it has not been used an aqueous system to dissolve the unencapsulated resveratrol because the solubility of resveratrol in water is very low.

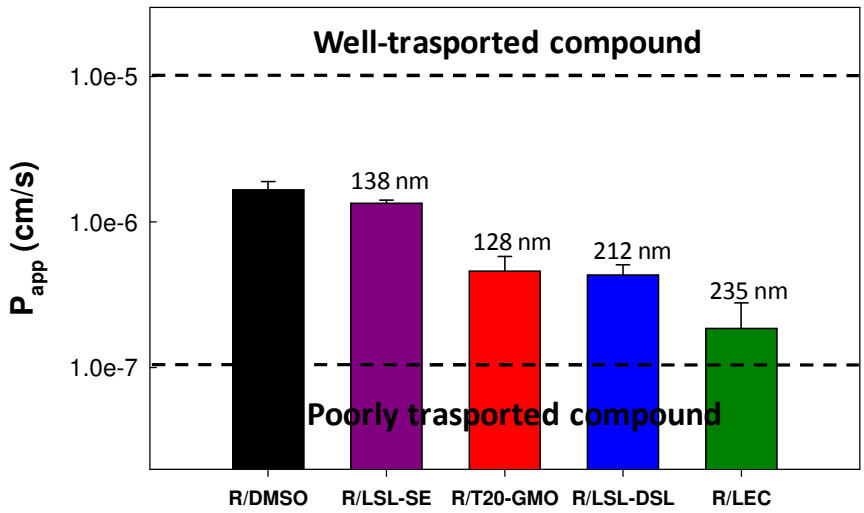

Figure VI.4 *The Apparent permeability coefficient, P_{app}, of unencapsulated resveratrol (R/DMSO) and encapsulated resveratrol into different nanoemulsion-based delivery systems.*

The low P_{app} values obtained for the nanoemulsions with bigger particle sizes (R/LSL-DSL and R/LEC) can be explained in terms of cellular uptake (Figure VI.5). While smaller particle sizes can favour the permeability, bigger droplets can be entrapped into the Caco-2 cells increasing the cellular uptake and reducing the permeability.

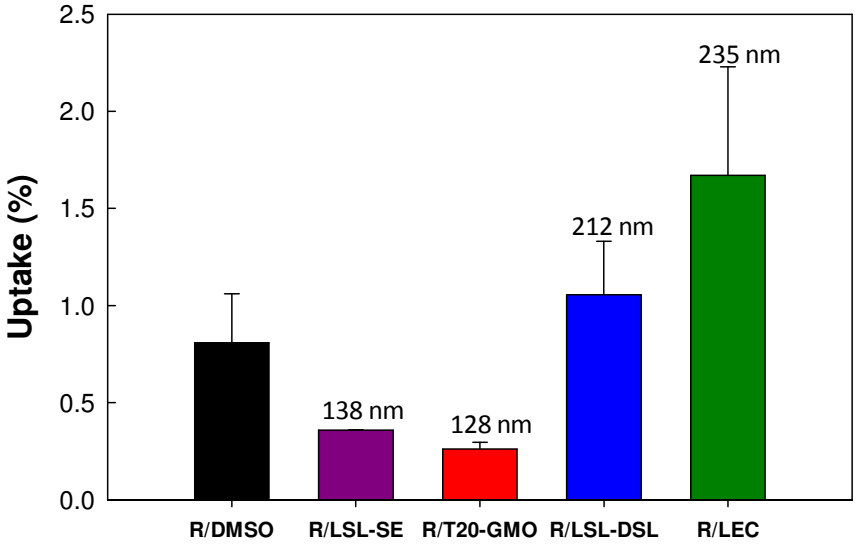

Figure VI.5 *The cellular uptake of unencapsulated resveratrol (R/DMSO) and encapsulated resveratrol into different nanoemulsion-based delivery systems.*

VI.3.3 In vitro release of nanoencapsulated resveratrol

Nanometric size delivery systems offer considerable advantages especially in the control of the release rate of resveratrol, as shown in Figure VI.6, where the *in vitro* release of resveratrol encapsulated in the different nanoemulsions is reported in comparison with unencapsulated resveratrol. For the unencapsulated resveratrol the release occurs rapidly, reaching the maximum concentration of 45% after 3 h. When resveratrol is encapsulated in nanoemulsions a more sustained release was obtained, with different maximum concentrations of resveratrol being released. In particular, the nanoemulsions R/LSL-SE and R/LSL-DSL seem to be the best delivery systems for a sustained release, reaching a maximum concentration of 80% of the bioactive released after 24 h, in comparison with the other two formulations, which show a maximum concentration of resveratrol released only of 60% after 24 h.

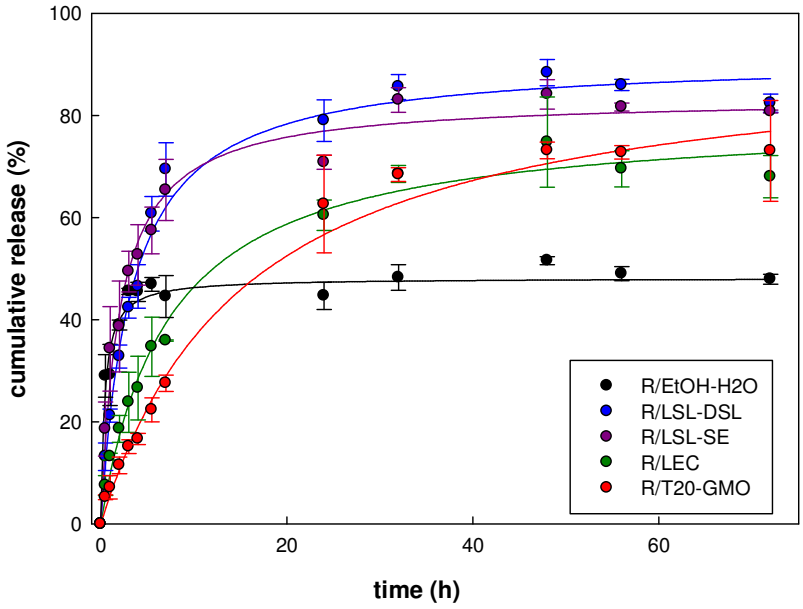

Figure VI.6 *Comparison of cumulative release into aqueous medium from dialysis bags of nanoencapsulated resveratrol with the unencapsulated compound.*

At the end of the *in vitro* release test, the mass balance between the resveratrol released and the compound still present in the dialysis bag was closed considering the aliquot of resveratrol chemical degraded during the test (Figure VI.7). On one side, when resveratrol was diluted in a water solution, 47% of compound was quickly released and the remaining 52% was degraded, being not protected from the interaction with external agent (O_2, temperature and light). On the other side, the nanoencapsulation improves the release and also protects resveratrol from degradation, reducing the amount of degraded compound to 25% for R/LEC and 15% for the other formulations.

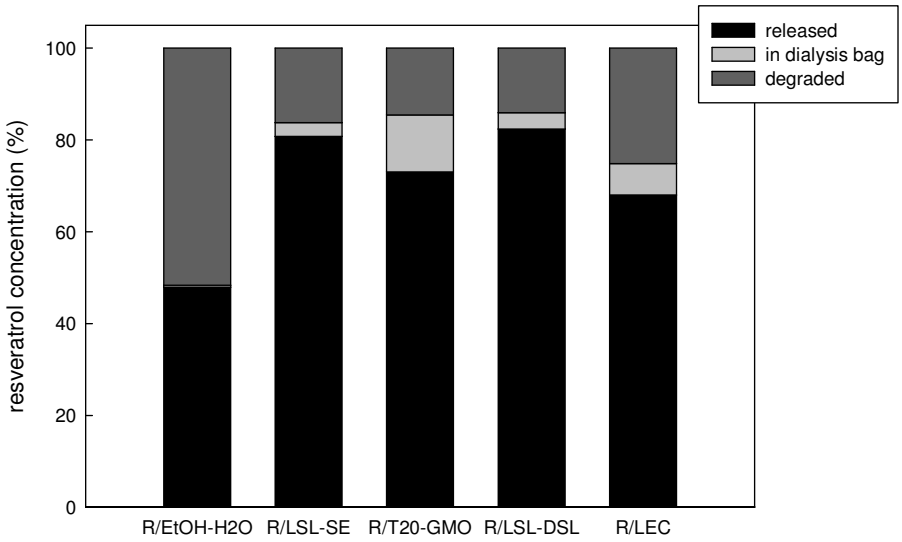

Figure VI.7 *The concentration of resveratrol released, in dialysis bag and chemical degraded after 72 h of in vitro release test.*

VI.4 Conclusions

Resveratrol, such as other bioactive compounds, has different therapeutic properties, whose exploitation is severely limited by its low bioavailability and rapid metabolism, because of poor solubility in water. For this reason, the use of nanoemulsion-based delivery systems seems to be ideal for increasing the bioavailability, protecting the bioactive compound during digestion and favouring a sustained release to reach in its active form the target sites.

In particular, in this section has been demonstrated that resveratrol encapsulated into O/W nanoemulsions, produced only with natural and food-grade ingredients, was not metabolized during *in vitro* gastric and intestinal digestion. Moreover, the formulations with smaller mean droplet diameters (below 200 nm) remain physically stable during the digestion process, allowing the resveratrol to reach the intestinal wall entrapped in the lipid droplets. These formulations, having subcellular diameters, show also higher apparent permeability coefficients in comparison with the other formulations (R/LSL-DSL and R/LEC), which, having bigger mean droplet diameters, remain uptaken into the cells.

Furthermore, lecithin-based nanoemulsions improve the transport through the cell monolayer, enhancing the passive transport mechanism due to their structure similar to the phospholipid bilayers of the cellular membrane.

Finally, the nanoencapsulation favors the sustained release of the bioactive compound, avoiding an undesired instantaneous drug release which reduces the ability to reach the target sites in the active form.

Chapter VII
Antioxidant activity of encapsulated compounds

This chapter reports the results related to the antioxidant activity of encapsulated bioactive compounds, measured with two different chemical assays (FRAP and ORAC) and a cellular antioxidant assay (CAA). The research was conducted at the Guelph Food Research Centre, Agriculture and AgriFood Canada.

VII.1 Introduction

Reactive oxygen species (ROS) are an entire class of highly reactive molecules derived from the metabolism of oxygen, which are often generated as by-products of biological reactions. *In vivo*, these species can play a positive role in cell physiology, but also damage the cell membranes and DNA, inducing the oxidation that causes membrane lipid peroxidation, decreased membrane fluidity and other DNA mutations, that may lead to cancer and degenerative diseases (Finkel and Holbrook, 2000).

Antioxidants are chemical substances that reduce or prevent oxidation. Many studies have shown that phenolic compounds display antioxidant activity as a result of their capacity to scavenge free radicals (Seyoum et al., 2006) or to chelate metal ions, preventing radical formation (Al-Azzawie and Alhamdani, 2006). Recently, polyphenols are receiving increasing interest as functional food ingredients or nutraceutical compounds because of their health beneficial properties, such as the antioxidant and reducing activity, as well as the capability of protecting cell constituents against oxidative damage and, therefore, limiting the risk of various degenerative diseases associated to oxidative stress (D'Archivio et al., 2007, Scalbert and Williamson, 2000).

The growing interest in the physiological benefits of natural antioxidants has been matched by acceleration in the development of analytical and biological methodologies for measurement of the antioxidant potential of these compounds. Several *in vitro* studies have been conducted to evaluate the total antioxidant capacity of food products. So far, however, there is no official standardized method, and therefore it is recommended that each evaluation should be made with various oxidation conditions and different methods of measurement (Frankel and Meyer, 2000).

The methods most commonly used to determine the total antioxidant capacity differ in terms of their assay principles and experimental conditions: assays based on a single electron transfer reaction, monitored through a change in colour as the oxidant is reduced, and assays based on a hydrogen atom transfer reaction, where the antioxidant and the substrate (probe) compete for free radicals (Huang et al., 2005).

Electron transfer reaction assays include the Trolox equivalent antioxidant capacity (TEAC or ABTS) assay, the ferric reducing ability of plasma (FRAP) assay, and the 2,2-diphenyl-1-picrylhydrazyl (DPPH) radical scavenging capacity assay. On the other side, hydrogen atom transfer reaction assays include the total peroxyl radical-trapping antioxidant parameter (TRAP) assay, and the oxygen radical absorbance capacity (ORAC) assay (Huang et al., 2005, Prior et al., 2005).

Among all these assays, ABTS, DPPH and ORAC are the most widely used. However, the ORAC assay is considered more relevant because it uses a biologically relevant radical source (Prior et al., 2003). Moreover, a major advantage of ORAC is that the method is automated and largely standardized; hence, values can be easily compared across laboratories.

Despite wide usage of these chemical antioxidant activity assays, their ability to predict *in vivo* activity is limited, because none of them take into account the bioavailability, uptake, and metabolism of the antioxidant compounds (Wolfe and Liu, 2007). Biological systems are much more complex than the simple chemical mixtures employed. The best antioxidant activity measurements are from animal models and human studies; however, these are expensive and time-consuming and not suitable for initial antioxidant screening of foods and dietary supplements (Liu and Finley, 2005). Cell culture models provide an approach that is cost-effective, relatively fast, and address some issues of uptake and metabolism.

Therefore, Wolfe and Liu developed a cell-based antioxidant activity assay to screen foods, phytochemicals and dietary supplements for potential biological activity (Wolfe and Liu, 2007).

The aim of this section was to evaluate the effect of nanometric delivery systems on the antioxidant activity of encapsulated polyphenols, comparing two chemical assays, FRAP and ORAC, with a cellular antioxidant activity assay.

VII.2 Materials and methods

VII.2.1 Chemicals

Ascorbic acid, 2,4,6-tripyridyl-s-triazine (TPTZ), fluorescein, dimethyl sulfoxide (DMSO) and 2',7'-dichlorofluorescein diacetate (DCFH-DA) were from Sigma Chemical Co. (St. Louis, MO), iron(III) chloride hexahydrate and hydrogen peroxide solution at 30% w/w were obtained from Sigma-Aldrich (Oakville, ON, Canada), 6-hydroxy-2,5,7,8-tetramethylchromane-2-carboxylic acid (Trolox) and 2,2'-azobis (2-methylpropionamidine) dihydrochloride (AAPH) were purchased from Aldrich Chemical Co. (Milwaukee, WI).

Caco-2 cells were obtained from the American Type Culture Collection (ATCC) (Rockville, MD). Dulbecco's Modified Eagle Medium (DMEM), Hanks' Balanced Salt Solution (HBSS) and antibiotic-antimycotic (100x) were purchased from Gibco Life Technologies (Grand Island, NY). Fetal bovine serum (FBS) was obtained from Thermo Scientific HyClone (Logan, UT).

VII.2.2 Chemical antioxidant activity

The antioxidant activity of encapsulated compounds was determined in comparison with unencapsulated compound diluted in DMSO or in methanol by using the Ferric Reducing Antioxidant Power assay (FRAP) and the Oxygen Radical Absorbance Capacity assay (ORAC).

The FRAP assay was conducted according to a previously reported procedure (Tsao et al., 2005) with minor modifications. Reagents included 300 mM acetate buffer, pH 3.6 (3.1 g $C_2H_3NaO_2 \cdot 3H_2O$ and 16 ml $C_2H_4O_2$), 10 mM TPTZ in 40 mM HCl and 20 mM $FeCl_3 \cdot 6H_2O$. Working FRAP reagent was prepared by mixing the reagents in a ratio 10:1:1 (acetate buffer:TPTZ solution:$FeCl_3 \cdot 6H_2O$ solution). Aqueous solutions of known L-(+)-ascorbic acid concentration, in the range of 10-1000 μM, were used for generating the calibration curve. FRAP values were expressed as μM ascorbic acid equivalent by using the standard curve calculated for each assay.

Nanoencapsulated compound (30 μl) was allowed to react with 900 μl of the working FRAP reagent for 30 min at room temperature. The sample was then centrifuged at 20000 xg for 3 min at 25 °C and 300 μl of the supernatant was used for analysis. Absorbance readings were taken using a visible-UV microplate reader (Power Wave XS2, Bio-Tek Instruments Inc., Winooski, VT, USA) set at 593 nm. A blank control was included at each time the assay also conducted for the samples and the standard. The blanks of the different delivery systems were the corresponding nanoemulsions

without the bioactive compound. All the reaction mixtures were prepared in triplicate.

The ORAC assay was conducted according to a previously reported method (Davalos et al., 2004) with some modifications. Analyses were conducted in 75 mM phosphate buffer (pH 7.4) and the final reaction mixture was 200 µl. Nanoemulsions (25 µl) containing the bioactive and fluorescein (150 µl; 86.8 nM, final concentration) solutions were placed in 96-well plate and preincubated for 30 min at 37 °C in a fluorescence microplate reader (FLx800, Bio-Tek Instruments Inc., Winooski, VT, USA). The reaction was initiated by the addition of 25 µl of AAPH (153 mM final concentration) reagent followed by shaking at maximum intensity for 10 s. The fluorescence was then monitored kinetically with data taken every minute for 1 h. The 96-well plate was also loaded with the blank controls including phosphate buffer with DMSO and different nanoemulsions without the bioactive compound, as well as the standard solutions of Trolox (6.25, 12.5, 25, 50, 100 µM). All the reaction mixtures were prepared in triplicate. The area under the fluorescence decay curve corresponding to a sample (net AUC) was calculated by subtracting the AUC corresponding to a blank. ORAC values were expressed as Trolox equivalents by using the standard curve calculated for each assay.

VII.2.3 Cellular antioxidant activity

Caco-2 cells were grown in growth medium (DMEM supplemented with 10% FBS, 1% antibiotic-antimycotic) and were maintained at 37 °C in an incubator with 5% CO_2. The medium was changed every 2 days. Cells used in this study were at passage 25-30.

Caco-2 cells were seeded at a density of 4 x 10^4/well on a 96-well microplate (collagen treated black plate) in 100 µL of growth medium/well and incubated for 15 days at 37 °C and 5% CO_2. The growth medium was then removed and the cells were washed with 100 µl of treatment medium (HBSS+10% FBS). Triplicate wells were treated with 100 µl of encapsulated bioactive compound suspended in 100 µl of treatment medium and incubated for 1 h at 37 °C. The wells were washed with 100 µl of treatment medium. Then the cells were treated with 200 µl of 100 µM DCFH-DA in treatment medium and incubated for 30 min at 37 °C. The wells were washed with 100 µl of treatment medium. Then 50 µM H_2O_2 was applied to the cells in 100 µl of treatment medium and the 96-well microplate was placed into a fluorescence microplate reader (FLx800, Bio-Tek Instruments Inc., Winooski, VT, USA) at 37 °C. Emission at 528 nm was measured with excitation at 485 nm every minute for 1 h. Each plate included triplicate control, blank and sample background wells: control wells contained cells treated with DCFH-DA and oxidant, blank wells contained cells treated with DCFH-DA without oxidant, sample background wells contained cells treated

with nanoemulsions and DCFH-DA without oxidant. The area under the curve of fluorescence versus time was integrated to calculate the CAA value, according to eq. (VII.1) (Wolfe and Liu, 2007):

$$CAA\ unit = \left(100 - \frac{\left(\int SA - \int BA \right)}{\int CA} \right) \times 100 \qquad \text{(VII.1)}$$

where $\int SA$ is the integrated area from the sample curve; $\int BA$ is the integrated area from the blank curve or sample background curve and $\int CA$ is the integrated area from the control curve.

VII.3 Results

VII.3.1 Antioxidant activity of nanoencapsulated resveratrol

Resveratrol was encapsulated into different peanut oil-based nanoemulsions, whose composition and mean droplet diameter is reported in Table VI.1, using a combination of hydrophilic and lipophilic emulsifiers. Moreover, the physicochemical stability of encapsulated resveratrol during *in vitro* digestion has been evaluated and described in section VI.3.1.

The retention of the antioxidant activity of nanoencapsulated resveratrol during *in vitro* digestion was preliminary assessed by two chemical assays, namely FRAP and ORAC, in comparison with the unencapsulated resveratrol diluted in DMSO (Figure VII.1).

It is important to investigate the antioxidant activity of resveratrol also in non-digested delivery systems, because one of the advantages of the nanometric delivery systems is the acceleration of the transport to the intestinal epithelial cells, due to the high dispersibility and hence diffusivity through the intestinal aqueous boundary layer (Acosta, 2009), making unnecessary the stage of bile emulsification.

The results of both FRAP and ORAC analyses, which were very consistent with each other, showed that the nanoencapsulated resveratrol controls retained an antioxidant activity comparable to the unencapsulated form, with higher values being observed for R/T20-GMO and R/LSL-SE.

In vitro digestion caused for all formulations a reduction of the antioxidant activity, which was particularly evident in the gastric step for R/LSL-DSL and R/LEC formulations. This result can be explained with the increase of the mean droplet sizes observed after gastric digestion (Figure VI.1), which was responsible for a significant reduction of the surface area (of two orders of magnitude), and consequently making resveratrol unavailable through the oil/water interfaces.

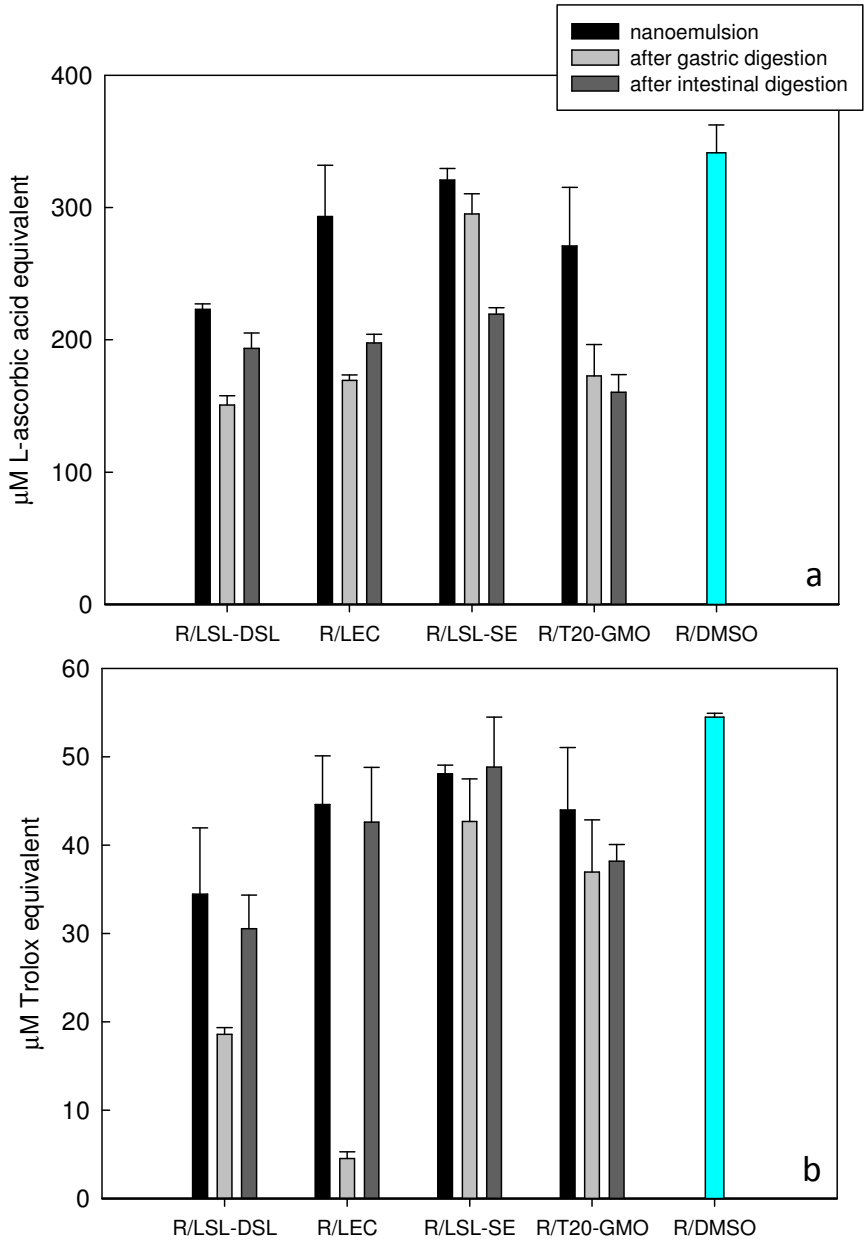

Figure VII.1 *Antioxidant activity of nanoemulsions containing resveratrol by FRAP assay (a) and ORAC assay (b) before and after the in vitro digestion process, in comparison with resveratrol dissolved in DMSO (R/DMSO).*

The antioxidant activity of the control (undigested nanocapsules) and digested samples was also assessed using a cell-based antioxidant assay system. Caco-2 cells were seeded on a 96-well microplate and the CAA assay was performed 15 days after seeding, in order to measure the antioxidant activity on mature differentiated intestinal cells with fully developed brush border enzymes and transporters.

Caco-2 cells were pre-treated with nanoencapsulated resveratrol, which due to the nanometric size of the capsules passed through the membrane to enter the cell. In this study Caco-2 cells were first pre-treated with the nanoencapsulated resveratrol, followed by DCFH-DA treatment, rather than pretreating the cells with the DCFH-DA and the antioxidant together, as suggested in a previous work (Wolfe and Liu, 2007). Preliminary results (not reported) showed that this modification eliminates the possibility of having the antioxidant effect outside the cells in the medium, and restricts the measured CAA solely to the interaction of intracellular resveratrol with DCFH. The cells were subsequently treated with H_2O_2, instead of a synthetic radical (Wolfe and Liu, 2007). H_2O_2 is a biologically relevant reactive oxygen species and is readily diffused into the cells. Once inside the cells, H_2O_2 oxidizes the intracellular DCFH to the fluorescent DCF. The nanoencapsulated resveratrol exerts its cellular antioxidant activity by preventing the oxidation of DCFH and reduce the formation of DCF.

Figure VII.2 shows the cellular antioxidant activity of the nanoemulsions containing resveratrol in comparison with the unencapsulated compound and the variation of the CAA during the *in vitro* digestion process. All formulations exhibited excellent antioxidant activity on Caco-2 cells, which, for R/LSL-SE, R/LEC and R/LSL-DSL was greater than 80% and comparable to the CAA of resveratrol dissolved in DMSO, suggesting that the nanometric size of the nanocapsules may improve the uptake of the antioxidant compound into the cells. Moreover, R/LEC and R/LSL-DSL showed a cellular antioxidant activity higher than expected considering the FRAP and ORAC results (Figure VII.1), which reported lower antioxidant activity for these formulations in comparison to the others due to a better resveratrol entrapment in the lipid phase and consequent reduction of the extent of its localization at the oil/water interface, as well as of the interaction with the oxidant reagents. The better entrapment of resveratrol can be likely attributed to the formation of reversed micelles of the more lipophilic emulsifier (i.e. glycerol monooleate, soy lecithin) within the lipid droplets stabilized by the more hydrophilic emulsifier (i.e. Tween 20, defatted soy lecithin, sugar ester).

The digestion process did not significantly affect the cellular antioxidant activity of encapsulated resveratrol, suggesting it being stable after gastric and intestinal digestion, and available to be absorbed by the cells in its active antioxidant form.

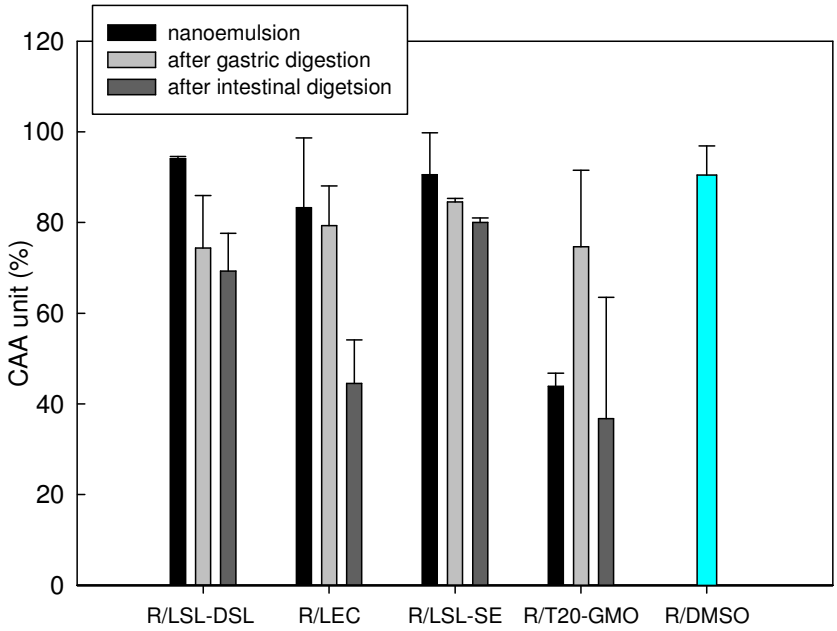

Figure VII.2 *Cellular antioxidant activity, CAA unit, of resveratrol-encapsulated nanoemulsions before and after in vitro digestion.*

It must be highlighted that, despite very surface active bile salts may have displaced some emulsifier molecules at the O/W interface, no significant changes were observed in the efficiency in delivering resveratrol to the cells in antioxidant activity measurements conducted before and after the gastric and intestinal digestion processes, probably thanks to the dual-emulsifier formulation that improved protection of resveratrol and its transport through the biological membranes.

Moreover, the most physically and chemically stable formulations also exhibited the highest chemical and cellular antioxidant activity, which was comparable to the undigested and unencapsulated resveratrol dissolved in DMSO.

VII.3.2 Antioxidant activity of encapsulated grape marc polyphenols

The antioxidant activity of grape marc polyphenols encapsulated in the O/W nanoemulsion-based delivery systems, whose compositions and mean droplet diameters have been reported in Table V.2, was measured in comparison to the unencapsulated grape marc extracts using both a chemical-based and a biological-based approach, in order to evaluate the capability of the delivery systems to efficiently protect the bioactive

compounds against degradation and to transport them to the intestinal epithelium in active form.

Figure VII.3 reports the chemical antioxidant activity of the encapsulated grape marc polyphenols in comparison with the unencapsulated compounds, according to two chemical assays, based on different mechanisms of antioxidant activity against free radicals: by single electron transfer reaction (FRAP assay) or by hydrogen atom transfer reaction (ORAC assay).

In fact, not always the ORAC and FRAP measurements of antioxidant activity correlate well with each other, with the observed discrepancies mainly depending on the nature of the bioactive compounds, as observed in the characterization of more than 900 vegetable extracts (Ou et al., 2002). The combined use of ORAC and FRAP assays can therefore provide more complete details on the dominant mechanisms of antioxidant activity of the tested extracts, both in encapsulated and unencapsulated form.

The results of the FRAP assay always showed a lower antioxidant activity of the encapsulated extracts in comparison with the unencapsulated compounds (Figure VII.3a). In contrast, the antioxidant activity of the encapsulated grape marc polyphenols measured with ORAC assay resulted comparable or higher than the antioxidant activity of unencapsulated compounds, except when the polyphenols were encapsulated in PO/GMO-DSL (Figure VII.3b), because of the already discussed issues of physicochemical stability of this formulation (Table V.3, Figure V.5c, Figure V.6c).

In the FRAP assay, the measure of antioxidant activity corresponds to a measure the capability of reducing the complex $Fe(TPTZ)_2(III)$ to $Fe(TPTZ)_2(II)$ (Benzie and Strain, 1996). In order to obtain an accurate measurement, the following conditions must be satisfied: 1) under the reaction conditions, $Fe(TPTZ)_2(III)$ should only interact with and hence be reduced by the antioxidant compounds object of measurement (other compounds with reducing activity might interfere with the measurement); 2) the reaction should be fast enough to get to completion within the assay time (30 min); 3) the oxidized antioxidant should have no absorption at 593 nm, where the absorption of $Fe(TPTZ)_2(II)$ is located (Ou et al., 2002).

Probably, the reaction rate of reduction of a ferric tripyridyltriazine complex, $Fe(TPTZ)_2(III)$, to the ferrous tripyridyltriazine, $Fe(TPTZ)_2(II)$, is faster for unencapsulated compounds (higher FRAP values) than for the encapsulated ones, which are embedded by the lipid phase and prevented from an optimal contact with Fe(III) complex.

The ORAC assay reflects instead the peroxyl radical scavenging activity, which is more relevant to the biological antioxidant activity. In fact, it was clearly demonstrated that hydrogen atom transfer reaction concurs with electron transfer reaction and plays a dominant role in biological redox reactions (Wright et al., 2001), with the consequence that the ORAC

principle is closely related to biological functions of chain-breaking antioxidants.

The comparable ORAC values for the antioxidant activity of encapsulated and unencapsulated polyphenols suggest their being similarly available for the peroxyl radical scavenging activity, which is apparently not affected by their inclusion in the lipid phases.

The total measured antioxidant activity resulting from FRAP assay is of about 3800 μM of ascorbic acid equivalents in the methanolic solution and 3000 μM in the prepared nanoemulsions (Figure VII.3a), corresponding to about 0.5 $g_{\text{ascorbic acid equivalents}}$/L. This antioxidant activity is comparable to that of a commercial orange juice, where the average concentration of ascorbic acid is about 0.3 g/L (Pisoschi et al., 2008). The equivalent concentration of ascorbic acid in the dried extracts is instead 0.5 g/g.

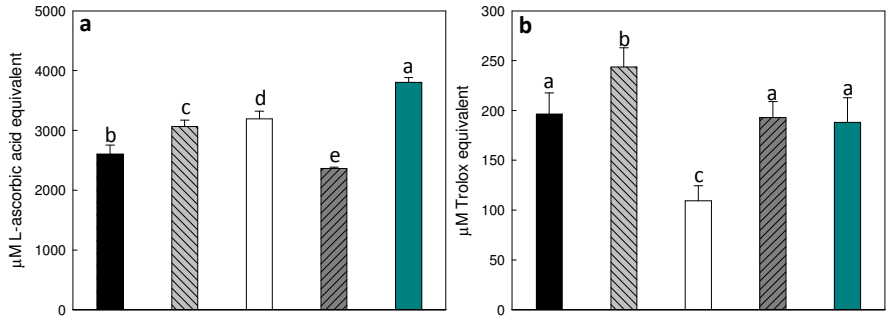

Figure VII.3 *Chemical antioxidant activity using (a) FRAP assay and (b) ORAC assay of grape marc polyphenols nanoencapsulated into:* (■) *SO/GMO-DSL,* (▨) *SO/LSL-DSL,* (▨) *PO/GMO-DSL and* (▨) *PO/LSL-DSL, in comparison with* (■) *unencapsulated grape marc polyphenols dissolved in methanol. Different letters indicate statistically (Student t test) significant differences ($p<0.05$).*

To overcome the limitations of biological significance of the FRAP and ORAC chemical assays, such as the redox reaction of a ferric/ferrous complex, and the use of pH values quite far from the physiological pH (FRAP), or the measurement of the antioxidant activity against peroxyl radicals, not considering other biologically relevant reactive oxygen species (ORAC), a biological-based approach was used to take into account also the bioavailability, uptake, and metabolism of the antioxidant compounds.

Remarkably, all the tested formulations exhibited a CAA value significantly higher than the unencapsulated grape marc polyphenols (Figure VII.4). This can be explained in terms of an increased transport through the Caco-2 cell membrane thanks to the nanometric size of the delivery systems, comprised between 176 and 220 nm. The PO/GMO-DSL system, despite its

large mean droplet size (1330 nm), also showed very high CAA value, comparable to the other nanometric delivery systems, probably due to its being composed of aggregated nanoparticles, which are able to adhere to the cell walls and possibly facilitate the penetration of the active compounds inside the cells.

The formulation of the delivery systems based with soy lecithin, which is a mixture of phospholipids similar to the phospholipid bilayer structure of the cellular membrane, seems to significantly contribute to their absorption into the cells, favouring the entrapment in the microvilli and the consequent transport through the cell membrane.

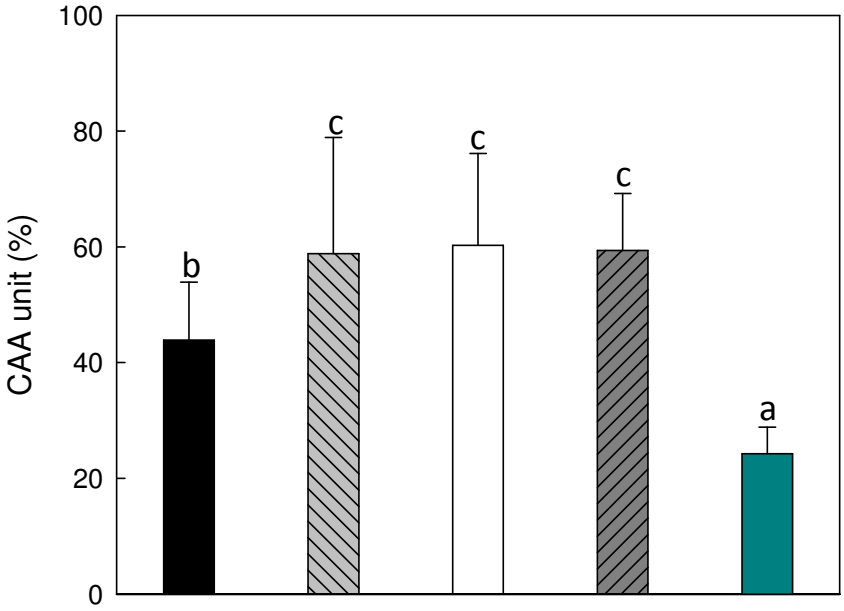

Figure VII.4 *Cellular antioxidant activity (CAA unit) of grape marc polyphenols nanoencapsulated into:* (■) *SO/GMO-DSL,* (▨) *SO/LSL-DSL,* (▨) *PO/GMO-DSL and* (▨) *PO/LSL-DSL, in comparison with* (■) *unencapsulated grape marc polyphenols dissolved in methanol. Different letters indicate statistically (Student t test) significant differences (p<0.05).*

VII.3.3 Antioxidant activity of encapsulated curcumin

Curcumin was encapsulated in solid lipid particles of micrometric sizes, using stearic acid as lipid phase and a combination of soy lecithin and sugar esters (C/LSL-SE) or lipophilic and defatted soy lecithins (C/LSL-DSL) as emulsifiers, as described in section V.3.

The influence of the delivery system on the antioxidant activity of curcumin was evaluated using a chemical-based approach (FRAP and ORAC assays) and a biological-based approach, based on the measurement of the cellular antioxidant activity on Caco-2 cells, to overcome the limitations of the chemical assays as previously described.

Figure VII.5a shows a very low antioxidant activity of encapsulated curcumin in comparison with unencapsulated form using FRAP assay, probably due to the presence of a solid lipid matrix which avoids the interaction of the encapsulated curcumin with FRAP reagents. On the contrary, when an ORAC assay is used, an higher antioxidant activity for the encapsulated curcumin was measured (Figure VII.5b). Moreover, the lecithin/sugar ester-based formulation shows an antioxidant activity comparable to the unencapsulated curcumin.

As already shown for the other nanoencapsulated polyphenols, the trend of the antioxidant activity using ORAC assay is similar to that obtained from the results of a cellular antioxidant activity assay, confirming that ORAC assay better simulates the biological processes.

In particular, a cellular antioxidant activity (> 60%) of curcumin encapsulated in lecithin/sugar°ester-based emulsion and comparable with the unencapsulated compound was observed using a biological approach. This latter behaviour is explained by the ability of the delivery system to improve the cellular uptake of the encapsulated bioactive compound.

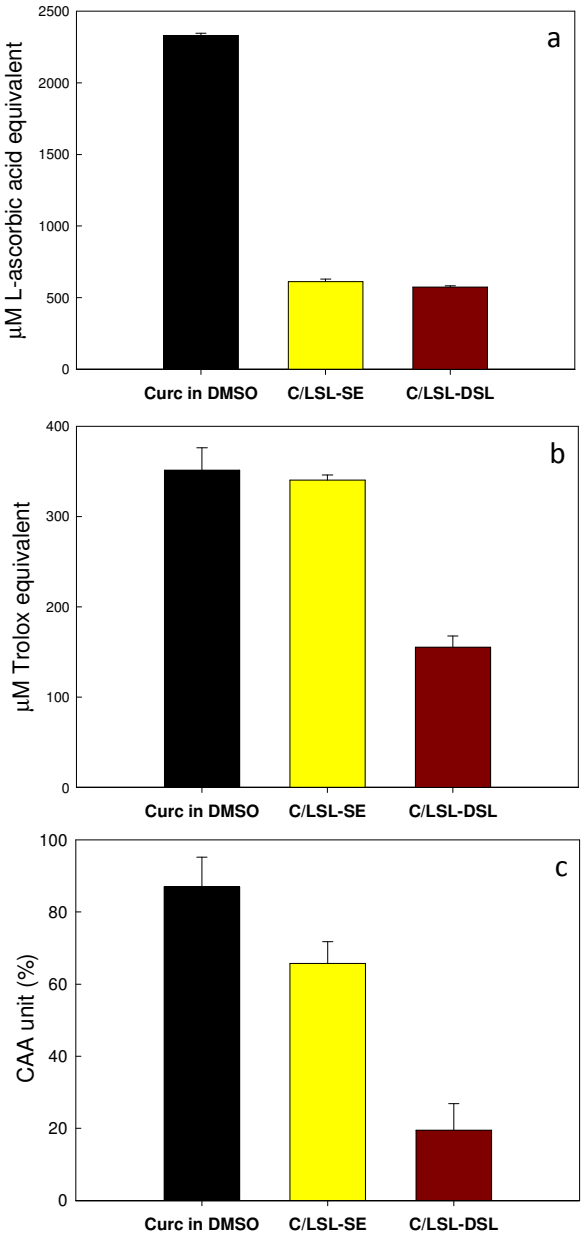

Figure VII.5 *Comparison of the antioxidant activity of encapsulated curcumin into solid lipid particles, produced by HPH using as emulsifiers lipophilic soy lecithin and sugar ester (C/LSL-SE) or lipophilic and defatted soy lecithin (C/LSL-DSL), with unencapsulated curcumin diluted in DMSO, using (a) FRAP assay, (b) ORAC assay and (c) Cellular Antioxidant Activity assay.*

VII.4 Conclusions

For the first time, the effect of nanoemulsion-based delivery systems on the antioxidant activity of encapsulated bioactive has been investigated.

The antioxidant activity of nanoencapsulated compounds has been measured using two chemical assays, FRAP and ORAC, based on different mechanisms. Moreover, an *ex vivo* antioxidant assay has been used to overcome the limitations of the chemical assays.

For this purpose, a novel method was proposed and tested for measuring the cellular antioxidant activity (CAA) exclusively due to the bioactive absorbed into the cells. In our modified method Caco-2 cells are pre-treated with the nanoencapsulated polyphenols first, followed by probe treatment. This modification eliminates the possibility of measuring any antioxidant effect outside the cells in the medium, and restricts the measured cellular antioxidant activity solely to the interaction of intracellular polyphenols with fluorescent probe.

The FRAP and ORAC assays showed that the antioxidant compounds, when encapsulated, are as available as unencapsulated polyphenols in scavenging the peroxyl radicals (ORAC), but are less available in reducing the ferric tripyridyltriazine complexes (FRAP). Remarkably, the cellular antioxidant activity was significantly higher for the encapsulated bioactive compounds than for the unencapsulated ones, suggesting the fundamental role of the nanoemulsions in favoring the delivery through the biological membranes.

Chapter VIII
Antimicrobial activity of nanoencapsulated essential oils

In this chapter is highlighted how the encapsulation on nanometric scale of essential oils (terpene mixture and D-limonene) represents a viable method to enhance the antimicrobial activity and minimize the alteration of the quality attributes of the product where the antimicrobials are incorporated.

The effect of the nanodelivery systems on the antimicrobial activity of essential oils was evaluated by determining the minimum inhibitory concentration (MIC) and minimum bactericidal concentration (MBC) for three different classes of microorganisms (*Lactobacillus delbrueckii*, *Saccharomyces cerevisiae*, *Escherichia coli*). Moreover, the different mechanisms of inactivation of encapsulated antimicrobials were investigated by fluorescence microscopy.

Finally, the incorporation of the most efficient antimicrobial nanocapsules was tested in real systems, such as fruit juices, inoculated with *L. delbrueckii*.

VIII.1 Essential oils as natural antimicrobials

Nowadays, the approaches that can be adopted in food preservation include: a) handling and aseptic packaging, to prevent the penetration of microorganisms in the food, b) the mechanical removal of microorganisms by washing or filtration, c) destruction of microorganisms by heat, pressure, radiation, electric or magnetic fields as well as by chemical sanitization, and finally d) the inhibition of pathogens through environmental control.

The latter approach has benefited most from the recent developments in nanotechnology. Inhibition of microbial growth through environmental control is achieved through the addition of chemical compounds

(antimicrobial preservatives) with an inhibitory or bactericidal/fungicide activity. In the last years, natural antimicrobials have attracted considerable attention due to the increased consumer awareness on the aspects of food quality and safety.

Similar to most bioactive compounds (aromas, antioxidants and nutraceuticals, etc.), antimicrobial agents are chemically reactive species, which can cause considerable problems when they are embedded into a complex food system. For antimicrobial compounds, this translates into the need to use concentrations which are high enough to inhibit microbial growth within the limits imposed by food regulations, but at the same time minimally alter the qualitative properties of the product (Weiss et al., 2009).

Nanoencapsulation of antimicrobial compounds represents a viable and efficient approach to increasing the concentration of the bioactive compounds in food areas where microorganisms are preferably located, for example water-rich phases or liquid-solid interfaces (Weiss et al., 2009).

A significantly large part of current literature on the encapsulation of essential oils deals with micrometric size capsules, which are used for the protection of the active compounds against those environmental factors, which contribute to their deterioration (e.g. oxygen, light, moisture, pH), as well as enhance their antimicrobial activity by increasing the mass transfer efficiency.

For example, solid lipid microparticles (delivery systems where the lipid phase is in a solid state) have been proposed for the encapsulation of juniper oil, in order to reduce the volatility of the antimicrobial agent, loaded inside the lipidic structure (Gavini et al., 2005).

Several authors have proposed the use of biopolymers for the formulation of microparticles in the encapsulation of essential oils, such as chitosan, whose use for oral cavity care was recently reviewed (Pedro et al., 2009), as well as Ca-alginate hydrogels (Wang et al., 2009). In particular, the entrapment of carvacrol in microcapsules made of Ca-alginate hydrogel, tested for oral administration to pigs, resulted in the reduced absorption of carvacrol in the upper gastrointestinal tract, therefore retaining its potential antibacterial activity for the small intestine in controlling enteric diseases (Wang et al., 2009).

In food applications, spray drying has been frequently investigated for the microencaspulation of antimicrobial agents. For example, milk protein-based matrices exhibited excellent properties for coating the essential oils of oregano as well as the aroma extracts of citronella and sweet marjoram (Baranauskiene et al., 2006). The use of a blend of Arabic gum, maltodextrin and modified starch as wall materials offered a good protection in encapsulating cardamom oleoresin against degradation (Krishnan et al., 2005).

While microcapsules may guarantee excellent protection of essential oils against degradation or evaporation, they in general do not affect

antimicrobial activity. In contrast, nanometric size delivery systems, due to the subcellular size, may increase the passive cellular absorption mechanisms, thus reducing mass transfer resistances and increasing antimicrobial activity.

Proof of this concept was given by the incorporation into liposomal delivery systems of *Origanum dictamnus L.* (Liolios et al., 2009), Citrus limon extracts (Gortzi et al., 2007) and *Artemisia arborescens L.* essential oil (Sinico et al., 2005): all these systems resulted in the improvement of the antimicrobial activity of encapsulated compounds.

The encapsulation of eugenol and carvacrol into nanometric surfactant micelles (microemulsions), also resulted in enhanced antimicrobial activity, which has been attributed to the increased solubility of essential oil components in the aqueous phase due to the presence of surfactants as well as to the improved interactions of antimicrobials with microorganisms (Gaysinsky et al., 2005). Nevertheless, when the encapsulated eugenol was added to milk, it resulted to be less or as inhibitory as unencapsulated eugenol against target pathogens (Gaysinsky et al., 2007). Moreover, the appreciable water solubility of eugenol appeared to promote a rapid diffusional mass transport of the essential oil molecules from microemulsions to the milk macroemulsions, especially for systems composed of phytophenols above a critical loading ratio (Gaysinsky et al., 2007).

In spite of the fact that nanoemulsions are potentially very promising antimicrobial carrier systems, thanks to the easy industrial scalability of the production process by high pressure homogenization, up to now very little systematic research has been carried out to evaluate their use in encapsulating antimicrobial essential oils (Weiss et al., 2009).

The results of current literature highlight that very often antimicrobial activity is reduced by nanoencapsulation. For example, the antimicrobial activity of chitosan in soybean lecithin or Polaxamer-based nanoemulsions resulted to be slightly lower than the activity of free chitosan (Jumaa et al., 2002), with it being most likely due to the adsorption of positively charged chitosan onto the surface of the emulsion droplets, thereby decreasing the concentration of chitosan in the aqueous phase as well as its overall activity.

Similarly, the encapsulation of different preservatives (such as benzalkonium chloride, methyl and propyl parabens as well as chlorocresol) into submicron emulsions induced instability phenomena and in some cases insufficient antimicrobial activity (Sznitowska et al., 2002).

In comparison with unencapsulated active compounds, corn-oil-in-water emulsions loaded with eugenol exhibited lower activity, inhibiting *E. coli* strains, but failed to inhibit the growth of *L. monocytogenes* strains (Weiss et al., 2009). When using Tween 20 and lauric arginate as emulsifiers, nanoemulsions containing eugenol displayed similar antimicrobial activities to unencapsulated eugenol against both microorganisms (Weiss et al., 2009).

The aforementioned studies show the need for more detailed research on the formulation, design and application of nanoemulsions as antimicrobial delivery systems, in order to maximize the antimicrobial efficacy of the encapsulated compounds.

This section focuses on the nanoencapsulation in nanoemulsion-based delivery systems of two antimicrobial compounds, a terpenes mixture extracted from *Melaleuca alternifolia* and D-limonene. It deals with the issues of formulation and fabrication in order to retain and possibly enhance the antimicrobial activity of the encapsulated compounds. The most promising formulations in terms of antimicrobial activity are tested at different concentrations in fruit juices inoculated with *Lactobacillus delbrueckii*, which can be considered as one of the potential spoilage microorganisms of fruit juices, in order to evaluate the possible shelf-life extension against the alteration of the quality parameters of the juices.

VIII.2 Materials and methods

VIII.2.1 Materials

The antimicrobial compounds tested were D-Limonene (Sigma-Aldrich, Germany) and a mixture of terpenes extracted from *Melaleuca alternifolia* (provided by Istituto Superiore della Sanità, Italy). In the emulsion fabrication, sunflower oil (Sagra, Italy) and palm oil (Sigma-Aldrich, Germany) were used as organic phases, while soy lecithin Solec Ip (a generous gift from Solae Italia s.r.l., Italy), Tween 20 and glycerol monooleate (Sigma-Aldrich, Germany), and CLEARGUM® CO 01 (a generous gift from Roquette, Italy) were used as emulsifying agents.

VIII.2.2 Preparation of nanoemulsions

The sunflower oil or essential oil-in-water nanoemulsions were prepared using a High Pressure Homogenization (HPH) technique. Primary emulsions were obtained by High Shear Homogenization (HSH), using an *Ultra Turrax T25* (IKA Labortechnik, *Jahnke und Kunkel, Germany*) at 24000 rpm for 5 min. The primary emulsions were then subjected to HPH by passing them through a high pressure homogenizer Nano DeBEE Electric Bench-top Laboratory (BEE International, USA) ten times at 350 MPa. When palm oil was used as a lipid phase, the antimicrobial agents were dissolved in the melted lipid and, in order to prevent recrystallisation, the temperature during processing was always kept about 5-10 °C above the lipid melting point. Crystallization of the lipid droplets was attained by rapid cooling of the hot nanoemulsions in an ice bath at the end of the HPH processing.

Droplet size distribution of the nanoemulsions produced was determined by photon correlation spectroscopy at 25 °C (HPPS, Malvern Instruments,

UK). Each measurement was replicated twice, with the means and the standard deviations being calculated.

VIII.2.3 Determination of MIC and MBC

Experiments were carried out on three different microbial strains grown to the stationary phase in an aerated incubator (Haeraeus Instruments): *Saccharomyces cerevisiae*, *Escherichia coli*, *Lactobacillus delbrueckii.*

S. cerevisiae yeast was grown in MRS broth (Oxoid, UK) at 32 °C for 48 h, *E. coli* in Tryptone Soya broth (Oxoid, UK) at 30 °C for 18-24 h, *L. delbrueckii* in MRS broth (Oxoid, UK) at 32 °C for 48 h.

The Minimum Inhibitory Concentration (MIC) of the antimicrobial agents was evaluated for the three microbial strains, for the following concentrations of antimicrobial agents in culture media: 25, 10, 5.0, 1.0 and 0.1 g/L. The sample were inoculated with 100 µl of a microbial suspension (10^7 CFU/ml) and incubated for 24 h at 32 °C for *S. cerevisiae* and *L. delbrueckii* and at 30 °C for *E. coli.* The MIC value was determined as the lowest concentration of the antimicrobial agent that inhibited the visible growth of the test microorganism, evaluating the absorbance of the sample with a spectrophotometer (Jasco V-650) in the range of 590-600 nm.

The Minimum Bactericidal Concentration (MBC) was also determined following MIC determination. A sample of 1 ml was collected from each tested sample and inoculated on sterile Plate count agar (Oxoid, UK) for *E. coli* and MRS agar (Oxoid, UK) for *S. cerevisiae* and *L. delbrueckii*. The plates were incubated at 37 °C for 24 h. The highest dilution that yielded a decrease in microbial concentration in comparison to the control sample was considered as MBC. Each measurement was replicated three times.

VIII.2.4 Kinetics of inactivation

The inactivation kinetics of three microorganisms (*S. cerevisiae*, *L. delbrueckii* and *E. coli*) in the presence of an encapsulated terpenes mixture were carried out on two levels of antimicrobial concentration (1.0 and 2.5 g/L), in comparison to a control, where terpenes were replaced by sunflower oil.

The microorganisms, centrifuged at 5000 rpm for 10 min at 4 °C, were resuspended in 100 ml of sterile distilled water in test tubes, with nanoemulsions being added to the desired final antimicrobial concentrations. The test tubes were then incubated at 32 °C for *S. cerevisiae* and *L. delbrueckii* and at 30 °C for *E. coli*. After 30 min for the antimicrobial concentration of 2.5 g/L and after 90 min and 24 h for the antimicrobial concentration of 1.0 g/L, the surviving cells were evaluated by a standard plate count method. In brief, 1 ml of each sample was used to prepare decimal dilutions, which were plated in duplicate with Plate Count agar for

E. coli and MRS agar for *S. cerevisiae* and *L. delbrueckii.* The plates were incubated at 30 °C for 24 h for *E. coli* and at 32 °C for 48 h for *S. cerevisiae* and *L. delbrueckii*.

Kinetics experiments were carried out in duplicate. From the linear regression of the common logarithm of the survival fraction vs. the exposure time to the antimicrobials, the decimal reduction time *D*, defined according to eq. (VIII.1), was calculated.

$$D = \frac{\log \frac{N_0}{N(t)}}{t - t_0} \qquad \text{(VIII.1)}$$

VIII.2.5 GC-MS analysis

The composition of the terpenes mixture after homogenization (either HSH or HPH) was evaluated through a gas chromatography-mass spectrometry method (GC-MS). The terpenes mixture was extracted by adding 4 ml of dichloromethane to 500 µl of nanoemulsion, followed by three vortex agitations of 10 s each. The organic phase was recovered with a Pasteur pipette and anhydrous sodium sulphate was added to remove any traces of water. The extract was micro-filtered and placed for 15 min under a nitrogen flow in order to completely evaporate the solvent. 2 µl of the resulting terpenes were added to 2 ml of n-pentane and analyzed by Focus-GC-DSQ (Thermo Finnigan) gascromatograph, equipped with a capillary column Rtx-5Sil MS (30 m, ID 0.25 mm, film thickness 0.25 µm; Restek), using helium as a carrier gas (1 ml/min). The column temperature was kept at 40 °C for 3 min and then increased by 3 °C/min to 280 °C. The mass selective detector was used in the electron ionisation mode, with the mass range between 35 and 500 being scanned. The mass spectra were compared to both the NIST Mass Spectral Library as well as an in-house library for peak identification.

VIII.2.6 Fluorescence microscopy

Fluorescence microscopy was used to visualize the transport of nanoencapsulated antimicrobials through the cell membrane into *S. cerevisiae*. The fluorescence microscope consisted of a Eclipse TE2000S inverted microscope (Nikon), equipped with a B-2A filter (Excitation Filter Wavelengths: 450-490 nm, Dichromatic Mirror Cut-on Wavelength: 500 nm, Barrier Filter Wavelengths: 515 nm cut-on), fitted with a high-pressure mercury burner as a light source. The images were acquired with a digital camera (DS-5M Digital Sight Camera System, Nikon), through a 20x lens (Nikon).

Nile red (Sigma-Aldrich, Germany) was used as a fluorescent lipophilic stain. It excites at 485 nm, and emits at 525 nm. The Nile Red was dissolved in ethanol at a concentration of 1 mg/ml; a sample of 100 µl of this solution were added to 1 ml of nanoemulsion to stain the oil droplets. 100 µl of nanoemulsion with Nile Red were subsequently added to 1 ml of culture medium containing 10^8 cfu/ml of yeast cells in a stationary phase to a final antimicrobial concentration of 5.0 g/L. At a fixed time (1 min, 30 min, 1 h, 2 h, 3 h, 24 h), a drop of the sample was mounted onto a glass slide, enclosed with a cover slip and observed.

VIII.2.7 Shelf life of fruit juices

The effect of the addition of the encapsulated antimicrobial on the microbiological stability of two fruit juices, orange juice (Tropicana Pure Premium PepsiCo, France) and pear juice (Yoga, Italy), was evaluated over time. The juices were inoculated with 10^3 cfu/ml of *Lactobacillus delbrueckii*. Different concentrations (10, 5.0 and 1.0 g/L) of terpenes nanoemulsions were tested under accelerated shelf life conditions at 32 °C.

The concentration of microorganisms in each sample expressed in CFU/ml was evaluated over time by standard plate count method, as previously described. Moreover, the evolution of color, pH and °Brix of the fruit juices over storage time was also evaluated by Chroma Meter (CR-200b, Minolta), pH-meter (Basic 20+, Crison) and Abbe Refractometer (Atago) respectively.

The color was measured registering the following parameters: *L* (brightness), *a* (red-green component) and *b* (yellow-blue component). The global color difference (*ΔE*) was calculated with the following equation:

$$\Delta E = \sqrt{(\Delta L)^2 + (\Delta a)^2 + (\Delta b)^2} \qquad \text{(VIII.2)}$$

The values provided were the average of three replicates.

VIII.3 Results

VIII.3.1 Mechanisms of inactivation of encapsulated essential oils

Different formulations and fabrication methods were used to produce stable nanoemulsions encapsulating the antimicrobial compounds. In general, the nanoemulsions contained 50 g/kg of the active compounds (a terpenes mixture or D-limonene), eventually mixed in the organic phase (palm oil or sunflower oil). Soy lecithin, modified starch (clear gum) or a mixture (50:50) of Tween 20 and glycerol monooleate were used as emulsifiers.

Table VIII.1 reports all those nanoemulsions, which resulted physically stable over 4 weeks with neither visible creaming nor significant variation of the mean droplet diameter.

Only the lecithin-based nanoemulsions, whose mean droplet diameter ranged from 75 nm (High Pressure Homogenization processing, HPH) to 175 nm (High Shear Homogenization processing, HSH), represented a stable delivery system for the terpenes mixture, without any additional organic phase. In contrast, the production of stable lecithin-based nanoemulsions (240 nm) required the blending of D-limonene with palm oil (1:1).

Table VIII.1 *Composition, dimension (Z-diameter) and production method of the tested nanoemulsions.*

Sample	Composition	Process	Z-diameter [nm]
T/SL-HPH	50 g/kg terpenes 10 g/kg soy lecithin 940 g/kg water	10 HPH passes at 300 MPa 3°C	74.4 ± 2.6
T/SL-HSH	50 g/kg terpenes 10 g/kg soy lecithin 940 g/kg water	HSH at 24000 rpm for 5 min	174.8 ± 5.7
L/PO-SL	50 g/kg D-limonene 50 g/kg palm oil 20 g/kg soy lecithin 880 g/kg water	10 HPH passes at 300 MPa 30°C	235.9 ± 9.6
L/CG	50 g/kg D-limonene 100 g/kg clear gum 850 g/kg water	10 HPH passes at 300 MPa 3°C	365.7 ± 7.5
L/SO-T20-GMO	50 g/kg D-limonene 50 g/kg sunflower oil 15 g/kg Tween 20 15 g/kg glycerol monooleate 870 g/kg water	10 HPH passes at 300 MPa 3°C	130.9 ± 1.3
L/T20-GMO	50 g/kg D-limonene 7.5 g/kg Tween 20 7.5 g/kg glycerol monooleate 935 g/kg water	10 HPH passes at 300 MPa 3°C	154.6 ± 1.4

A stable nanoemulsion (365 nm) was obtained with pure D-limonene as the organic phase only when clear gum was used as an emulsifier.

D-limonene was also encapsulated, alone or blended with sunflower oil (1:1), into stable delivery systems made of Tween 20 and glycerol

monooleate–based nanoemulsions, with a very fine mean droplet diameter (from 130 to 155 nm).

To evaluate the activity of an antimicrobial agent the Minimum Inhibitory Concentration (MIC) and the Minimum Bactericidal Concentration (MBC) can be measured. When the antimicrobial agent is encapsulated, the MIC and MBC can provide information on the efficiency of the delivery system to transport the active compound across the cell membrane of the target microorganisms.

Table VIII.2 reports the MIC and MBC values of a nanoencapsulated terpenes mixture as well as nanoencapsulated D-limonene in comparison to pure compounds.

Table VIII.2 *MIC and MBC measurements of pure and encapsulated essential oils on different microbial strains.*

	E. coli		***L. delbrueckii***		***S. cerevisiae***	
	MIC (g/L)	MBC (g/L)	MIC (g/L)	MBC (g/L)	MIC (g/L)	MBC (g/L)
Terpenes mixture	**5.0**	**5.0**	**5.0**	**25**	**10**	**10**
T/SL-HPH	1.0	5.0	10	10	1.0	5.0
T/SL-HSH	5.0	5.0	5.0	10	1.0	5.0
D-Limonene	**>25**	**>25**	**>25**	**>25**	**>25**	**>25**
L/CG	10	>25	10	>25	10	25
L/PO-SL	10	>25	10	>25	10	>25
L/SO-T20-GMO	5.0	>25	5.0	>25	5.0	>25
L/T20-GMO	5.0	>25	25	>25	25	>25

The MIC and MBC values of the antimicrobial agents encapsulated in nanoemulsions resulted always lower or equal to pure compounds, therefore suggesting the enhancement of transport mechanisms through the cell membrane of the target microorganisms.

The effect of the encapsulation system on the antimicrobial activity of the terpenes mixture depended on the target microorganism. For *S. cerevisiae,* the MIC and MBC values were reduced from 10 g/L to 1.0 g/L and 5.0 g/L respectively when the terpenes mixture was encapsulated in both nanoemulsion T/SL-HPH and T/SL-HSH. For *L. delbrueckii,* the

nanoencapsulation caused a reduction of only the MBC values for both T/SL-HPH and T/SL-HSH from 25 to 10 g/L, while the MIC values remained unchanged at 5.0 g/L for nanoemulsion T/SL-HSH and increased to 10 g/L for nanoemulsion T/SL-HPH. Interestingly, encapsulation of the terpenes mixture did not significantly reduce the MIC and MBC values for *E. coli.*

The antimicrobial activity of D-limonene is significantly lower than that of the terpenes mixture, with the MIC and MBC values being always higher than 25 g/L. Experimental measurements were intentionally limited to 25 g/L due to higher concentrations being considered unsuitable for food applications.

In contrast with what was observed with the terpenes mixture, the encapsulation of D-limonene never reduced the MBC values, but affected only the MIC values.

For L/CG and L/PO-SL nanoemulsions, the MIC values were reduced from >25 g/L to 10 g/L for all the microorganisms. For nanoemulsion L/SO-T20-GMO, the MIC reached the smallest value (5.0 g/L) for all the microorganisms, which is probably due to the fine droplet diameter of the delivery system. Whereas, nanoemulsion L/T20-GMO induced a reduction of the MIC value to 5.0 g/L for *E. Coli* and only to 25 g/L for the other microorganisms.

The results reported in Table VIII.2 show that the effect of encapsulation on the different delivery systems tested depends on the active compounds. The encapsulation of the terpenes mixture enhances both the bacteriostatic and bactericidal activity (MIC values are close to MBC values) for selected microorganisms (*S. Cerevisiae* and *E. coli*). This is probably due to the fact that *L. delbrueckii* is, unlike the other tested microorganisms, a gram-positive bacterium with a thick cell wall formed by 40 layers of peptidoglycan chains. In contrast, the encapsulation of D-limonene enhanced only its bacteriostatic activity (the MIC values were significantly smaller than the MBC values) on all the tested microorganisms.

In particular, previous studies showed that the antimicrobial activity of cyclic hydrocarbons is limited by their solubility, being available for interaction with cells only those molecules which are dissolved in the aqueous phase (Sikkema et al., 1995). This implies that the effect of an antimicrobial compound would be expected to be maximal under conditions of maximum solubility: for example, essential oil components, such as carvacrol, need to be dissolved in concentrations approaching or exceeding their maximum solubility in order to exhibit bactericidal activity (Gill and Holley, 2006). In contrast, limonene, which is characterized by a very limited water solubility (at least 1 order of magnitude smaller than carvacrol), exhibits only a bacteriostatic activity unless its concentration in the aqueous phase is enhanced. It is possible to increase the concentration of limonene in the aqueous phase by changing the emulsion lipid phase, and

therefore acting on the partitioning on limonene between the two phases, or by choosing an emulsifier which is able to solubilize in micelle assemblies the limonene molecules. From the results obtained, no apparent difference could be observed when using a solid lipid such as palm oil on the limonene activity, despite the possibility that limonene may be expelled from the emulsion droplets by the solid fat crystallization. In contrast, the use of emulsifiers, such as the combination of Tween 20 and glycerol monooleate, resulted in a slight increase of the bacteriostatic activity of limonene, suggesting that the water solubility of limonene might have been increased by micelle solubilization.

The bacteriostatic activity of D-limonene as well as the bactericidal activity of the terpenes mixture were visualized by fluorescence microscopy observations. Images of the *S. cerevisiae* cells exposed to the nanoemulsion L/CG (Figure VIII.1) as well as the nanoemulsion T/SL-HPH (Figure VIII.2), both loaded with fluorescent dye (Nile Red), were recorded after 5 min and 24 h.

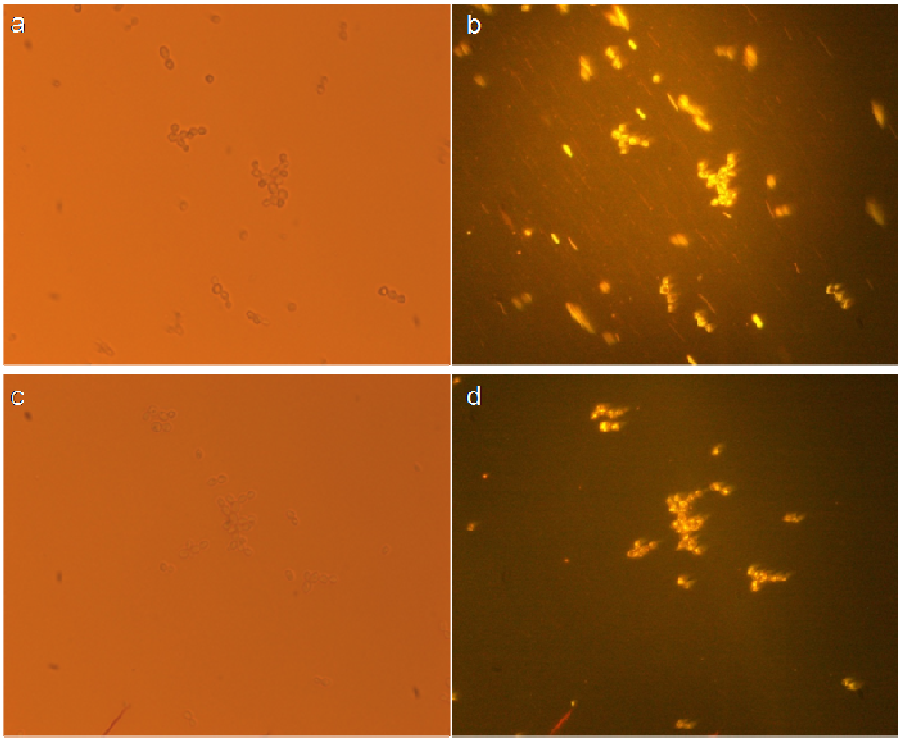

Figure VIII.1 *Brightfield (a and c) and fluorescence micrographs (b and d) of S. cerevisiae cells exposed to nanoemulsion L/CG captured by fluorescence microscopy after 5 min (a and b) and 24 h (c and d).*

Under a fluorescent light, the nanoemulsion droplets cannot be distinguished when they are dispersed in an aqueous system due to their nanometric size, with only a fluorescent halo being observed. In contrast, when the nanoemulsion droplets accumulate in the cell membrane as well as the intracellular space, the yeast cells became fluorescent and can be observed. Figures VIII.1 and VIII.2 show that both nanoemulsions can readily permeate the cell membrane: after 5 min, the yeast cells became fluorescent, suggesting that the antimicrobial agents have reached the action sites. After 24 h, there was a significant difference between the nanoemulsion T/SL-HPH and L/CG. The yeast cells exposed to the terpenes mixture exhibited a shrunk cell membrane, which suggests their death probably due to the loss of intracellular material (Figure VIII.2). On the other hand, the yeast cells exposed to nanoencapsulated D-limonene did not show any apparent change in shape and size, therefore suggesting a merely bacteriostatic effect of this compound, leaving the cells alive (Figure VIII.1).

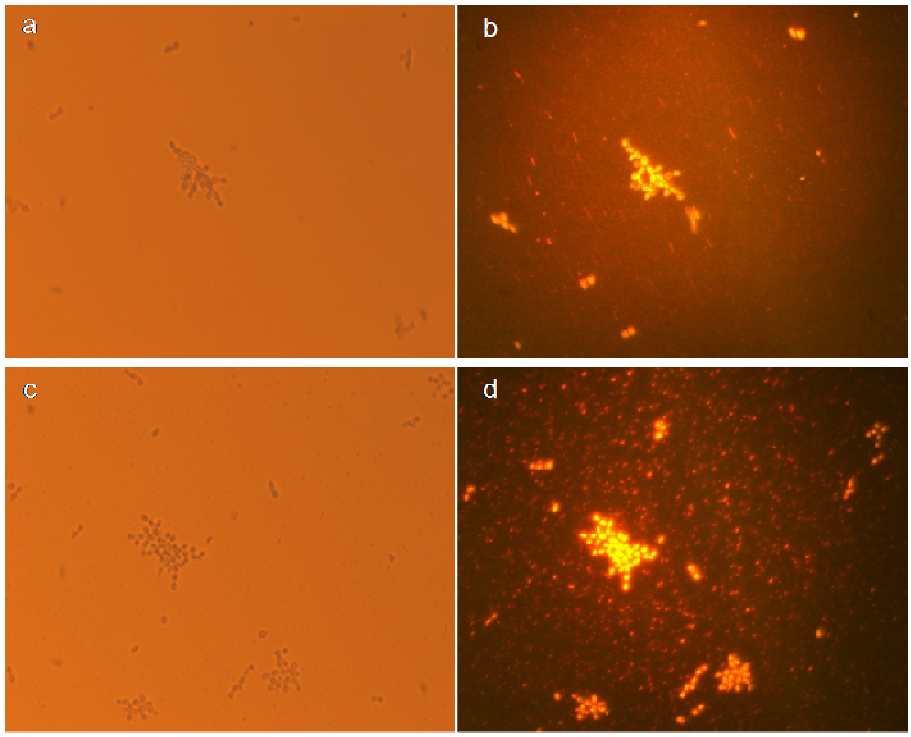

Figure VIII.2 *Brightfield (a and c) and fluorescence micrographs (b and d) of S. cerevisiae cells exposed to nanoemulsion T/SL-HPH captured by fluorescence microscopy after 5 min (a and b) and 24 h (c and d).*

VIII.3.2 Kinetics of inactivation

The inactivation kinetics of the three target microorganisms exposed to the terpenes mixture encapsulated in nanoemulsions T/SL-HPH and T/SL-HSH were determined in water at two different antimicrobial concentrations (1.0 and 2.5 g/L).

Table VIII.3 reports the decimal reduction time of inactivation, *D*, defined as the time required to reduce by an order of magnitude the number of surviving microorganisms, and calculated by the linear regression of the semi-log plots of inactivation of *E. coli*, *L. delbrueckii* and *S. cerevisiae*.

Table VIII.3 *The decimal reduction time of inactivation of target microorganisms exposed to the terpenes mixture encapsulated in T/SL-HPH and T/SL-HSH delivery systems.*

	Decimal reduction time D [min]		
	E. coli	***L. delbrueckii***	***S. cerevisiae***
T/SL-HPH 2.5 g/L	7.57 ± 0.36 $R^2 = 0.977$	10.2 ± 2.8 $R^2 = 0.655$	312 ± 72 $R^2 = 0.587$
T/SL-HPH 1.0 g/L	556 ± 542 $R^2 = 0.215$	714 ± 12 $R^2 = 0.995$	∞
T/SL-HSH 2.5 g/l	7.68 ± 0.14 $R^2 = 0.966$	6.69 ± 0.38 $R^2 = 0.834$	30.7 ± 2.2 $R^2 = 0.924$
T/SL-HSH 1.0 g/l	909 ± 23 $R^2 = 0.992$	588 ± 19 $R^2 = 0.975$	∞

While the control systems (nanoemulsions where the terpenes mixture was substituted by sunflower oil) did not cause any measurable microbial inactivation over 24 h (data not reported), the terpenes–loaded nanoemulsions inactivated the three microorganisms with characteristic times (*D* in Table VIII.3) of the order of minutes at 2.5 g/L and of hours at 1.0 g/L. Interestingly, the nanoemulsion T/SL-HSH caused a faster inactivation than nanoemulsion T/SL-HPH, despite the larger mean droplet diameter: the decimal reduction time of nanoemulsion T/SL-HSH is always shorter than for nanoemulsion T/SL-HPH for *L. delbrueckii* and *S. cerevisiae*, while no significant difference can be observed for *E. coli*. Moreover, it can be observed that the larger droplet diameter system (nanoemulsion T/SL-HSH) induced also a higher reduction of the MIC and MBC values for *L. delbrueckii* (Table VIII.2). In contrast to what was

expected, a straightforward correlation between the efficiency of the antimicrobial delivery system and its mean droplet diameter is not possible. These unexpected results can be explained in terms of the degradation of some active compounds during HPH processing. Table VIII.4 reports the GC-MS analysis of the pure terpenes mixture, which was not subjected to any fluid dynamic stresses, and the analysis of the terpenes mixture as extracted from nanoemulsion T/SL-HPH, subjected to high intensity stresses during the HPH treatment, and from nanoemulsion T/SL-HSH, subjected to mild intensity stresses during the HSH treatment.

GC-MS analysis revealed that, due to fluid dynamic stresses, both the HSH and HPH processing caused the degradation of some active compounds, such as α-fellandrene, terpinolene, p-cymene, thujene, δ-terpinene, 2-carene/isoterpinolene, trans-2-caren-4-ol, carveol, thujol, carvacrol. Interestingly, only carvacrol, which is a compound with a well-known antimicrobial activity (Ben Arfa et al., 2006, Veldhuizen et al., 2006), was significantly reduced when increasing the process intensity from HSH to HPH. Therefore, it can be assumed that the different performance observed for T/SL-HPH and T/SL-HSH, which share the same composition, is due to the fact that the theoretical higher delivery efficiency of nanoemulsion T/SL-HPH, associated with its smaller mean droplet diameter, is counter-balanced by the partial degradation of some active compounds, and in particular, carvacrol.

Table VIII.4 *Composition of the pure terpenes mixture and the terpenes extracted from nanoemulsions T/SL-HPH and T/SL-HSH.*

Compound	***Retention index***	***% Content***		
		Terpenes mixture	***Nanoemulsion T/SL-HSH***	***Nanoemulsion T/SL-HPH***
α-fellandrene	14.10	0.150	0.020	0.036
terpinolene	14.63	1	0.07	0.12
p-cymene	15.06	1.39	0.20	0.38
thujene	15.28	0.30	0.06	0.09
δ-terpinene	16.7	0.68	0.06	0.10
2-carene/isoterpinolene	17.99	0.28	0.02	0.04
trans-2-caren-4-ol	18.33	0.14	0.02	0.03
cis-α-terpineol	19.09	0.04	0.06	0.07
cyclohexanol (4-isopropil-1-methyl)-cis/cis-sabinene hydrate	20.12	0.15	0.30	0.36
carveol	20.39	0.08	0.02	0.02
1-terpineol	20.7	0.06	0.04	0.06
cyclohexanol(4-isopropil-1-methyl)-trans	21	0.04	0.10	0.14
terpinen-4-ol	22.8	94.61	98.27	97.73
5-coranol	23.95	0.05	0.06	0.09
thujol	27.84	0.30	0.20	0.20
carvacrol	29.21	0.43	0.12	0.05

VIII.3.3 Addition of encapsulated antimicrobial agents to fruit juices

Nanoemulsion T/SL-HPH was added at different concentrations to two fruit juices (orange juice and pear juice) inoculated with *L. delbrueckii* in order to test the microbiological stability as well as the alteration of the chemical and physical characteristics of the juices stored at 32 °C.

The results of the accelerated shelf life studies are reported in Figures VIII.3-VIII.4. Figure VIII.3 shows that for both fruit juices after 2 days, the total inactivation of the initial microbial load of 10^3 CFU/ml was already reached for the terpenes concentrations of 5.0 g/L and 10 g/L. At a terpenes concentration of 1.0 g/L, microorganism growth is delayed by 5 days in orange juice and 2 days in pear juice in comparison to the control.

°Bx and pH were not significantly altered by the addition of the nanoemulsion. This was also observed during the storage period, unless significant microbial growth occurred, such as for the control sample and the 1.0 g/L terpenes sample (Figure VIII.4a, b, c and d).

In contrast, major color deviations were observed when 10 g/L nanoencapsulated terpenes were added to the juices, while the addition of the terpenes mixture at lower concentrations (5.0 and 1.0 g/L) can be considered acceptable, with it inducing much smaller color deviations (Figure VIII.4e and f). The color remained stable over the storage time for all those systems where no significant microbial growth occurred.

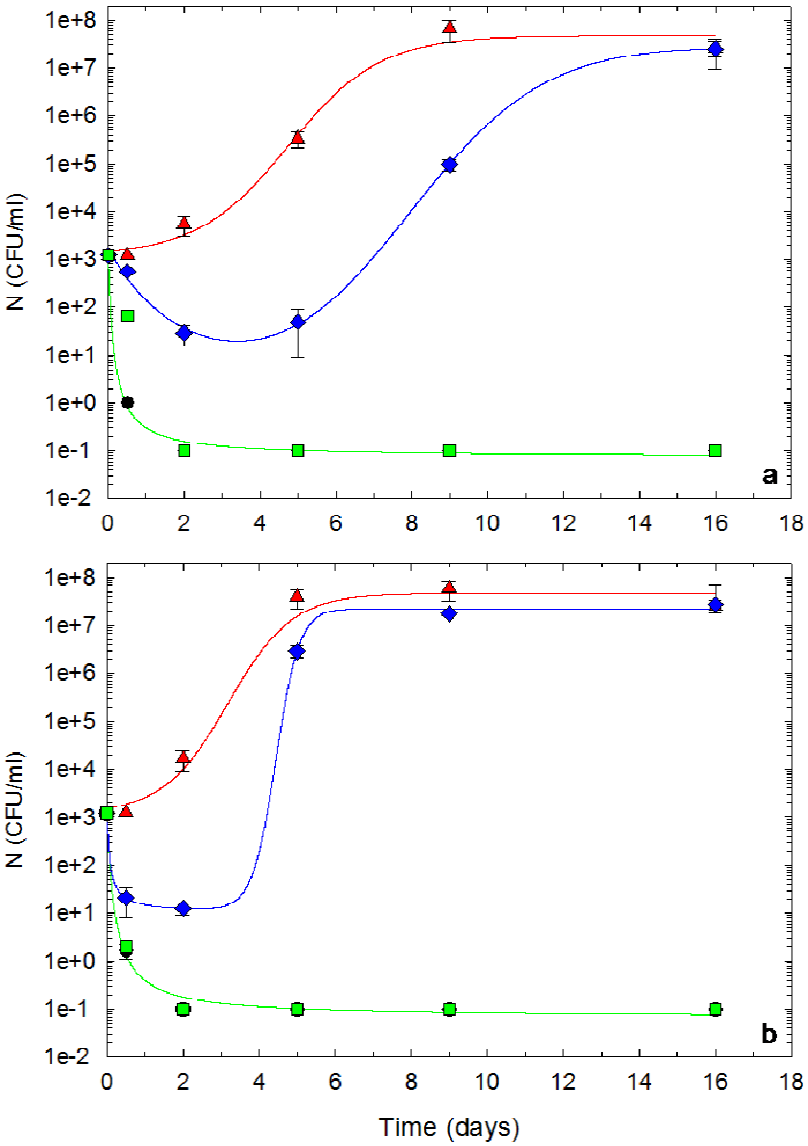

Figure VIII.3 *Inactivation curve of L. delbrueckii suspended in (a) orange juice and (b) pear juice treated with terpenes nanoemulsion T/SL-HPH at 32 °C. Experimental data: control juice (▲), juice added with the nanoemulsion to a final concentration of 1.0 g/L (◆), 5.0 g/L (●) and 10 g/L (■) of the terpenes mixture.*

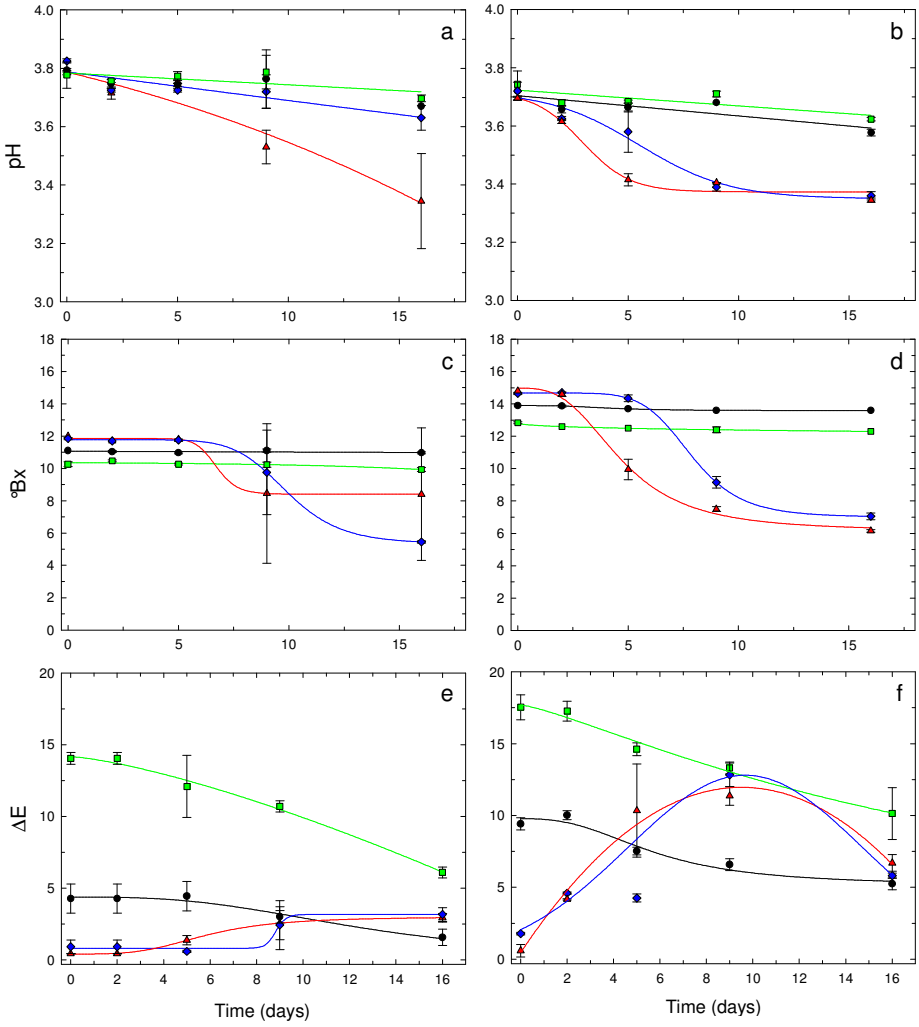

Figure VIII.4 *Variation over time of (a and b) pH, (c and d) °Bx and (e and f) global color difference, ΔE, of (a, c and e) orange juice and (b, d and f) pear juice with different concentrations of terpenes nanoemulsion T/SL-HPH at 32 °C. Experimental data: control juice (▲), juice added with the nanoemulsion to a final concentration of 1.0 g/L (◆), 5.0 g/L (●) and 10 g/L (■) of the terpenes mixture.*

VIII.4 Conclusions

In this section, the nanoencapsulation of two essential oils, a terpenes mixture extracted from *Melaleuca alternifolia* and D-limonene, was investigated as a method to improve the safety and quality of foods through the addition of natural preservatives.

Nanoemulsions based on food grade ingredients were fabricated by high pressure homogenization processing at 300 MPa, obtaining physically stable antimicrobial delivery systems. In particular, lecithin-based nanoemulsion with a mean droplet diameter of 75 nm resulted as being a highly efficient carrier system for the terpenes mixture, while D-limonene was successfully nanoencapsulated pure using clear gum as emulsifier, or in a blend with palm oil using soy lecithin as emulsifier.

The stable nanoemulsions produced were tested by MIC and MBC measurements on three target microorganisms (*E. coli, L. delbrueckii* and *S. cerevisiae*), in order to verify the ability of the delivery systems to enhance the bacteriostatic and bactericidal capability of the antimicrobials.

The MIC and MBC values of the nanoencapsulated terpenes resulted always lower than or equal to the values of the unencapsulated mixture, suggesting the activation of passive transport mechanisms through the cell membrane of the tested microorganisms. On the other hand, the nanoencapsulation of D-limonene was able to reduce only the MIC values, without any significant variation of the MBC values in comparison to the unencapsulated D-limonene.

The terpenes nanocapsules were tested in real systems, such as orange juice and pear juice, inoculated with *L. delbrueckii*. The addition of low concentrations of the nanoencapsulated terpenes was able to delay the microbial growth (1.0 g/L terpenes) or completely inactivate the microorganisms (5.0 g/L terpenes) while minimally altering the organoleptic properties of the fruit juices.

Chapter IX
Conclusions and perspectives

The functional food and nutraceutical industries have consolidated in the last years a growing interest in nanotechnology, in order to improve delivery of bioactive compounds, as well as to create novel food functionalities.

Nevertheless, the science, technology and engineering behind the existing nanotechnology applications are still at a basic level, in comparison to the potential they can express according to the current and prospective results of scientific research.

This work highlights the potentialities of food-grade nanometric systems, such as nanoemulsions and solid lipid nanoparticles, to efficiently encapsulate and deliver bioactive compounds. In particular, novel formulations were developed to increase the solubility in aqueous systems of bioactive compounds, insoluble in water and poor soluble in oil. Curcumin was encapsulated in stearic acid-based nanoemulsions at a maximum concentration of 1000 mg/L, 1600 higher than its solubility in water. Moreover, the design of nanoemulsion-based delivery systems with a combined use of hydrophilic (sugar ester, defatted soy lecithin, polysorbate 20) and lipophilic emulsifiers (soy lecithin, glycerol monooleate) was resulted an efficient method to encapsulate resveratrol and disperse it in aqueous systems at a concentration ten time higher than the therapeutic blood concentration (10 mg/L). The double layer of emulsifiers, limiting hydrophobic interactions, was also able to improve protection of thermolabile and photosensitive compounds against degradation under accelerated ageing and after gastro-intestinal digestion in comparison to unencapsulated compounds.

For the first time the properties of food emulsifiers, in terms of interfacial properties and characteristic times of adsorption, have been correlated to the efficiency of the emulsification process. In particular, the high pressure homogenization process resulted to be controlled not only by disruption efficiency achieved in the homogenization valve, but also by capability of the emulsifiers used to prevent recoalescence phenomena of newly formed droplets by rapid absorption at the O/W interface.

From this work has appeared also that a specific design and formulation may add specific functionalities to the nanodelivery systems. For example, uptake and bioavailability may be enhanced on one side by the reduction of mean droplet diameter of delivery system at subcellular size, improving the passive transport mechanisms through the intestinal wall, on the other side by a suitable choice of the lipid phase, whose co-administration with the bioactive compounds, may promote their adsorption from intestinal cells. In this regard the results obtained demonstrated that the formulations with smaller mean droplet diameters (below 200 nm), resulting physically stable after the digestion process and allowing the resveratrol to reach the intestinal wall entrapped in the lipid droplets, have increased the cumulative amount of nanoencapsulated resveratrol transported from the apical to the basolateral side across Caco-2 cell monolayers. In particular, soy lecithin/sugar esters-based nanoemulsion showed an higher permeability due to the presence of soy lecithin, which, having a structure similar to the phospholipid bilayers of the cellular membrane, favours the absorption and the entrapment of the oil droplets in the microvilli and their consequent transport through the cell membrane.

Similarly, has been demonstrated that an efficient design of nanoemulsion-based delivery systems in terms of mean droplet diameters achieved and choice of emulsifier used can affect the possible mechanisms of antimicrobial action of nanoencapsulated essential oils. The antimicrobial activity of nanoencapsulated essential oils can be carried out through the transport of the antimicrobial compounds across the cellular membrane, where they are released and can act from the inner side on the cytoplasmic membrane, as well as through the controlled release of antimicrobial compounds in the aqueous phase from the nanoemulsion droplets, therefore maintaining the essential oils active in the food system over an extended period of time, despite their limited solubility in aqueous phase. Moreover, the results obtained showed that the addition of low concentrations of nanoencapsulated essential oils in real food was able to delay the microbial growth (1.0 g/L terpenes) or completely inactivate the microorganisms (5.0 g/L terpenes), while minimally altering the organoleptic properties of the fruit juices.

In the future, seems possible to think to integrate consolidated top-down techniques, such as high pressure homogenization, with bottom-up approaches, based on thermodynamic self-assembling at molecular levels, in order to incorporate complex structures with advanced functionalities in unfavorable environments, such as most foods, during their manufacturing, storage and preparation. More efforts are also needed to enhance the ability of nano-engineered particles and emulsions to resist to the detrimental effects of processing conditions during food production, due to the thermolabile nature of the bioactive compounds and/or to the possibility of binding irreversibly to the food structure. The redesign of the processing

flow sheet and the optimization of the processing conditions for the production of foods supplemented with nanobioactive compounds are also a perspective and a challenge in order to prevent the loss of bioavailability.

References

ACOSTA, E. 2009. Bioavailability of nanoparticles in nutrient and nutraceutical delivery. *Current Opinion in Colloid & Interface Science,* 14**,** 3-15.

AL-AZZAWIE, H. F. & ALHAMDANI, M. S. S. 2006. Hypoglycemic and antioxidant effect of oleuropein in alloxan-diabetic rabbits. *Life Sciences,* 78**,** 1371-1377.

ALIAKBARIAN, B., CASAZZA, A. A. & PEREGO, P. 2011. Valorization of olive oil solid waste using high pressure-high temperature reactor. *Food Chemistry,* 128**,** 704-710.

AMENDOLA, D., DE FAVERI, D. M. & SPIGNO, G. 2010. Grape marc phenolics: Extraction kinetics, quality and stability of extracts. *Journal of Food Engineering,* 97**,** 384-392.

AMRI, A., CHAUMEIL, J. C., SFAR, S. & CHARRUEAU, C. 2011. Administration of resveratrol: What formulation solutions to bioavailability limitations? *Journal of Controlled Release*.

ASENSI, M., MEDINA, I., ORTEGA, A., CARRETERO, J., BANO, M. C., OBRADOR, E. & ESTRELA, J. M. 2002. Inhibition of cancer growth by resveratrol is related to its low bioavailability. *Free Radical Biology and Medicine,* 33**,** 387-398.

BARANAUSKIENE, R., VENSKUTONIS, P. R., DEWETTINCK, K. & VERHE, R. 2006. Properties of oregano (Origanum vulgare L.), citronella (Cymbopogon nardus G.) and marjoram (Majorana hortensis L.) flavors encapsulated into milk protein-based matrices. *Food Research International,* 39**,** 413-425.

BASPINAR, Y., KECK, C. M. & BORCHERT, H. H. 2010. Development of a positively charged prednicarbate nanoemulsion. *International Journal of Pharmaceutics,* 383**,** 201-208.

BEN ARFA, A., COMBES, S., PREZIOSI-BELLOY, L., GONTARD, N. & CHALIER, P. 2006. Antimicrobial activity of carvacrol related to its chemical structure. *Letters in Applied Microbiology,* 43**,** 149-154.

BENZIE, I. F. F. & STRAIN, J. J. 1996. The ferric reducing ability of plasma (FRAP) as a measure of "antioxidant power": The FRAP assay. *Analytical Biochemistry,* 239**,** 70-76.

BEVERUNG, C. J., RADKE, C. J. & BLANCH, H. W. 1998. Adsorption dynamics of L-glutamic acid copolymers at a heptane/water interface. *Biophysical Chemistry,* 70**,** 121-132.

BONILLA, F., MAYEN, M., MERIDA, J. & MEDINA, M. 1999. Extraction of phenolic compounds from red grape marc for use as food lipid antioxidants. *Food Chemistry,* 66**,** 209-215.

BOOCOCK, D. J., FAUST, G. E. S., PATEL, K. R., SCHINAS, A. M., BROWN, V. A., DUCHARME, M. P., BOOTH, T. D., CROWELL, J. A., PERLOFF, M., GESCHER, A. J., STEWARD, W. P. & BRENNER, D. E. 2007. Phase I dose escalation pharmacokinetic study in healthy volunteers of resveratrol, a potential cancer chemopreventive agent. *Cancer Epidemiology Biomarkers & Prevention,* 16**,** 1246-1252.

BOYER, J., BROWN, D. & LIU, R. H. 2005. In vitro digestion and lactase treatment influence uptake of quercetin and quercetin glucoside by the Caco-2 cell monolayer. *Nutr J,* 4**,** 1.

BRADAMANTE, S., BARENGHI, L. & VILLA, A. 2004. Cardiovascular protective effects of resveratrol. *Cardiovascular Drug Reviews,* 22**,** 169-188.

BROSEL, S. & SCHUBERT, H. 1999. Investigations on the role of surfactants in mechanical emulsification using a high-pressure homogenizer with an orifice valve. *Chemical Engineering and Processing,* 38**,** 533-540.

BROSEL, S. & SCHUBERT, H. 2000. Investigations on the role of surfactants in mechanical emulsification using a high-pressure homogenizer with an orifice valve (vol 38, pg 533, 1999). *Chemical Engineering and Processing,* 39**,** 553-554.

BURYANOVSKYY, L., FU, Y., BOYD, M., MA, Y. L., HSIEH, T. C., WU, J. M. & ZHANG, Z. T. 2004. Crystal structure of quinone reductase 2 in complex with resveratrol. *Biochemistry,* 43**,** 11417-11426.

CASAZZA, A. A., ALIAKBARIAN, B., MANTEGNA, S., CRAVOTTO, G. & PEREGO, P. 2010a. Extraction of phenolics from Vitis vinifera wastes using non-conventional techniques. *Journal of Food Engineering,* 100**,** 50-55.

CASAZZA, A. A., ALIAKBARIAN, B., MONTOYA, E. Y. O. & PEREGO, P. 2010b. t-resveratrol recovery from grape skins using high pressure and temperature extraction. *Journal of Biotechnology,* 150**,** S333-S333.

CASAZZA, A. A., ALIAKBARIAN, B., SANNITA, E. & PEREGO, P. 2011. High pressure and temperature process extraction of phenolic

compounds from grape skins. *International Journal of Food Science and Technology,* In Press.

CHAU, C.-F., WU, S.-H. & YEN, G.-C. 2007. The development of regulations for food nanotechnology. *Trends in Food Science & Technology,* 18**,** 269-280.

CHAUHAN, D. P. 2002. Chemotherapeutic potential of curcumin for colorectal cancer. *Current Pharmaceutical Design,* 8**,** 1695-1706.

CHEN, H., KHEMTONG, C., YANG, X., CHANG, X. & GAO, J. 2011. Nanonization strategies for poorly water-soluble drugs. *Drug Discovery Today,* 16**,** 354-360.

CIMINO, S., DONSI, F., RUSSO, G. & SANFILIPPO, D. 2008. Optimization of ethylene production via catalytic partial oxidation of ethane on Pt-LaMnO3 catalyst. *Catalysis Letters,* 122**,** 228-237.

D'ARCHIVIO, M., FILESI, C., DI BENEDETTO, R., GARGIULO, R., GIOVANNINI, C. & MASELLA, R. 2007. Polyphenols, dietary sources and bioavailability. *Annali dell'Istituto superiore di sanita,* 43**,** 348-61.

DA SILVA, C. A. S., SANAIOTTI, G., LANZA, M., FOLLEGATTI-ROMERO, L. A., MEIRELLES, A. J. A. & BATISTA, E. A. C. 2010. Mutual Solubility for Systems Composed of Vegetable Oil plus Ethanol plus Water at Different Temperatures. *Journal of Chemical and Engineering Data,* 55**,** 440-447.

DAVALOS, A., GOMEZ-CORDOVES, C. & BARTOLOME, B. 2004. Extending applicability of the oxygen radical absorbance capacity (ORAC-fluorescein) assay. *Journal of Agricultural and Food Chemistry,* 52**,** 48-54.

DJORDJEVIC, D., CERCACI, L., ALAMED, J., MCCLEMENTS, D. J. & DECKER, E. A. 2008. Chemical and physical stability of protein- and gum arabic-stabilized oil-in-water emulsions containing limonene. *Journal of Food Science,* 73**,** C167-C172.

DONSI, F., ANNUNZIATA, M., SESSA, M. & FERRARI, G. 2011a. Nanoencapsulation of essential oils to enhance their antimicrobial activity in foods. *Lwt-Food Science and Technology,* 44**,** 1908-1914.

DONSI, F., FERRARI, G., LENZA, E. & MARESCA, P. 2009. Main factors regulating microbial inactivation by high-pressure homogenization: Operating parameters and scale of operation. *Chemical Engineering Science,* 64**,** 520-532.

DONSI, F., SENATORE, B., HUANG, Q. & FERRARI, G. 2010a. Development of Novel Pea Protein-Based Nanoemulsions for Delivery of Nutraceuticals. *Journal of Agricultural and Food Chemistry,* 58**,** 10653-10660.

DONSI, F., SENATORE, B., HUANG, Q. R. & FERRARI, G. 2010b. Development of Novel Pea Protein-Based Nanoemulsions for

Delivery of Nutraceuticals. *Journal of Agricultural and Food Chemistry,* 58**,** 10653-10660.

DONSI, F., SESSA, M. & FERRARI, F. 2011b. Effect of emulsifier type and disruption chamber geometry on the fabrication of food nanoemulsions by high pressure homogenization. *Industrial Engineering & Chemistry Research,* submitted.

DONSI, F., SESSA, M. & FERRARI, G. 2010c. Nanoencapsulation of essential oils to enhance their antimicrobial activity in foods. *Journal of Biotechnology,* 150**,** S67-S67.

DONSI, F., WANG, Y. & HUANG, Q. 2011c. Freeze-thaw stability of lecithin and modified starch-based nanoemulsions. *Food Hydrocolloids,* 25**,** 1327-1336.

DONSI, F., WANG, Y., LI, J. & HUANG, Q. 2010d. Preparation of Curcumin Sub-micrometer Dispersions by High-Pressure Homogenization. *Journal of Agricultural and Food Chemistry,* 58**,** 2848-2853.

FANG, J. Y., HUNG, C. F., LIAO, M. H. & CHIEN, C. C. 2007. A study of the formulation design of acoustically active lipospheres as carriers for drug delivery. *European Journal of Pharmaceutics and Biopharmaceutics,* 67**,** 67-75.

FATHI, M., MOZAFARI, M. R. & MOHEBBI, M. 2011. Nanoencapsulation of food ingredients using lipid based delivery systems. *Trends in Food Science & Technology,* article in press.

FERRER, J., PAEZ, G., MARMOL, Z., RAMONES, E., CHANDLER, C., MARIN, M. & FERRER, A. 2001. Agronomic use of biotechnologically processed grape wastes. *Bioresource Technology,* 76**,** 39-44.

FILIP, V., PLOCKOVA, M., SMIDRKAL, J., SPICKOVA, Z., MELZOCH, K. & SCHMIDT, S. 2003. Resveratrol and its antioxidant and antimicrobial effectiveness. *Food Chemistry,* 83**,** 585-593.

FINKEL, T. & HOLBROOK, N. J. 2000. Oxidants, oxidative stress and the biology of ageing. *Nature,* 408**,** 239-247.

FIORI, L., DE FAVERI, D., CASAZZA, A. A. & PEREGO, P. 2009. Grape by-products: extraction of polyphenolic compounds using supercritical CO2 and liquid organic solvent - a preliminary investigation Subproductos de la uva: extraccion de compuestos polifenolicos usando CO2 supercritico y disolventes organicos liquidos - una investigacion preliminar. *Cyta-Journal of Food,* 7**,** 163-171.

FLOURY, J., BELLETTRE, J., LEGRAND, J. & DESRUMAUX, A. 2004a. Analysis of a new type of high pressure homogeniser. A study of the flow pattern. *Chemical Engineering Science,* 59**,** 843-853.

FLOURY, J., DESRUMAUX, A., AXELOS, M. A. V. & LEGRAND, J. 2002a. Degradation of methylcellulose during ultra-high pressure homogenisation. *Food Hydrocolloids,* 16**,** 47-53.

FLOURY, J., DESRUMAUX, A. & LEGRAND, J. 2002b. Effect of ultra-high-pressure homogenization on structure and on rheological properties of soy protein-stabilized emulsions. *Journal of Food Science,* 67**,** 3388-3395.

FLOURY, J., LEGRAND, J. & DESRUMAUX, A. 2004b. Analysis of a new type of high pressure homogeniser. Part B. Study of droplet break-up and recoalescence phenomena. *Chemical Engineering Science,* 59**,** 1285-1294.

FRANKEL, E. N. & MEYER, A. S. 2000. The problems of using one-dimensional methods to evaluate multifunctional food and biological antioxidants. *Journal of the Science of Food and Agriculture,* 80**,** 1925-1941.

GAO, J., HUGGER, E. D., BECK-WESTERMEYER, M. S. & BORCHARDT, R. T. 2001. Estimating intestinal mucosal permeation of compounds using caco-2 cell monolayers. *Current protocols in pharmacology / editorial board, S.J. Enna (editor-in-chief) ... [et al.],* Chapter 7.

GAO, L., LIU, G., WANG, X., LIU, F., XU, Y. & MA, J. 2011. Preparation of a chemically stable quercetin formulation using nanosuspension technology. *International Journal of Pharmaceutics,* 404**,** 231-237.

GAVINI, E., SANNA, V., SHARMA, R., JULIANO, C., USAI, M., MARCHETTI, M., KARLSEN, J. & GIUNCHEDI, P. 2005. Solid lipid microparticles (SLM) containing juniper oil as anti-acne topical carriers: Preliminary studies. *Pharmaceutical Development and Technology,* 10**,** 479-487.

GAYSINSKY, S., DAVIDSON, P. M., BRUCE, B. D. & WEISS, J. 2005. Growth inhibition of Escherichia coli O157 : H7 and Listeria monocytogenes by carvacrol and eugenol encapsulated in surfactant micelles. *Journal of Food Protection,* 68**,** 2559-2566.

GAYSINSKY, S., TAYLOR, T. M., DAVIDSON, P. M., BRUCE, B. D. & WEISS, J. 2007. Antimicrobial efficacy of eugenol microemulsions in milk against Listeria monocytogenes and Escherichia coli O157 : H7. *Journal of Food Protection,* 70**,** 2631-2637.

GHAFOOR, K., CHOI, Y. H., JEON, J. Y. & JO, I. H. 2009. Optimization of Ultrasound-Assisted Extraction of Phenolic Compounds, Antioxidants, and Anthocyanins from Grape (Vitis vinifera) Seeds. *Journal of Agricultural and Food Chemistry,* 57**,** 4988-4994.

GILL, A. O. & HOLLEY, R. A. 2006. Disruption of Escherichia coli, Listeria monocytogenes and Lactobacillus sakei cellular membranes by plant oil aromatics. *International Journal of Food Microbiology,* 108**,** 1-9.

GORTZI, O., LALAS, S., TSAKNIS, J. & CHINOU, I. 2007. Enhanced bioactivity of Citrus limon (Lemon Greek cultivar) extracts, essential oil and isolated compounds before and after encapsulation in liposomes. *Planta Medica,* 73**,** P 184.

HAILONG, Y. & QINGRONG, H. 2010. Enhanced in vitro anti-cancer activity of curcumin encapsulated in hydrophobically modified starch. *Food Chemistry,* 119**,** 669-674.

HAKANSSON, A., TRAGARDH, C. & BERGENSTAHL, B. 2009a. Dynamic simulation of emulsion formation in a high pressure homogenizer. *Chemical Engineering Science,* 64**,** 2915-2925.

HAKANSSON, A., TRAGARDH, C. & BERGENSTAHL, B. 2009b. Studying the effects of adsorption, recoalescence and fragmentation in a high pressure homogenizer using a dynamic simulation model. *Food Hydrocolloids,* 23**,** 1177-1183.

HASLAM, E. 1996. Natural polyphenols (vegetable tannins) as drugs: Possible modes of action. *Journal of Natural Products,* 59**,** 205-215.

HOLME, A. L. & PERVAIZ, S. 2007. Resveratrol in cell fate decisions. *Journal of Bioenergetics and Biomembranes,* 39**,** 59-63.

HOLST, B. & WILLIAMSON, G. 2008. Nutrients and phytochemicals: from bioavailability to bioefficacy beyond antioxidants. *Current Opinion in Biotechnology,* 19**,** 73-82.

HUANG, D. J., OU, B. X. & PRIOR, R. L. 2005. The chemistry behind antioxidant capacity assays. *Journal of Agricultural and Food Chemistry,* 53**,** 1841-1856.

HUANG, M. T., LOU, Y. R., MA, W., NEWMARK, H. L., REUHL, K. R. & CONNEY, A. H. 1994. INHIBITORY EFFECTS OF DIETARY CURCUMIN ON FORESTOMACH, DUODENAL, AND COLON CARCINOGENESIS IN MICE. *Cancer Research,* 54**,** 5841-5847.

HUANG, M. T., NEWMARK, H. L. & FRENKEL, K. 1997. Inhibitory effects of curcumin on tumorigenesis in mice. *Journal of cellular biochemistry. Supplement,* 27**,** 26-34.

HUANG, Q. R., YU, H. L. & RU, Q. M. 2010. Bioavailability and Delivery of Nutraceuticals Using Nanotechnology. *Journal of Food Science,* 75**,** R50-R57.

HUBATSCH, I., RAGNARSSON, E. G. E. & ARTURSSON, P. 2007. Determination of drug permeability and prediction of drug absorption in Caco-2 monolayers. *Nature Protocols,* 2**,** 2111-2119.

HUNG, C. F., CHEN, J. K., LIAO, M. H., LO, H. M. & FANG, J. Y. 2006. Development and evaluation of emulsion-liposome blends for resveratrol delivery. *Journal of Nanoscience and Nanotechnology,* 6**,** 2950-2958.

HUNG, C. F., LIN, Y. K., HUANG, Z. R. & FANG, J. Y. 2008. Delivery of resveratrol, a red wine polyphenol, from solutions and hydrogels via the skin. *Biological & Pharmaceutical Bulletin,* 31**,** 955-962.

HUSSAIN, N., JAITLEY, V. & FLORENCE, A. T. 2001. Recent advances in the understanding of uptake of microparticulates across the gastrointestinal lymphatics. *Advanced Drug Delivery Reviews,* 50**,** 107-142.

JANG, M. S., CAI, E. N., UDEANI, G. O., SLOWING, K. V., THOMAS, C. F., BEECHER, C. W. W., FONG, H. H. S., FARNSWORTH, N. R., KINGHORN, A. D., MEHTA, R. G., MOON, R. C. & PEZZUTO, J. M. 1997. Cancer chemopreventive activity of resveratrol, a natural product derived from grapes. *Science,* 275**,** 218-220.

JENNING, V., GYSLER, A., SCHAFER-KORTING, M. & GOHLA, S. H. 2000. Vitamin A loaded solid lipid nanoparticles for topical use: occlusive properties and drug targeting to the upper skin. *European Journal of Pharmaceutics and Biopharmaceutics,* 49**,** 211-218.

JOHNSON, J. J., NIHAL, M., SIDDIQUI, I. A., SCARLETT, C. O., BAILEY, H. H., MUKHTAR, H. & AHMAD, N. 2011. Enhancing the bioavailability of resveratrol by combining it with piperine. *Molecular Nutrition & Food Research,* 55**,** 1169-1176.

JUMAA, M., FURKERT, F. H. & MULLER, B. W. 2002. A new lipid emulsion formulation with high antimicrobial efficacy using chitosan. *European Journal of Pharmaceutics and Biopharmaceutics,* 53**,** 115-123.

KAPETANOVIC, I. M., MUZZIO, M., HUANG, Z., THOMPSON, T. N. & MCCORMICK, D. L. 2011. Pharmacokinetics, oral bioavailability, and metabolic profile of resveratrol and its dimethylether analog, pterostilbene, in rats. *Cancer Chemotherapy and Pharmacology,* 68**,** 593-601.

KING, R. E., KENT, K. D. & BOMSER, J. A. 2005. Resveratrol reduces oxidation and proliferation of human retinal pigment epithelial cells via extracellular signal-regulated kinase inhibition. *Chemico-Biological Interactions,* 151**,** 143-149.

KLEINIG, A. R. & MIDDELBERG, A. P. J. 1998. On the mechanism of microbial cell disruption in high-pressure homogenisation. *Chemical Engineering Science,* 53**,** 891-898.

KONG, M., CHEN, X. G., KWEON, D. K. & PARK, H. J. 2011. Investigations on skin permeation of hyaluronic acid based nanoemulsion as transdermal carrier. *Carbohydrate Polymers,* 86**,** 837-843.

KRISHNAN, S., BHOSALE, R. & SINGHAL, R. S. 2005. Microencapsulation of cardamom oleoresin: Evaluation of blends of gum arabic, maltodextrin and a modified starch as wall materials. *Carbohydrate Polymers,* 61**,** 95-102.

KUMAR, M., MISRA, A., MISHRA, A. K., MISHRA, P. & PATHAK, K. 2008. Mucoadhesive nanoemulsion-based intranasal drug delivery

system of olanzapine for brain targeting. *Journal of Drug Target,* 16**,** 806-814.

LI, Y., SKOUROUMOUNIS, G. K., ELSEY, G. M. & TAYLOR, D. K. 2011. Microwave-assistance provides very rapid and efficient extraction of grape seed polyphenols. *Food Chemistry,* 129**,** 570-576.

LIEDTKE, S., WISSING, S., MULLER, R. H. & MADER, K. 2000. Influence of high pressure homogenisation equipment on nanodispersions characteristics. *International Journal of Pharmaceutics,* 196**,** 183-185.

LIN, C.-C., LIN, H.-Y., CHEN, H.-C., YU, M.-W. & LEE, M.-H. 2009. Stability and characterisation of phospholipid-based curcumin-encapsulated microemulsions. *Food Chemistry,* 116**,** 923-928.

LIN, J. K., CHEN, Y. C., HUANG, Y. T. & LIN-SHIAU, S. Y. 1997. Suppression of protein kinase C and nuclear oncogene expression as possible molecular mechanisms of cancer chemoprevention by apigenin and curcumin. *Journal of cellular biochemistry. Supplement,* 28-29**,** 39-48.

LIOLIOS, C. C., GORTZI, O., LALAS, S., TSAKNIS, J. & CHINOU, I. 2009. Liposomal incorporation of carvacrol and thymol isolated from the essential oil of Origanum dictamnus L. and in vitro antimicrobial activity. *Food Chemistry,* 112**,** 77-83.

LIU, L. Y., ZHAO, Q. Z., LIU, T. X. & ZHAO, M. M. 2011. Dynamic surface pressure and dilatational viscoelasticity of sodium caseinate/xanthan gum mixtures at the oil-water interface. *Food Hydrocolloids,* 25**,** 921-927.

LIU, R. H. & FINLEY, J. 2005. Potential cell culture models for antioxidant research. *Journal of Agricultural and Food Chemistry,* 53**,** 4311-4314.

LO CURTO, R. B. & TRIPODO, M. M. 2001. Yeast production from virgin grape marc. *Bioresource Technology,* 78**,** 5-9.

LU, X. W., JI, C. B., XU, H. E., LI, X. L., DING, H. X., YE, M., ZHU, Z. S., DING, D., JIANG, X. Q., DING, X. S. & GUO, X. R. 2009. Resveratrol-loaded polymeric micelles protect cells from A beta-induced oxidative stress. *International Journal of Pharmaceutics,* 375**,** 89-96.

LUCAS-ABELLAN, C., FORTEA, I., LOPEZ-NICOLAS, J. M. & NUNEZ-DELICADO, E. 2007. Cyclodextrins as resveratrol carrier system. *Food Chemistry,* 104**,** 39-44.

MCCLEMENTS, D. J. 2005. Food emulsions: principles, practice and techniques. *in contemporary food science*.

MCCLEMENTS, D. J., DECKER, E. A. & WEISS, J. 2007. Emulsion-based delivery systems for lipophilioc bioactive components. *Journal of Food Science,* 72**,** R109-R124.

MCCLEMENTS, D. J. & LI, Y. 2010. Structured emulsion-based delivery systems: Controlling the digestion and release of lipophilic food components. *Advances in Colloid and Interface Science,* 159**,** 213-228.

MCCLEMENTS, J. D. 1999. *Food Emulsions: Principles, Practices and Techniques,* Boca Raton, Florida, CRC Press.

MEHNERT, W. & MADER, K. 2001. Solid lipid nanoparticles - Production, characterization and applications. *Advanced Drug Delivery Reviews,* 47**,** 165-196.

MIDDELBERG, A. P. J. 1995. PROCESS-SCALE DISRUPTION OF MICROORGANISMS. *Biotechnology Advances,* 13**,** 491-551.

MOSCHWITZER, J., ACHLEITNER, G., POMPER, H. & MULLER, R. H. 2004. Development of an intravenously injectable chemically stable aqueous omeprazole formulation using nanosuspension technology. *European Journal of Pharmaceutics and Biopharmaceutics,* 58**,** 615-619.

MOZAFARI, M. R., JOHNSON, C., HATZIANTONIOU, S. & DEMETZOS, C. 2008. Nanoliposomes and Their Applications in Food Nanotechnology. *Journal of Liposome Research,* 18**,** 309-327.

MULIK, R. S., MONKKONEN, J., JUVONEN, R. O., MAHADIK, K. R. & PARADKAR, A. R. 2010. Transferrin mediated solid lipid nanoparticles containing curcumin: Enhanced in vitro anticancer activity by induction of apoptosis. *International Journal of Pharmaceutics,* 398**,** 190-203.

MULLER, R. H., RADTKE, M. & WISSING, S. A. 2002. Solid lipid nanoparticles (SLN) and nanostructured lipid carriers (NLC) in cosmetic and dermatological preparations. *Advanced Drug Delivery Reviews,* 54**,** S131-S155.

MUN, S., DECKER, E. A., PARK, Y., WEISS, J. & MCCLEMENTS, D. J. 2006. Influence of interfacial composition on in vitro digestibility of emulsified lipids: Potential mechanism for chitosan's ability to inhibit fat digestion. *Food Biophysics,* 1**,** 21-29.

NAM, J. B., RYU, J. H., KIM, J. W., CHANG, I. S. & SUH, K. D. 2005. Stabilization of resveratrol immobilized in monodisperse cyano-functionalized porous polymeric microspheres. *Polymer,* 46**,** 8956-8963.

NARAYANAN, N. K., NARGI, D., RANDOLPH, C. & NARAYANAN, B. A. 2009. Liposome encapsulation of curcumin and resveratrol in combination reduces prostate cancer incidence in PTEN knockout mice. *International Journal of Cancer,* 125**,** 1-8.

NEGRO, C., TOMMASI, L. & MICELI, A. 2003. Phenolic compounds and antioxidant activity from red grape marc extracts. *Bioresource Technology,* 87**,** 41-44.

NILSSON, L. & BERGENSTAHL, B. 2006. Adsorption of hydrophobically modified starch at oil/water interfaces during emulsification. *Langmuir,* 22**,** 8770-8776.

NINO, M. R. R., SANCHEZ, C. C., RUIZ-HENESTROSA, V. P. & PATINO, J. M. R. 2005. Milk and soy protein films at the air-water interface. *Food Hydrocolloids,* 19**,** 417-428.

OLAS, B. & WACHOWICZ, B. 2005. Resveratrol, a phenolic antioxidant with effects on blood platelet functions. *Platelets,* 16**,** 251-260.

ORALLO, F. 2006. Comparative studies of the antioxidant effects of cis- and trans-resveratrol. *Current Medicinal Chemistry,* 13**,** 87-98.

OU, B. X., HUANG, D. J., HAMPSCH-WOODILL, M., FLANAGAN, J. A. & DEEMER, E. K. 2002. Analysis of antioxidant activities of common vegetables employing oxygen radical absorbance capacity (ORAC) and ferric reducing antioxidant power (FRAP) assays: A comparative study. *Journal of Agricultural and Food Chemistry,* 50**,** 3122-3128.

PALMA, M. & BARROSO, C. G. 2002. Ultrasound-assisted extraction and determination of tartaric and malic acids from grapes and winemaking by-products. *Analytica Chimica Acta,* 458**,** 119-130.

PAQUIN, P. 1999. Technological properties of high pressure homogenizers: the effect of fat globules, milk proteins, and polysaccharides. *International Dairy Journal,* 9**,** 329-335.

PEDRO, A. S., CABRAL-ALBUQUERQUE, E., FERREIRA, D. & SARMENTO, B. 2009. Chitosan: An option for development of essential oil delivery systems for oral cavity care? *Carbohydrate Polymers,* 76**,** 501-508.

PENG, H. L., XIONG, H., LI, J. H., XIE, M. Y., LIU, Y. Z., BAI, C. Q. & CHEN, L. X. 2010. Vanillin cross-linked chitosan microspheres for controlled release of resveratrol. *Food Chemistry,* 121**,** 23-28.

PISOSCHI, A. M., DANET, A. F. & KALINOWSKI, S. 2008. Ascorbic Acid determination in commercial fruit juice samples by cyclic voltammetry. *Journal of automated methods & management in chemistry,* 2008**,** 937651.

PORTER, C. J. H., POUTON, C. W., CUINE, J. F. & CHARMAN, W. N. 2008. Enhancing intestinal drug solubilisation using lipid-based delivery systems. *Advanced Drug Delivery Reviews,* 60**,** 673-691.

PRIOR, R. L., HOANG, H., GU, L. W., WU, X. L., BACCHIOCCA, M., HOWARD, L., HAMPSCH-WOODILL, M., HUANG, D. J., OU, B. X. & JACOB, R. 2003. Assays for hydrophilic and lipophilic antioxidant capacity (oxygen radical absorbance capacity (ORAC(FL))) of plasma and other biological and food samples. *Journal of Agricultural and Food Chemistry,* 51**,** 3273-3279.

PRIOR, R. L., WU, X. L. & SCHAICH, K. 2005. Standardized methods for the determination of antioxidant capacity and phenolics in foods and

dietary supplements. *Journal of Agricultural and Food Chemistry,* 53**,** 4290-4302.

QIAN, C. & MCCLEMENTS, D. J. 2011. Formation of nanoemulsions stabilized by model food-grade emulsifiers using high-pressure homogenization: Factors affecting particle size. *Food Hydrocolloids,* 25**,** 1000-1008.

QUE, F., MAO, L. C. & PAN, X. 2006. Antioxidant activities of five Chinese rice wines and the involvement of phenolic compounds. *Food Research International,* 39**,** 581-587.

RAVINDRANATH, V. & CHANDRASEKHARA, N. 1981. Metabolism of curcumin--studies with 3H curcumin. *Toxicology,* 22**,** 337-44.

ROLAND, I., PIEL, G., DELATTRE, L. & EVRARD, B. 2003. Systematic characterization of oil-in-water emulsions for formulation design. *International Journal of Pharmaceutics,* 263**,** 85-94.

SAGALOWICZ, L. & LESER, M. E. 2010. Delivery systems for liquid food products. *Current Opinion in Colloid & Interface Science,* 15**,** 61-72.

SALAGER, J. L. 1988. Phase transformation and emulsion inversion on the basis of catastrophe theory. *In:* DEKKER, M. (ed.) *Encyclopedia of Emulsion Technology*. New York.

SANGUANSRI, P. & AUGUSTIN, M. A. 2006. Nanoscale materials development - a food industry perspective. *Trends in Food Science & Technology,* 17**,** 547-556.

SCALBERT, A. & WILLIAMSON, G. 2000. Dietary intake and bioavailability of polyphenols. *Journal of Nutrition,* 130**,** 2073S-2085S.

SCHUBERT, M. A. & MULLER-GOYMANN, C. C. 2005. Characterisation of surface-modified solid lipid nanoparticles (SLN): Influence of lecithin and nonionic emulsifier. *European Journal of Pharmaceutics and Biopharmaceutics,* 61**,** 77-86.

SCHULTZ, S., WAGNER, G., URBAN, K. & ULRICH, J. 2004. High-pressure homogenization as a process for emulsion formation. *Chemical Engineering & Technology,* 27**,** 361-368.

SESSA, M., TSAO, R., LIU, R. H., FERRARI, G. & DONSI, F. 2011. Evaluation of the Stability and Antioxidant Activity of Nanoencapsulated Resveratrol during in Vitro Digestion. *Journal of Agricultural and Food Chemistry,* 59**,** 12352-12360.

SEYOUM, A., ASRES, K. & EL-FIKY, F. K. 2006. Structure-radical scavenging activity relationships of flavonoids. *Phytochemistry,* 67**,** 2058-2070.

SHAO, J. F., LI, X. L., LU, X. W., JIANG, C., HU, Y., LI, Q. P., YOU, Y. P. & FU, Z. 2009. Enhanced growth inhibition effect of Resveratrol incorporated into biodegradable nanoparticles against glioma cells is

mediated by the induction of intracellular reactive oxygen species levels. *Colloids and Surfaces B-Biointerfaces,* 72**,** 40-47.

SHARMA, S., STUTZMAN, J. D., KELLOFF, G. J. & STEELE, V. E. 1994. SCREENING OF POTENTIAL CHEMOPREVENTIVE AGENTS USING BIOCHEMICAL MARKERS OF CARCINOGENESIS. *Cancer Research,* 54**,** 5848-5855.

SHI, G. R., RAO, L. Q., YU, H. Z., XIANG, H., YANG, H. & JI, R. 2008. Stabilization and encapsulation of photosensitive resveratrol within yeast cell. *International Journal of Pharmaceutics,* 349**,** 83-93.

SHI, T. F., ZIEGLER, V. E., WELGE, I. C., AN, L. J. & WOLF, B. A. 2004. Evolution of the interfacial tension between polydisperse "immiscible" polymers in the absence and in the presence of a compatibilizer. *Macromolecules,* 37**,** 1591-1599.

SHIRGAONKAR, I. Z., LOTHE, R. R. & PANDIT, A. B. 1998. Comments on the mechanism of microbial cell disruption in high-pressure and high-speed devices. *Biotechnology Progress,* 14**,** 657-660.

SIKKEMA, J., DEBONT, J. A. M. & POOLMAN, B. 1995. MECHANISMS OF MEMBRANE TOXICITY OF HYDROCARBONS. *Microbiological Reviews,* 59**,** 201-222.

SINICO, C., DE LOGU, A., LAI, F., VALENTI, D., MANCONI, M., LOY, G., BONSIGNORE, L. & FADDA, A. M. 2005. Liposomal incorporation of Artemisia arborescens L. essential oil and in vitro antiviral activity. *European Journal of Pharmaceutics and Biopharmaceutics,* 59**,** 161-168.

SOUTO, E. B., ANSELMI, C., CENTINI, M. & MULLER, R. H. 2005. Preparation and characterization of n-dodecyl-ferulate-loaded solid lipid nanoparticles (SLN (R)). *International Journal of Pharmaceutics,* 295**,** 261-268.

SPIGNO, G. & DE FAVERI, D. M. 2007. Antioxidants from grape stalks and marc: Influence of extraction procedure on yield, purity and antioxidant power of the extracts. *Journal of Food Engineering,* 78**,** 793-801.

STANG, M., KARBSTEIN, H. & SCHUBERT, H. 1994. ADSORPTION-KINETICS OF EMULSIFIERS AT OIL-WATER INTERFACES AND THEIR EFFECT ON MECHANICAL EMULSIFICATION. *Chemical Engineering and Processing,* 33**,** 307-311.

STANG, M., SCHUCHMANN, H. & SCHUBERT, H. 2001. Emulsification in High-Pressure Homogenizers. *Engineering in Life Sciences,* 1**,** 151-157.

STEPANEK, P. 1993. STATIC AND DYNAMIC PROPERTIES OF MULTIPLE LIGHT-SCATTERING. *Journal of Chemical Physics,* 99**,** 6384-6393.

SZNITOWSKA, M., JANICKI, S., DABROWSKA, E. A. & GAJEWSKA, M. 2002. Physicochemical screening of antimicrobial agents as

potential preservatives for submicron emulsions. *European Journal of Pharmaceutical Sciences,* 15**,** 489-495.

TESKAC, K. & KRISTL, J. 2010. The evidence for solid lipid nanoparticles mediated cell uptake of resveratrol. *International Journal of Pharmaceutics,* 390**,** 61-69.

THAKUR, R. K., VILLETTE, C., AUBRY, J. M. & DELAPLACE, G. 2007. Formulation-composition map of a lecithin-based emulsion. *Colloids and Surfaces a-Physicochemical and Engineering Aspects,* 310**,** 55-61.

TIYABOONCHAI, W., TUNPRADIT, W. & PLIANBANGCHANG, P. 2007. Formulation and characterization of curcuminoids loaded solid lipid nanoparticles. *International Journal of Pharmaceutics,* 337**,** 299-306.

TSAO, R., YANG, R., XIE, S., SOCKOVIE, E. & KHANIZADEH, S. 2005. Which polyphenolic compounds contribute to the total antioxidant activities of apple? *Journal of Agricultural and Food Chemistry,* 53**,** 4989-4995.

VACCARINO, C., LOCURTO, R. B., TRIPODO, M. M., PATANE, R. & RAGNO, A. 1992. GRAPE MARC AS A SOURCE OF FEEDSTUFF AFTER CHEMICAL TREATMENTS AND FERMENTATION WITH FUNGI. *Bioresource Technology,* 40**,** 35-41.

VATAI, T., SKERGET, M. & KNEZ, Z. 2009. Extraction of phenolic compounds from elder berry and different grape marc varieties using organic solvents and/or supercritical carbon dioxide. *Journal of Food Engineering,* 90**,** 246-254.

VELDHUIZEN, E. J. A., TJEERDSMA-VAN BOKHOVEN, J. L. M., ZWEIJTZER, C., BURT, S. A. & HAAGSMAN, H. P. 2006. Structural requirements for the antimicrobial activity of carvacrol. *Journal of Agricultural and Food Chemistry,* 54**,** 1874-1879.

VIAN, M. A., TOMAO, V., GALLET, S., COULOMB, P. O. & LACOMBE, J. M. 2005. Simple and rapid method for cis- and trans-resveratrol and piceid isomers determination in wine by high-performance liquid chromatography using Chromolith columns. *Journal of Chromatography A,* 1085**,** 224-229.

WALLE, T., HSIEH, F., DELEGGE, M. H., OATIS, J. E. & WALLE, U. K. 2004. High absorption but very low bioavailability of oral resveratrol in humans. *Drug Metabolism and Disposition,* 32**,** 1377-1382.

WANG, Q., GONG, J., HUANG, X., YU, H. & XUE, F. 2009. In vitro evaluation of the activity of microencapsulated carvacrol against Escherichia coli with K88 pili. *Journal of Applied Microbiology,* 107**,** 1781-1788.

WANG, X., JIANG, Y., WANG, Y. W., HUANG, M. T., HO, C. T. & HUANG, Q. 2008. Enhancing anti-inflammation activity of curcumin through o/w nanoemulsions. *Food Chemistry,* 108**,** 419-424.

WEISS, Q., GAYSINSKY, S., DAVIDSON, M. & MCCLEMENTS, J. 2009. Nanostructured encapsulation systems: food antimicrobials. *In:* BARBOSA-CANOVAS, G. V., MORTIMER, A., LINEBACK, D., SPIESS, W. AND BUCKLE, K. (ed.) *IUFoST World Congress Book: Global Issues in Food Science and Technology.* Amsterdam: Elsevier Inc.

WENZEL, E., SOLDO, T., ERBERSDOBLER, H. & SOMOZA, V. 2005. Bioactivity and metabolism of trans-resveratrol orally administered to Wistar rats. *Molecular Nutrition & Food Research,* 49**,** 482-494.

WENZEL, E. & SOMOZA, V. 2005. Metabolism and bioavailability of trans-resveratrol. *Molecular Nutrition & Food Research,* 49**,** 472-481.

WOLFE, K. L. & LIU, R. H. 2007. Cellular antioxidant activity (CAA) assay for assessing antioxidants, foods, and dietary supplements. *Journal of Agricultural and Food Chemistry,* 55**,** 8896-8907.

WOOSTER, T. J., GOLDING, M. & SANGUANSRI, P. 2008. *Impact of oil type on nanoemulsion formation and Ostwald ripening stability*.

WRIGHT, J. S., JOHNSON, E. R. & DILABIO, G. A. 2001. Predicting the activity of phenolic antioxidants: Theoretical method, analysis of substituent effects, and application to major families of antioxidants. *Journal of the American Chemical Society,* 123**,** 1173-1183.

YOUN, J., LEE, J.-S., NA, H.-K., KUNDU, J. K. & SURH, Y.-J. 2009. Resveratrol and Piceatannol Inhibit iNOS Expression and NF-kappa B Activation in Dextran Sulfate Sodium-Induced Mouse Colitis. *Nutrition and Cancer-an International Journal,* 61**,** 847-854.

YU, L., SUN, Z. J., WU, S. L. & PAN, C. E. 2003. Effect of resveratrol on cell cycle proteins in murine transplantable liver cancer. *World Journal of Gastroenterology,* 9**,** 2341-2343.

YUAN, Y., GAO, Y., ZHAO, J. & MAO, L. 2008. Characterization and stability evaluation of b-carotene nanoemulsions prepared by high pressure homogenization under various emulsifying conditions. *Food Research International,* 41**,** 61-68.

ZHUANG, C. Y., LI, N., WANG, M., ZHANG, X. N., PAN, W. S. & PENG, J. J. 2010. Preparation and characterization of vinpocetine loaded nanostructured lipid carriers (NLC) for improved oral bioavailability. *International Journal of Pharmaceutics,* 394**,** 179-185.